

**Design of Spacecraft
for
Exploration of the Moon and Mars**

by

Brenden P. Epps

Submitted to the Department of Mechanical Engineering
in partial fulfillment of the requirements for the degree of

Master of Science in Mechanical Engineering

at the

MASSACHUSETTS INSTITUTE OF TECHNOLOGY

February 2006

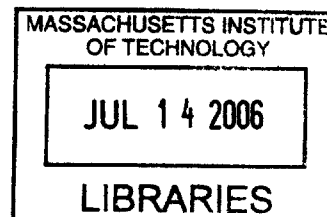
© Massachusetts Institute of Technology 2006. All rights reserved.

Author
Department of Mechanical Engineering
January 18, 2006

Certified by
Edward F. Crawley
Professor, Aeronautics and Astronautics
Thesis Supervisor

Certified by
Daniel Frey
Professor, Mechanical Engineering
Thesis Reader

Accepted by
Lallit Anand
Chairman, Department Committee on Graduate Students



BARKER

[THIS PAGE INTENTIONALLY LEFT BLANK]

Design of Spacecraft
for
Exploration of the Moon and Mars

by
Brenden P. Epps

Submitted to the Department of Mechanical Engineering
on January 18, 2006, in partial fulfillment of the
requirements for the degree of
Master of Science in Mechanical Engineering

Abstract

In this thesis, I develop the conceptual design of the spacecraft required for human-Lunar and human-Mars exploration. The requirements for these vehicles are derived in the context of the NASA Concept Exploration & Refinement project. Similarly, the concepts generated are intended to operate within the transportation architecture developed during this project. Therefore, this thesis serves as a vehicle-level design exercise. Four vehicle architecture options are synthesized by combining system concepts in a logical fashion. These four options are evaluated on several performance criteria, and one vehicle design concept is selected for detailed modeling. In addition, I investigate the conceptual design of the airlock system, as a system-level design exercise. This research project culminated in a set of vehicle concept designs and design recommendations for NASA.

Thesis Supervisor: Edward F. Crawley
Title: Professor, Aeronautics and Astronautics

Thesis Reader: Daniel Frey
Title: Professor, Mechanical Engineering

[THIS PAGE INTENTIONALLY LEFT BLANK]

Collagen Implants to Promote Regeneration of the Adult Rat Spinal Cord

by

Rahmatullah H. Cholas

B.S. Aerospace Engineering
Embry-Riddle Aeronautical University, 2002

SUBMITTED TO THE DEPARTMENT OF MECHANICAL ENGINEERING IN
PARTIAL FULFILLMENT OF THE REQUIREMENTS OF THE DEGREE OF

MASTER OF SCIENCE IN MECHANICAL ENGINEERING
AT THE
MASSACHUSETTS INSTITUTE OF TECHNOLOGY

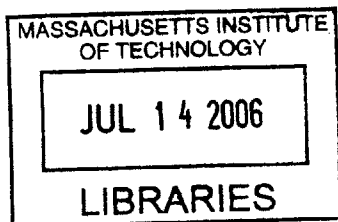
JUNE 2006

©2006 Massachusetts Institute of Technology
All rights reserved

Signature of Author: _____
Department of Mechanical Engineering
May 12, 2006

Certified by: _____
Myron Spector, Ph.D.
Senior Lecturer, Department of Mechanical Engineering, MIT
Professor of Orthopedic Surgery (Biomaterials), Harvard Medical School
Thesis Supervisor

Accepted by: _____
Lallit Anand, Ph.D.
Professor of Mechanical Engineering
Chairman, Mechanical Engineering Graduate Committee



BARKER

Collagen Implants to Promote Regeneration of the Adult Rat Spinal Cord

by

Rahmatullah H. Cholas

Submitted to the Department of Mechanical Engineering
on May 12, 2006 in Partial Fulfillment of the
Requirements for the Degree of Master of Science in
Mechanical Engineering

ABSTRACT

Over 250,000 people in the United States currently live with a spinal cord injury and approximately 11,000 new cases occur every year. People with spinal cord injuries experience a significant reduction in quality of life due to the many problems that arise from damage to the spinal cord including paralysis and loss of sensation below the location of injury, loss of bowel and bladder function, loss of sexual function, and impaired respiration. Despite considerable ongoing research in the area of nerve regeneration by various institutions, satisfactory treatment for spinal cord injury has not yet been discovered.

Previous studies have had considerable success in facilitating the regeneration of severed peripheral nerves through the use of collagen based implants used to bridge the resulting gap between the severed nerve stumps. The current study aims to apply this same regenerative approach to a defect created in the spinal cord of adult rats. The objective is to evaluate the efficacy of three different collagen implants toward the regeneration of the spinal cord. The experimental spinal cord injury was a complete transection at T7 and T9 and the removal of the spinal cord segment between the two transections, creating a 5 mm gap.

This study contained four experimental groups. Group I was the control group. The animals in this group had a complete spinal cord transection as described above but received no implantation. Group II received a resorbable dura replacement sheet of collagen, 1 mm thick, cut from the BioGide® membrane which was placed extradurally over the dorsal aspect of the wound site. Group III used the BioGide® membrane as a wrap which bridged the gap between the two cord stumps. Group IV used a collagen tube, fabricated using a freeze-drying process, to bridge the gap.

Histological analysis at 6 weeks after implantation showed Groups III and IV to have more longitudinally oriented reparative tissue filling the defect area as well as fewer fluid-filled cysts. Quantitative analysis of axonal regeneration showed the collagen implants to be supportive of the regeneration of axons into the center of the defect.

Thesis Supervisor: Myron Spector

Title: Senior Lecturer, Department of Mechanical Engineering

Professor of Orthopedic Surgery (Biomaterials), Harvard Medical School

Acknowledgements

My work on the spinal cord project has truly been a learning experience. Despite my limited background in the biological and biomedical fields I was able to finally bring this research together and I am grateful to my advisor, Dr. Spector, for allowing me to work on this project solely based on my heightened interest of the topic. I have learned a lot from Dr. Spector, and I appreciate his patience and enthusiasm no matter what the situation.

I would also like to thank the other members of the spinal cord regeneration team for their support and encouragement even during the times when the work could get a bit wearing like when we had to go to the animal research facility every night at midnight to express rat bladders. Dr. Hu-Ping Hsu was an invaluable resource; bringing his skills and expertise on animal surgery to the project.

On a more personal note, I would like to thank my parents for their continued love and encouragement, no matter what. Also, I thank my friends for not giving up on me despite my “disappearance” while I worked on putting this thesis together. I am truly grateful to have the friends that I do.

Table of Contents

ABSTRACT	2
ACKNOWLEDGEMENTS	3
TABLE OF CONTENTS	4
LIST OF FIGURES.....	5
LIST OF TABLES.....	6
CHAPTER 1: INTRODUCTION	7
1.1 MOTIVATION OF RESEARCH	7
1.2 THE NERVOUS SYSTEM.....	7
1.3 THE SPINAL CORD	10
1.4 NORMAL INJURY RESPONSE OF THE PERIPHERAL NERVOUS SYSTEM.....	13
1.5 NORMAL INJURY RESPONSE OF THE SPINAL CORD.....	15
1.6 CURRENT CLINICAL TREATMENTS OF SCI AND ONGOING RESEARCH.....	15
1.7 AIM OF RESEARCH PROJECT AND SPECIFIC GOALS OF THIS THESIS	17
CHAPTER 2: METHODS AND MATERIALS	18
2.1 COLLAGEN IMPLANTS	18
2.1.1 <i>Tube Fabrication Materials</i>	18
2.1.2 <i>Tube Fabrication Protocol</i>	19
2.1.2 <i>BioGide® Membrane</i>	21
2.2 SPINAL CORD INJURY MODEL.....	22
2.3 ANIMAL MODEL.....	23
2.4 RAT STRAIN CHOICE.....	23
2.5 RAT SURGERY	24
2.6 SPINAL TISSUE REMOVAL.....	29
2.7 HISTOLOGY.....	30
2.7.1 <i>Plastic Embedded Specimen</i>	30
2.7.2 <i>Wax Embedded Specimen</i>	31
2.7.3 <i>Method for the Quantitative Analysis of Axonal Regeneration</i>	31
CHAPTER 3: RESULTS.....	33
3.1 SURVIVAL POST-SURGERY	33
3.2 FUNCTIONAL ABILITY.....	33
3.3 MORPHOLOGICAL OBSERVATIONS	34
3.4 HISTOLOGICAL FINDINGS.....	36
3.5 AXONAL QUANTIFICATION.....	40
CHAPTER 4: DISCUSSION.....	43
CHAPTER 5: CONCLUSION	45
APPENDIX A: DEHYDROTHERMAL CROSSLINKING PROTOCOL (ADAPTED FROM HARLEY, 2002).....	46
APPENDIX B: PLASTIC EMBEDDING PROTOCOL.....	47
APPENDIX C: HEMATOXYLIN AND EOSIN (H & E) STAINING PROTOCOL	49
REFERENCES	50

List of Figures

No.	Description	Page
1.1	Neuron.....	8
1.2	Axon myelination.....	8
1.3	Neural synapse.....	9
1.4	Astrocyte in close proximity of a neuron and capillary.....	9
1.5	Oligodendrocyte.....	10
1.6	Spinal cord within vertebra and meninges.....	11
1.7	Spinal cord with gray and white matter.....	12
1.8	Human body showing spinal root locations for innervation.....	13
1.9	Vasculature of the spinal cord.....	13
1.10	Peripheral nerve regeneration.....	14
2.1	Mold used for fabricating collagen tubes.....	18
2.2	Side view of closed mold.....	19
2.3	Glass rod with a silicone sheath and Teflon spacers.....	19
2.4	Collagen tube.....	21
2.5	Microstructure of the BioGide® membrane.....	22
2.6	Section of exposed spinal cord and image showing 5mm gap.....	25
2.7	Schematic diagram of spinal cord transection with implants.....	26
2.8	Surgical implantation procedures.....	27
2.9	Collagen membrane placed over the defect area.....	28
2.10	Rat post-operative care.....	28
2.11	Steps for the extraction of the thoracic spinal column.....	29
2.12	Extracted spinal cord.....	30
2.13	Image of plastic embedded spinal cord section.....	31
2.14	Example images used for axon quantification.....	32
3.1	Snapshots of tube implanted rat and normal rat.....	34
3.2	Comparison of lesion center areas for experimental groups.....	35
3.3	Aspect ratios of lesion center cross-sections.....	36
3.4	Sectioning strategy.....	36
3.5	Normal rat spinal cord.....	37
3.6	Explanted spinal cord of control group showing large cyst.....	38
3.7	Explanted spinal cord of Group II rat showing numerous cysts.....	38
3.8	Explanted spinal cord of Group III (wrap) rat.....	38
3.9	Explanted spinal cord of Group IV (tube) rat demonstrating fewer cysts.....	38
3.10	High magnification of defect center.....	39
3.11	Cross-section of the defect-center of control animal.....	40
3.12	Cross-section of the defect-center of dorsal barrier implanted animal.....	40
3.13	Cross-section of the defect-center of a wrap implanted animal.....	41
3.14	Cross-section of the defect-center of a tube implanted animal.....	41
3.15	Comparison of mean number of axons found at the lesion centers.....	42

List of Tables

No.	Description	Page
3.1	Experimental groups	33

Chapter 1: Introduction

1.1 Motivation of Research

There are currently 250,000 people in the United States who have suffered a spinal cord injury and there are approximately 11,000 new cases every year. Motor vehicle crashes account for the majority of new spinal cord injury (SCI) cases. The most common neurologic level of injury is tetraplegia (57.6% for both complete and incomplete injuries) followed by paraplegia (35.9% for both complete and incomplete injuries). Only less than 1% of patients with SCI experience full neurological recovery [1].

Patients with SCI often suffer significant reduction in quality of life. In addition to suffering paralysis and the loss of sensation below the level of injury, other basic bodily functions are often impaired including breathing, bowel and bladder control and sexual function. As a result, sufferers of spinal cord injuries lose a great deal of their independence. Additional complications that often arise with SCI are orthostatic hypotension, autonomic dysreflexia, osteoporosis, chronic pain, and pressure ulcers [2].

The financial toll that SCI imposes is quite staggering. Lifetime costs that are directly attributed to SCI vary depending on the severity of injury and are as high as \$2.8 million for high tetraplegia and \$900,000 for paraplegia [1].

1.2 The Nervous System

The nervous system is composed of a network of cells, or neurons, which are distributed throughout the body and function to transmit information as electrochemical impulses to and from and within the brain. Some of the information that is transmitted via the neural network is in response to stimuli received from both the external and internal environment of the body (sensory information), while other information transmitted by neurons is in the form of motor commands which cause muscles to contract or glands to function.

The cells of the central nervous system include neurons (which transmit information) and glia, which support neuronal function.

1.5 Normal Injury Response of the Spinal Cord

Injury to the spinal cord results in two distinct modes of tissue damage. The first is acute tissue damage which results directly from the disruption of the tissue and causes extensive cell death at the injury site. The second mode of tissue damage, or secondary tissue damage, is tissue degeneration that continues well after the initial injury.

Secondary damage occurs as a result of various events which occur in response to the acute injury. Immediately following the initial injury, there is considerable hemorrhaging that takes place and affects the normal oxygen and nutrient supply to the affected tissue. The body then responds to the acute injury with a strong inflammatory response which leads to edema of the spinal tissue. As this occurs, neural cells begin to die and release excitotoxins such as glutamate which causes further neural cell death [6]. Another adverse occurrence is the formation of free radicals which cause extended damage to surrounding nervous tissue. The unfavorable conditions are heightened by the demyelization of remaining axons due to the loss of oligodendrocytes. As spinal tissue is lost and removed by phagocytes, fluid-filled cysts are formed within the lesion. Dense fibrous and glial scar formation occurs at the injury site which impedes any attempts of the axons to spontaneously regenerate across the defect. Reactive astrocytes, which form the glial scar, express chondroitin sulphate proteoglycans, which inhibit axonal growth. Other inhibitory molecules are found in the degenerating myelin including NOGO-A, MAG, and OMpg [7]. In response to being severed, the distal segments of damaged axons undergo Wallerian degeneration while the proximal segments retract away from the injury site.

The rather hostile environment ensuing injury to the spinal cord impedes the spontaneous regenerative processes, including axonal sprouting, that occur following nerve damage.

1.6 Current Clinical Treatments of SCI and Ongoing Research

The emphasis of the initial treatment of a spinal injury is on immobilization of the spinal column to prevent further nerve damage. Surgical intervention is commonly required to provide realignment and stabilization of the spine and decompression of the spinal cord. The intravenous administration of methylprednisolone in high dosages

within 8 hours of injury was reported by Bracken et al. to significantly reduce the effect of secondary injury in a multicenter randomized clinical trial. Methylprednisolone was reported to be of benefit only if administered within the 8 hour period following spinal cord injury [8]. Despite the broad acceptance of methylprednisolone as a clinical treatment for SCI there is still considerable controversy over the efficacy of this steroid treatment [9]. To date there are no clinical therapies which actively promote the regeneration of the damaged nervous tissue.

Many experimental SCI treatment strategies are being investigated in animal models and reported in the literature with varying degrees of promise. Some approaches to spinal cord regeneration involve development and evaluation of various substrates to provide guidance and act as a bridge to axonal growth across a defect in the spinal cord [10-12]. The focus of some studies is the ability of certain neurotrophic factors and gene therapy strategies for creating favorable conditions for axonal growth. Other studies have looked at the implantation of various cell types into the damaged spinal cord to replace lost cells and facilitate nerve repair [14]. Various stem cell approaches have been studied, including the implantation of neural stem and progenitor cells into spinal cord lesions [15]. In many studies the implanted cells are first genetically encoded to express specific neurotrophic factors [16]. Bone marrow mesenchymal stem cells implanted into damaged spinal cords of adult rats have been reported to simulate nerve regeneration [17-20]. Lu et al. reported that BDNF-expressing marrow stromal cells supported axonal regeneration in adult rats [21]. Furthermore, olfactory ensheathing glia have been reported to promote long distance axonal growth when implanted into the defect of a transected rat spinal cord [22-24]. In another study, neurotrophin-3 (NT-3) expressing olfactory ensheathing glia cells were reported to promote spinal sparing and regeneration in adult rats [25]. While some researchers only implant cells into the spinal cord lesion others implant them in combination with a biomaterial scaffold [26-28]. The identification of inhibitors to regeneration (such as NOGO-A) and the application of agents to block or overcome these inhibitors has shown promise in improving axon recovery after spinal cord injury [7, 29-31]. In one study, the use of an oscillating field stimulator, which produced an electric field across a lesion in the spinal cord, was shown

to induce limited sensory recovery and improve motor function in patients participating in a phase 1 clinical trial [32].

Previous work in our laboratory has shown the effectiveness of collagen tubes in promoting axonal regeneration across significant gaps in the rat peripheral nerve [33, 34]. The tubes performed better than the nerve autograft “gold standard”. Our laboratory has also investigated the use of collagen tubes for spinal cord regeneration. Results showed that tubulation of a transected adult rat spinal cord had beneficial effects on spinal cord healing such as a reduction in scar formation and improved axonal and connective tissue orientation within the defect [35, 36]. This past work forms the basis for the current hypothesis that collagen based implants have beneficial effects on spinal cord regeneration.

Notwithstanding the encouraging results for spinal cord regeneration that many researchers have reported in the literature, there has yet to be a single therapy which can provide satisfactory recovery from traumatic spinal cord injury. It is likely that an effective treatment for spinal cord injury will require a multifaceted approach to nerve regeneration; combining various spinal cord regeneration strategies.

1.7 Aim of Research Project and Specific Goals of this Thesis

The long term objective of this research project is the development of an implant for the treatment of spinal cord injuries in humans. The implant will likely make use of a combination of therapies shown to support regeneration of the spinal cord. The therapies currently investigated include porous, structurally aligned, bioresorbable collagen scaffolds, stem cell therapies, inhibitor blocking antibodies, and the use of neurotrophic factors delivered via scaffold binding and/or cellular transfection.

The specific aim of this thesis is to compare select collagen implants for their abilities to promote axon regeneration in the adult rat spinal cord. The goal is to find an optimal entubulation strategy which can be used in the future in combination with the spinal cord regeneration therapies mention above. The primary method for the evaluation of the efficacy of the various implants will be qualitative histology and quantitative axonal regeneration analysis.

The BioGide® sheets were prepared into a slurry suspension (5% w/w) by cutting them into small pieces (1 mm²) then mixing with a 0.5 M acetic acid solution. The collagen slurry was thoroughly mixed until a homogenous mixture was achieved. A 10-ml syringe containing the collagen slurry was attached to another 10-ml syringe with a Luer-lock assembly, and mixed by injecting collagen slurry from one syringe into the other (approximately 30-40 times) until the collagen fibers began to hydrate and the solution appeared uniform.

After letting the slurry sit for 3 hours at room temperature to allow for the collagen fibers to swell, the collagen slurry was centrifuged in order to de-gas the collagen so that any macroscopic air bubbles were removed from the slurry.

During centrifugation the slurry tended to separate into two phases. In order to re-homogenize the slurry, it was gently mixed using the syringes and Luer-lock assembly 2-3 times very slowly taking care not to allow any air to be mixed into the solution.

The collagen slurry was injected into the Teflon mold. The slurry (~0.8 ml per tube) was injected into one side of a channel in the closed mold until it started to come out of the other side of the channel. The glass rod with its silicone sheath was then inserted into the channel which had been filled with slurry. The rod was rotated during its insertion so as to keep the rod centered in the channel and to maintain a uniform coverage of the rod with the collagen slurry throughout the channel. When the rod came out of the other side of the channel, a centering ring/spacer was slipped over the rod. This procedure was repeated for each of the 6 channels in the mold.

The mold was placed into a freeze-drier (set to -40°C) for 1 hour. After freezing, the mold was removed from the freeze-drier and quickly split open, in order for the frozen collagen tube to be gently removed from the mold. The glass/silicone rods were kept inside of the collagen tubes. The tubes with the rods in place were inserted back into the freeze-drier (at -40°C).

A vacuum below 100 mTorr (taking ~30-60 minutes to reach) was applied to the freeze-drier. The temperature was then raised to 0°C and the samples left overnight under vacuum in the freeze-drier (17 hours). The temperature was subsequently raised to 20°C and the vacuum released.

implant a device for facilitating axonal regeneration. Unilateral hemesectional models offer the advantage of being able to assess an implanted device while still preserving the structural integrity and function of one side of the spinal cord [26].

For this study the complete transection model was chosen as it offers the best method for evaluating the effects of an implanted device on axonal regeneration.

2.3 Animal Model

The most common animal model used for spinal cord injury research is the adult rat. For this reason there is an abundance of data in the literature that allows for easy comparison of result from different studies. Compared to other animals, rats are inexpensive, can be studied in large numbers, require less intensive post operative care, and have relatively low mortality rates. Transgenic mice offer the researcher the distinctive ability to control particular genetic characteristics; however, the small size of mice may prohibit certain surgical procedures and device implantations [37].

Larger animal models such as cats, dogs, pigs and primates are not used as widely in the literature. These animal models are less attractive due to the higher cost and more intensive animal care; however, using a large animal model may be important before performing trials on humans.

In this study, the rat was chosen as the animal model for the reasons mention above and also due to the fact that our laboratory has extensive experience in using rats for both peripheral nerve and spinal cord regeneration studies [13, 33-36, 39, 40].

Female rats were used in this study because they allow for easier management of the loss of reflex bladder control following spinal cord transection. The loss of bladder function necessitates the manual expression of urine from the bladders of the rats following complete spinal cord transection. Using female rats facilitates the manual expression of the bladder.

2.4 Rat Strain Choice

The first three experimental groups in this study used Sprague-Dawley (SD) rats weighing between 250 to 300 grams. There was an approximately 40% incidence of self-mutilation in the SD rats, most commonly in the form of extreme biting of the skin of the

Chapter 1

Introduction

On January 14, 2004, President G.W. Bush announced his Vision for Space Exploration: complete the construction of the International Space Station, develop a new launch vehicle to replace the Space Shuttle when it is retired in 2010, return to the Moon by year 2020 and establish an extended human presence there, and begin a program of human-Mars exploration [4]. To achieve this long-term vision, NASA must design a sustainable, safe system of systems geared towards delivering the value of space exploration to all key stakeholders.

It isn't enough to just "land a man on the Moon and return him safely" [14], as was the case in the Apollo program. The American people want to see vivid video and images of humans on Mars; scientists want to conduct experiments in space environments; and politicians want public approval. In order to satisfy all stakeholders to at least some degree, a carefully engineered system of systems is required. A team of over fifty research assistants, MIT faculty, and Draper Laboratory employees studied the problem of designing such a system for NASA.

1.1 Background

NASA commissioned the MIT-Draper team to investigate the design of the overarching system of systems architecture, including the transportation architecture, and specifically, the Crew Exploration Vehicle. This body of work is funded under this grant, and thus, the analyses and results align to the work that has been done by the MIT-Draper Concept Exploration & Refinement (CE&R) team.

My role in the team was twofold. During the first half of the project, I investigated the risk and safety of the candidate transportation system architectures. The results of my analysis were used as a metric to select the Lunar and Martian exploration architectures presented in this thesis. In addition, my analysis pointed to several technical risks (such as landing stability) which could be mitigated by a robust vehicle design. During the second half of the project, I conducted several analyses (such as landing gear design) which allowed the team to make decisions regarding the design of the vehicles themselves. My specific contributions are detailed in Section 1.4.1.

1.2 Governing Equations

This thesis is written for those with a general understanding of physics and advanced mathematics. The pertinent equations governing space-flight are presented here in order to give the reader an appreciation for how and why spacecraft are designed as they are.

1.2.1 Orbits and Transfers

The general mission sequence consists of launch from Earth to low Earth orbit (LEO), travel to Mars (or the Moon), operations in low Mars (or low Moon) orbit, descent, surface operations, ascent to M-orbit, transfer to Earth orbit, and Earth atmospheric entry, descent, landing, and recovery. In order to gain insight into the mechanics

of this mission, let us first examine the spacecraft in low Earth orbit. This craft's motion can be described mathematically, using Newton's law of gravitation for a satellite orbiting the Earth:

$$\begin{aligned}
 F &= \frac{GMm}{r^2} \\
 &= \frac{\mu m}{r^2}
 \end{aligned}
 \tag{1.2.1}$$

where G is the universal constant of gravitation, M is the Earth's mass, m is the satellite's mass, and r is the distance between their centers. The gravitational constant is, $\mu = GM = 3.99 \times 10^8 \text{ m}^3/\text{s}^2$, for Earth.

Assuming that the Earth and the satellite are the only bodies interacting and that the satellite travels in a circular orbit, we may readily write its velocity:

$$v_c = \sqrt{\frac{\mu}{r}}
 \tag{1.2.2}$$

where v_c is the velocity and r is the radius of the orbit. Clearly, a lower orbit requires a faster speed, and a higher orbit requires a lower speed. Why, then, does a satellite stay in orbit? Let us consider the general orbit to deduce the answer.

To derive the general equation for the motion in an orbit, we combine (1.2.1) with Newton's second law to yield the *two-body equation of motion*:

$$\ddot{\mathbf{r}} + \left(\frac{\mu}{r^3}\right) \mathbf{r} = 0
 \tag{1.2.3}$$

which has the solution:

$$r = \frac{a(1 - e^2)}{1 + e \cos \nu}
 \tag{1.2.4}$$

where a is the semimajor axis, $e = c/a$ is the eccentricity, c is the distance from the center of the orbit to one of the foci, and ν is the polar angle, defined to be zero at

the perigee (closest point to Earth) and π at the apogee (farthest point from Earth). See Figure 1-1.

Equation (1.2.4) may either describe a circle, ellipse, parabola, or hyperbola, depending on the satellite's *specific mechanical energy*, ϵ , given by the *energy equation*:

$$\epsilon = \frac{v^2}{2} - \frac{\mu}{r} = -\frac{\mu}{2a} \quad (1.2.5)$$

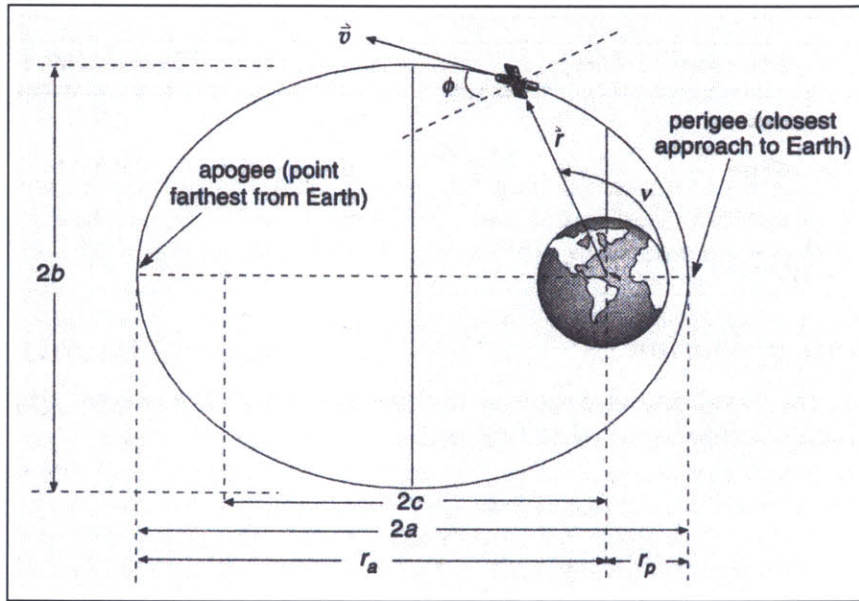


Figure 1-1: Geometry of an elliptical orbit, from [16].

Since gravity is a conservative force, the specific mechanical energy is always constant ($-\mu/2a$). By inspection of (1.2.5), we see that the energy is negative for a circular or elliptical orbit. In fact, the energy is minimum for a circular orbit (when $a = r$). Negative energy means that the craft will remain in orbit.

Suppose one wants to move from a low circular orbit to a higher circular orbit. If the velocity is boosted slightly, mechanical energy is increased, and the satellite now travels in an elliptical orbit. At a later time, when the satellite is further from Earth, the velocity is retarded, and the satellite falls into the larger-radius circular orbit. This process is called a *Hohmann Transfer* and is illustrated in Figure 1-2.

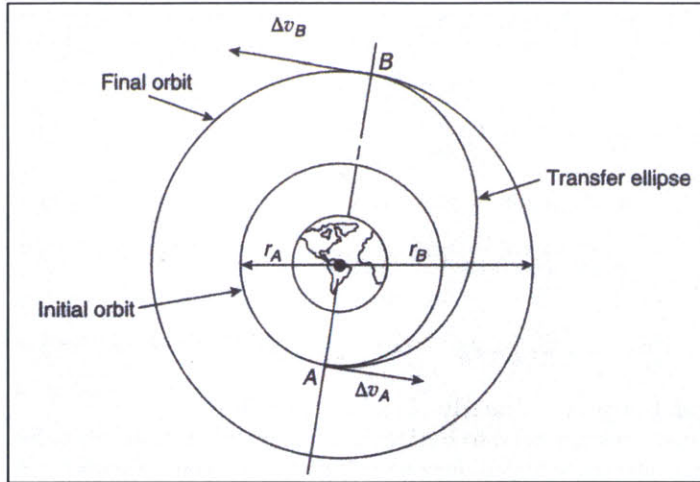
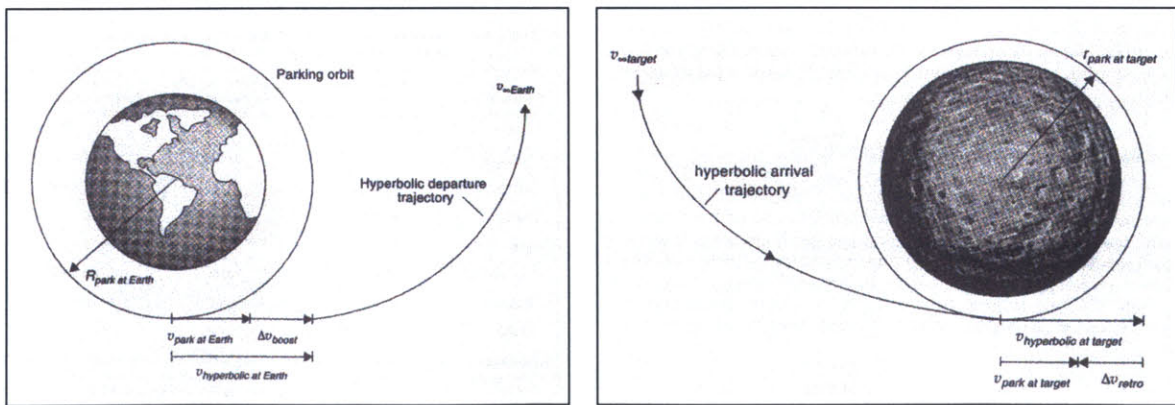


Figure 1-2: Hohmann Transfer between two circular, coplanar orbits, from [16].

By setting the energy to zero, we may solve (1.2.5) for the *escape velocity*, the velocity required to leave Earth orbit altogether.

$$v_{esc} = \sqrt{\frac{2\mu}{r}} \quad (1.2.6)$$

So by boosting the velocity the amount $\Delta v = \sqrt{\frac{2\mu}{r}} - \sqrt{\frac{\mu}{r}}$, the satellite will leave low Earth orbit. A similar delta-V is required to insert into circular orbit around the Moon or Mars. See Figure 1-3.



(a) Earth-escape

(b) M-orbit insertion

Figure 1-3: Depiction of delta-V required for orbit transfers, from [16].

Once in an orbit, the satellite will remain in that orbit. Propulsive events which change the velocity (i.e. produce a delta-V) are required to transfer between orbits. Let us now consider how these changes in velocity occur by rocket propulsion.

1.2.2 Rocket Propulsion

A standard rocket fuel is methane (CH_4) and oxygen (O_2), which react in the engine combustion chamber to exhaust steam (H_2O) and carbon dioxide (CO_2). The propellant is stored at rest in tanks, and the exhaust leaves the rocket at a tremendous velocity. Newton's third law asserts that this increase in momentum of the fluid leaving the rocket is balanced by an equal and opposite increase of momentum of the rocket. Knowing this much, we may anticipate that the rocket will require large amounts of fuel to change its velocity appreciably. Let us now derive the governing equation.

Consider a rocket performing an engine burn in the absence of gravity at a constant exhaust velocity relative to the rocket, V_e and thus, constant exhaust mass flow rate, \dot{M}_e . Conservation of Momentum then simply states:

$$\begin{aligned}
 0 = \frac{d(MV)}{dt} &= \underbrace{\frac{dM}{dt} V_e}_{\text{momentum lost out exit}} + \underbrace{M \frac{dV}{dt}}_{\text{momentum gained by rocket}} \\
 &= -\dot{M}_e V_e + (M_0 - \dot{M}_e t) \frac{dV}{dt}
 \end{aligned}$$

where V is the velocity and $M = M_0 - \dot{M}_e t$ is the mass of the rocket at any instant in time. We now integrate to find the so-called *Rocket Equation* [7]:

$$\Delta V = V_e \ln \frac{M_0}{M} \tag{1.2.7}$$

where $\Delta V = V - V_0$ is the change in velocity of the rocket and M_0 and M are the initial and final masses of the rocket, respectively. The ratio $\frac{M_0}{M}$, referred to as

the *mass fraction*, is used to determine the amount of fuel required for a particular maneuver.

Clearly, the landed mass is a design driver, since it is carried through several propulsive events, thus requiring a large amount of propellant mass. Since spaceflight costs approximately \$10,000 per kilogram launched to low Earth orbit [8], engineers strive to minimize total system mass. We see that minimizing landed mass reduces propellant mass, but minimizing delta-V also saves fuel mass. Aerocapture is one means to reduce the required delta-V.

1.2.3 Aerocapture

Aerocapture offers an opportunity to reduce the required propellant mass by reducing the delta-V required for Mars orbit insertion. In the nominal aerocapture maneuver, a vehicle approaches Mars at high speed (5.5-8.5 km/s) on a hyperbolic transfer trajectory. As the vehicle passes through the atmosphere, the aerodynamic drag force reduces the speed of the craft. Kinetic energy is dissipated in the form of heat, much the same way brakes work on a car. The spacecraft is protected from the high heat loads by a Thermal Protection System (TPS), nominally consisting of a heat shield of ablative materials that burn off during the aerocapture maneuver.

To execute aerocapture, the vehicle must approach Mars within a narrow corridor. At the limit furthest from the surface, the vehicle has to orient itself such that the lift force is directed towards the planet, thereby assisting gravity in pulling the vehicle into orbit. The vehicle sweeps a large arc through the atmosphere, thus experiencing the lowest peak deceleration and peak heating rate, but due to the long duration of the event, the highest integrated heat load. At the near limit, the vehicle must direct its lift away from the planet in order not crash into the surface. In this scenario, a shorter arc is swept, the peak deceleration and peak heat rate are highest, and the integrated heat load is lowest. The entry corridor is further narrowed by the fact that

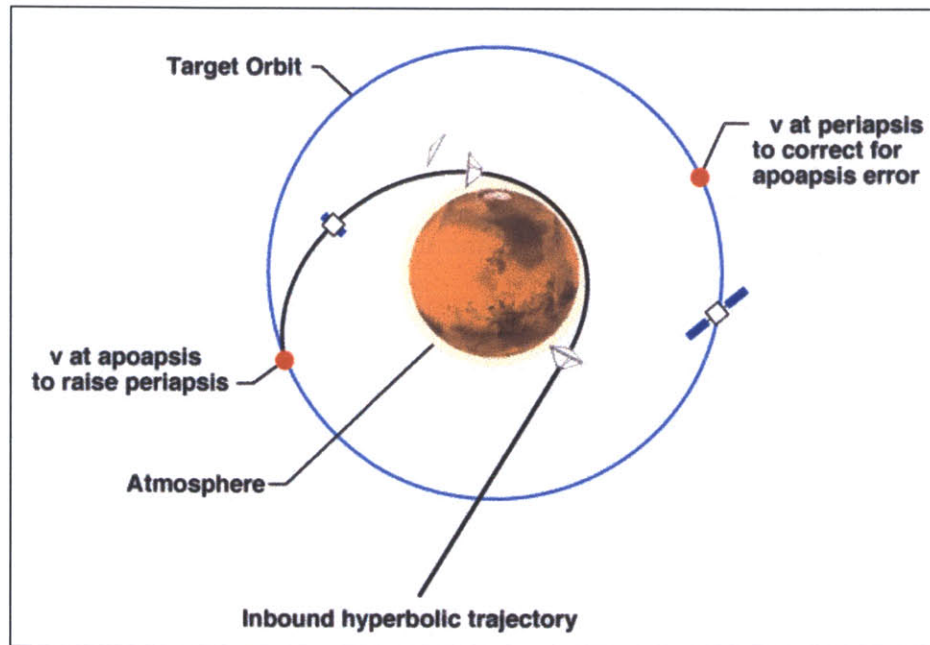


Figure 1-4: Aerocapture may be used to decelerate from a hyperbolic trajectory into a circular parking orbit with substantial delta-V savings.

the crew can not withstand loads higher than 5 Earth g's.

While there is some level of risk associated with the hazardous aerocapture maneuver, some other hazards are mitigated. Decoupling the Mars arrival time and the Mars descent time allows the crew to wait in orbit in the case of a severe dust storm or other atmospheric conditions. This also allows the crew to choose the entry point, which eliminates the need for massive cross-range requirements. Further, the peak entry deceleration loads are reduced, since speed is scrubbed off during two maneuvers rather than one entry and descent upon arrival.

Clearly, the use of aerocapture is a high-level design decision. Using aerocapture incurs some level of risk, but saves some amount of fuel mass. In order to make the design decision whether or not to use aerocapture, we need a formal design methodology.

1.3 Space Systems Design Methodology

A product design approach was used as a framework for considering this problem. The general product design process [9], [10], [21], [26] is summarized in Figure 1-5. This general process may be used to design anything from toys to automobiles to spacecraft. This process may even be used to design the broad architecture of a space exploration mission. In fact, the formal space mission design methodology presented in [16] and shown in Figure 1-6, is very similar. This methodology is used to determine the architecture of a space exploration mission.

One important note is that the mission architecture comprises much more than simply the transportation elements. Orbits and trajectories, of which there are many choices, define the delta-V requirements for the transportation system. Surface elements, such as rovers, science equipment, and bases, allow astronauts to do useful work on the surface. The crew is supported by a mission operations command and control center (e.g. “Houston”), their link to Earth. And finally, the crew themselves are a biological system, whose number, physiology and psychology, and skills may be carefully crafted. The full mission architecture is a system of systems, each a complex engineering task in and of themselves. This thesis focuses solely on the transportation architecture, and the vehicle elements therein.

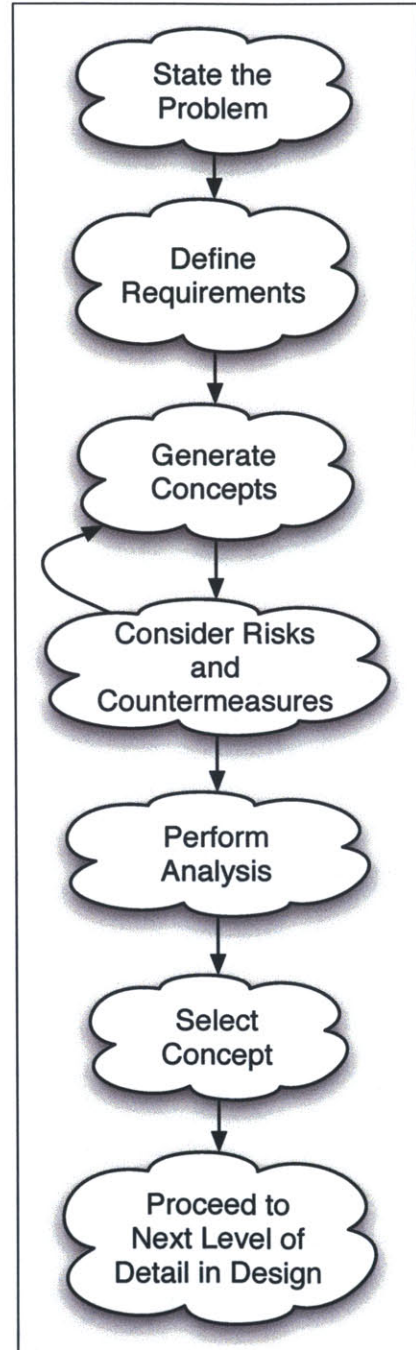


Figure 1-5: General Mechanical Engineering design process.

1. Define broad mission objectives
2. Define mission requirements and constraints
3. Develop alternative mission concepts and architectures
 - (a) Mission-level and element-level architecture
4. Identify system drivers and critical requirements for each concept and architecture
5. Select a baseline mission concept and architecture
 - (a) Evaluate concepts and architectures
6. Define system and subsystem requirements
7. Iterate

Figure 1-6: Space mission design methodology, adapted from [16]

1.3.1 Systems Engineering

Throughout this thesis, terms such as *architecture*, *system*, and *sub-system*, will be used. The formal framework is presented here. By definition, an architecture is “the embodiment of concept, and the allocation of physical/informational function to elements of form, and definition of interfaces among the elements and with the surrounding context” [5]. The architecture is the essence of a thing. An architecture is comprised of “elements of form”, commonly dubbed systems. Each system may itself be comprised of elements of form, and thus, a system may be defined recursively, as shown in Figure 1-7. The base unit that makes up a system is a *part*. “A part is an element that you cannot take apart and then reconstitute in its original form - it has been irreversibly implemented” [5].

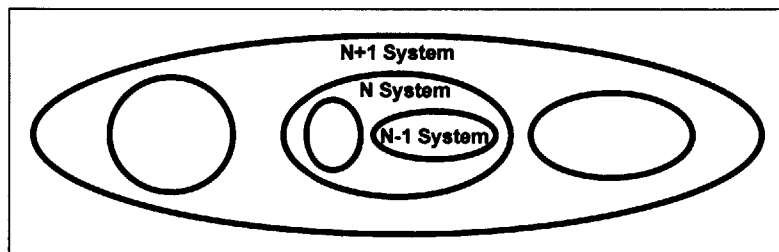


Figure 1-7: By definition, “every system operates as an element of a larger system and is itself composed of smaller systems” [5].

A spacecraft is a system. It is comprised of sub-systems (propulsion, avionics, life-support, etc), and itself is an element in the entire transportation system. Decomposing the propulsion system, we see that it is made up of tanks, tubing, engines, etc. One may declare the ignition switch a part, an element that may not be decomposed further. A spacecraft operates as part of an overarching transportation system. Let us also introduce the term *vehicle*, to be synonymous with spacecraft, but slightly more abstract semantically.

This thesis is concerned with the design of the vehicles that land on Mars or the Moon. Hence, we may refer to the final landed configuration of these vehicles as the *lander*.

By viewing the lander in light of the systems of systems it operates within, one puts into perspective the engineering trades that must be made. While the design of each of the subsystems in the lander may not be the absolute best on every metric, their aggregation may in fact produce the best vehicle system as a whole.

1.4 Results

The result of the MIT-Draper team's efforts was the conceptual design of the vehicles in the Moon and the Mars transportation architectures. The trades and analyses performed in order to converge on this design yielded an understanding of the design drivers and a set of key recommendations for the design of the spacecraft.

The key design drivers are:

- Launch vehicle architecture: side-mounted restricts aeroshell diameter.
- Habitat volume of 285 m^3 : dilates aeroshell diameter.
- Aeroentry stability: restricts aeroshell height.

Key recommendations include:

- Mars AEDL should be achieved using a 15-m diameter conic entry capsule.
- A 15 m-diameter fairing, in-line heavy lift launch vehicle is required for Mars exploration.
- A 15 m-diameter in-line or a 7.5 m-diameter side-mounted HLLV may be used for the Moon.
- Cargo should be mounted on the sides of the descent stage to increase aero-entry and landing stability and to ease deployment.
- Inflatable habitats are recommended for use on the surface of the Moon or Mars.

In this thesis, the design process leading to these and other conclusions is documented. The packaging of the vehicles was arrived at by working both inside-out and outside-in. By assuming a core propulsion stage geometry, one may build the habitat, cargo, and landing gear outwards and upwards from it. Similarly, by assuming an aeroshell shape, one bounds these contents to fit within. By working both inside-out and outside-in, one converges to a package with the optimum exterior shape, scaled to fit the volume required by its contents.

1.4.1 Contributions

Several persons contributed to the final output of our team. My contributions were twofold: analysis of the risk and safety of the candidate transportation architectures; and analysis of the vehicle system concepts in support of vehicle design.

During the first half of the project, over one thousand candidate architectures were identified regarding transportation systems to and from the Moon and Mars. The transportation architecture comprises the number and type of vehicles, their functions, and their interactions. I analyzed the risk and safety of these architectures

using a hazard-based analysis method. The results of my analysis were used as one metric to select the Lunar and Martian exploration architectures presented in the following chapter.

Safety & mission assurance is determined based on two criterion: the mitigation of hazards; and the availability of contingency plans if a hazard occurs. A *hazard mitigation assessment* is conducted as follows:

- Identify high-level hazards for each mission phase.
- Determine the maximum severity (1-4 scale) of each hazard for two categories of potential losses.

Categories: Crew (C), Mission (M)

- Determine extent of mitigation achieved by each architectural option, for each hazard, for each category.

Mitigation levels: Eliminate (4), Prevent (3), Control (2), Reduce (1)

- Generate a database of available mitigations for each architecture.
- Compute a metric for risk mitigation for each architecture by category (C,M) and overall.
- Support architecture trade studies with metrics and safety/risk information.

The process for the *contingency analysis* is similar. Performing each event in a mission sequence has associated hazards which may result in one or more error states. Unless a hazard is completely nonexistent in an architecture, one assumes that it will occur and that each error state will be realized. In response to each error state, the crew may: recover and continue the mission without loss; continue the mission in an impaired state; abort and return to Earth; or wait for rescue in a safe-haven location. If none of these options are available, the error state results in a catastrophic loss.

Each architecture is evaluated chronologically, as depicted in Figure 1-8, to determine which options are available for each hazard, for each error state. Finally, a metric is computed reflecting how often the architecture responds in each way to the error states.

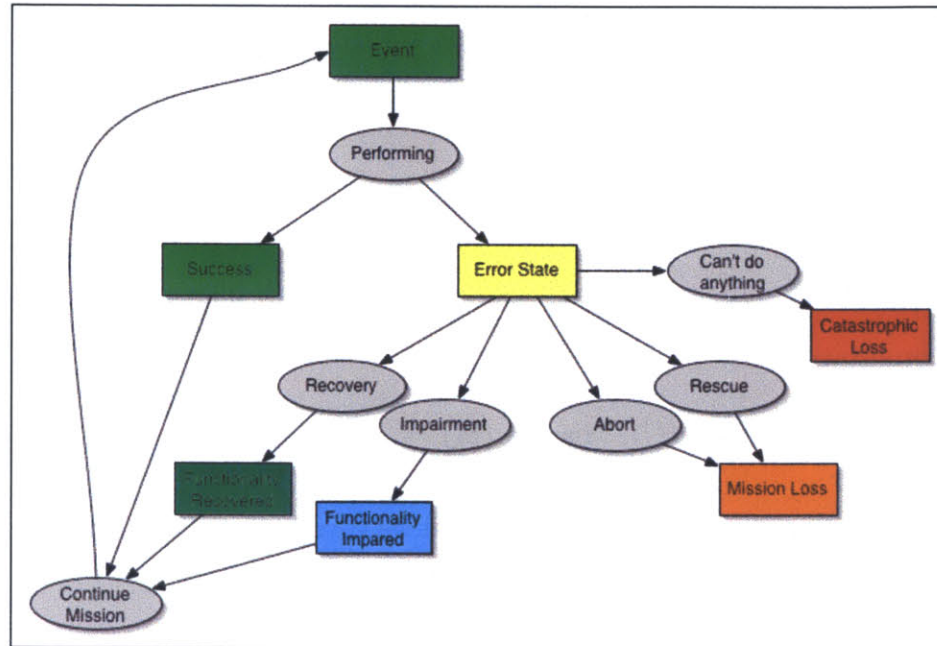


Figure 1-8: The hazard contingency analysis.

By assessing the mitigation levels and availability of contingency plans for each transportation architecture, I made recommendations regarding architectural-level trades and ultimately regarding the architecture selection. The results of this work are not published here in great detail, since this thesis is concerned with the design of the individual vehicles, not the transportation system architecture itself.

During the second half of the project, I performed several of the analyses which allowed the team to make decisions regarding the design of the five vehicles in the two selected transportation architectures (two vehicles for the Moon architecture, and three for the Mars). Many of these analyses are presented in this body of work. I derived the landing gear requirements from first principles, using the Apollo Lunar Module as a reference in the design process. I then sized suspension members and

determined the mass of the landing gear subsystem; this information was fed back into the vehicle mass allocation for subsequent iterations of the design. Moreover, my landing gear concept also served as the benchmark for an *Axiomatic Design* team to investigate alternative suspension designs.

During the landing gear design process, I was required to determine the center of gravity of the landed vehicles in order to determine the landing gear footprint. This led naturally to the analysis of the center of gravity of the vehicles during aerocapture, and aeroentry and descent to the Mars surface. The information gained from these analyses led to several design decisions, namely:

- The biconic aeroentry vehicle design is infeasible for the required volume and mass of the lander propulsion system and habitat.
- All cargo shall be located in low-hanging, side-mounted cargo bays in order to minimize the center of gravity height and maximize the moment of inertia.
- Cargo stored in side-mounted cargo bays may be deployed automatically via a hinged cargo bay or may be deployed manually via similar techniques used in the Apollo program.
- The airlock shall also be located in a low-hanging, side-mounted bay and may be a deployable structure.
- The radiation shelter shall be located surrounding the command and control center, which shall be located about the center of gravity of the vehicle. This minimizes g-loading on the crew during Mars aeroentry and descent as well as grants crew access to the command and control center during solar events.

Finally, I analyzed the costs and benefits of using inflatable structures and/or airlocks. Inflatable habitats offer a significant advantage in the landed mass of the Mars Transfer and Surface Habitat and the Lunar Long-Duration Surface Habitat.

Furthermore, they offer significant risk mitigation regarding Lunar dust intrusion, and the operational advantage of being able to perform scientific experiments within a pressurized structure at ground-level. Inflatable airlocks offer the advantage of lower ascent mass for the Crew Exploration Vehicle (CEV) or Mars Ascent Vehicle, as well as risk advantages regarding Lunar dust intrusion and crew illness.

The details of all of these analyses are found in Chapter 4.

1.5 Thesis Objective

The focus of this thesis is on the design of a common landing system for the Moon and Mars. We first generate requirements for vehicle mass, propulsive events, habitable volume, etc. Using these requirements, we navigate the design space and arrive at four acceptable concepts for the landing system. We specifically address the questions of: What is the optimal package of the landing craft? Can common hardware be used for many vehicles? Can we design for modularity? What is the minimum size heat shield needed? What is the minimum size launch vehicle needed? What is the optimal configuration of the habitat on the lander? How do we deploy large cargo elements (size on the order of magnitude of a small car) to the surface after landing? What, if any, features can we build into the system to mitigate the hazards of lunar (and Martian) dust contamination? and What are the implications on the Earth launch system or other systems due to the design of the lander?

The subsequent chapters follow the space mission design process. In Chapter 2, the mission statement is given, the transportation architecture is developed, and vehicle and system level requirements are derived. In Chapter 3, concepts are generated. Analyses are performed in Chapter 4, and conclusions are drawn in Chapter 5.

Chapter 2

Requirements

The initial phase of system design encompasses definition of the problem and generation of requirements. We answer the questions: what are we designing; what does it have to do; and how well does it have to do it? Requirements are cascaded from the architectural-level down to the vehicle-, system-, sub-system-, and finally, part-level. In this thesis, we highlight the pertinent vehicle-level requirements, and we explore the landing gear system requirements as an example of a lower-level cascade. While there are thousands of requirements, only a subset particularly pertinent to the design of these vehicles and systems are discussed herein.

2.1 Problem Definition

What are we designing? We seek to design the set of vehicles that will transport crew and cargo to the surface of the Moon or Mars in order to explore and conduct science experiments.

2.1.1 Mission Statement

What do these vehicles have to do? The goal of a Mars exploration mission is to send a human crew to the surface of Mars to perform exploration and in-situ science activities. These science activities include gathering samples from a wide search area, processing them on site, and returning selected samples to Earth for further analysis. A typical Mars mission will be approximately two years long (720 days), with one year spent on the surface and two, six-month transit periods [27].

We can translate these broad objectives into specific functional requirements for the space transportation system:

- Transport a human crew of five astronauts to the surface of Mars

Provide life support for $5 \text{ crew} \cdot 720 \text{ days} = 3600 \text{ crew} \cdot \text{days}$

Provide habitable volume for five astronauts

Provide power for two years of operations and for science activities

- Transport science cargo of 10-100 m³ volume and 5-10 mt mass
- Provide propulsion for required delta-V and landed mass
- Provide aerothermal protection during aerocapture and atmospheric entry
- Safely and reliably attenuate the kinetic energy of the lander at touchdown

With this abbreviated list of functional requirements, we can design a space transportation architecture to satisfy the broad mission objectives. The transportation architecture characterizes the number and type of vehicles, their destinations, and the crew usage of each during the mission.

2.1.2 Space Exploration Architectures

With mission-level requirements defined, the MIT-Draper team searched the design space for capable vehicle architectures. Using a tool developed in the Object Process Network (OPN) programming language, 1162 distinct architectures were identified [23]. These were ranked according to metrics such as initial mass in low Earth orbit, cost, risk/safety, and the common sense test. After further analysis, Mars architecture 969 (similar to 1993 NASA Design Reference Mission) and Moon architecture 1 (Lunar Direct Return) were selected for the concept generation design phase.

Mars Architecture 969

Mars architecture 969 is representative of the 1993 NASA Design Reference Mission. The architecture prescribes three vehicles, as shown in Figure 2-1. The Mars Ascent Vehicle (MAV) and Earth Return Vehicle (ERV) are staged on the Martian surface

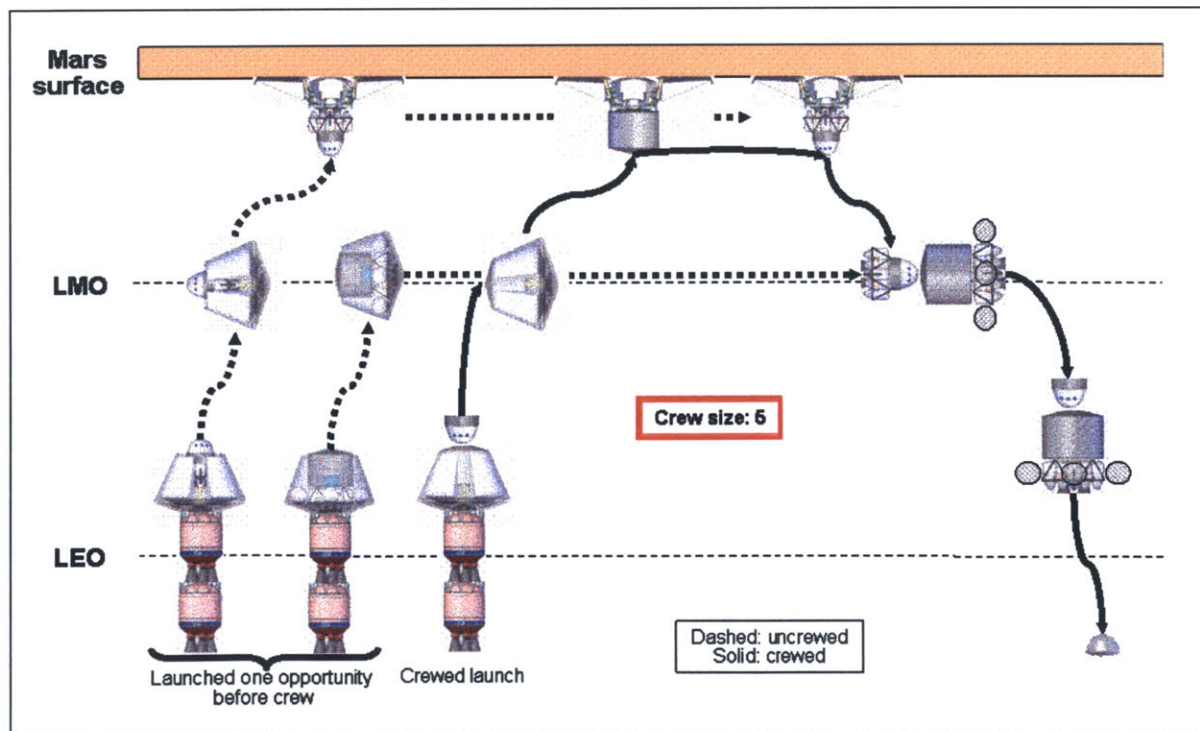


Figure 2-1: Mars Transportation System Architecture 969

and in Mars orbit, respectively. Once they have been positioned and their health verified, the crew is transported from Earth to the Martian surface in the Transfer and Surface Habitat (TSH). The TSH is home base for the astronauts for the duration of their time on Mars. At the conclusion of surface operations, the crew travels to the Mars Ascent Vehicle, ascends and rendezvous with the Earth Return Vehicle, and proceeds back to Earth.

The delta-V requirements, time of flight, and entry velocity for the Mars mission, assuming aerocapture is used, are listed in Figure 2-2.

	Dep. ΔV (km/s)	TOF (days)	Entry Velocity (km/s)
Outbound	3.8 ~ 4.5	180 ~ 270	5.5-7 (@Mars)
Inbound	2.0 ~ 3.0	180 ~ 270	11-14 (@Earth)

Figure 2-2: Trajectory data for the baseline Earth-Mars mission

Moon Architecture 1

The Lunar Direct Return was the first architecture identified by the OPN tool. See Figure 2-3. On a short mission (three to five days), the Lunar Crew Transfer System (LCTS) houses the crew, traveling from Earth to the surface of the Moon and back. In architecture 1, no rendezvous are required. For long-duration missions (60 days or more), the crew operates on the surface from the Lunar Long-Duration Surface Habitat (LLDSH), which is pre-positioned before the crew arrive in the LCTS, just as the MAV is propositioned in Mars architecture 969.

The delta-V requirements, time of flight, and entry velocity for the Lunar mission are listed in Figure 2-4.

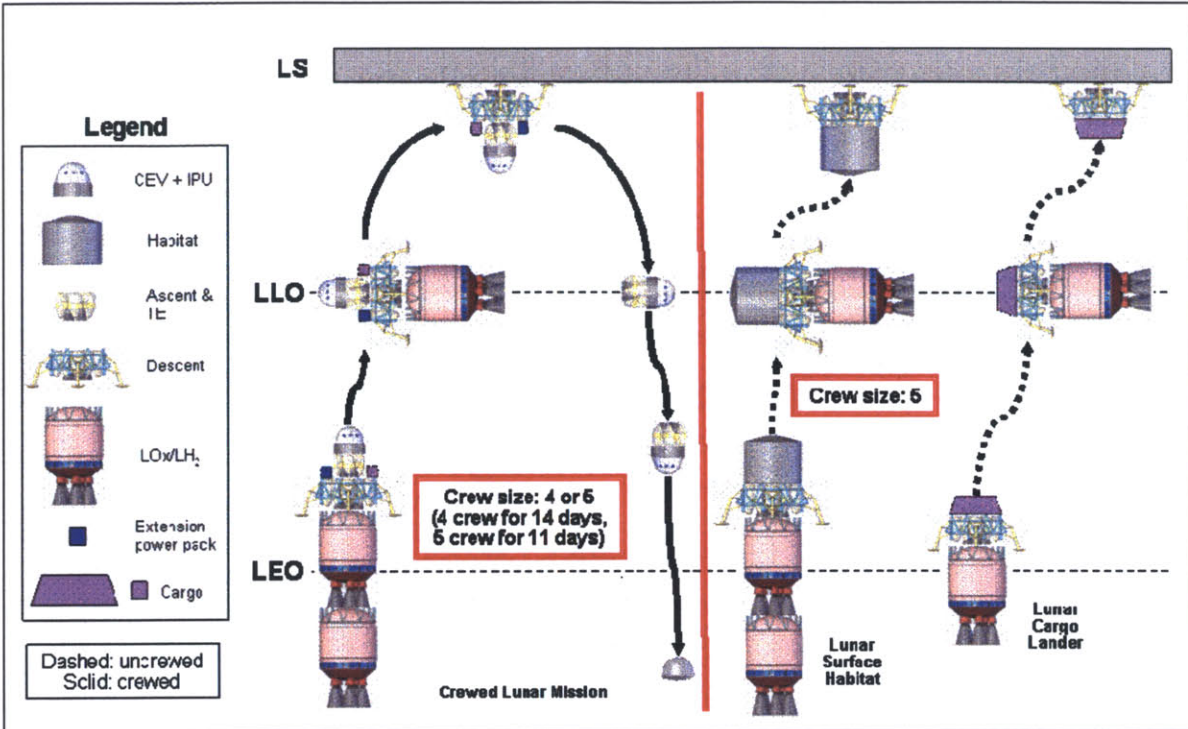


Figure 2-3: Moon Transportation Architecture 1

	Departure ΔV	Time of Flight	Arrival ΔV
LEO to LLO	3.2 km/s	3.5 days	0.9 km/s
LLO to LS (Descending)	2.1 km/s		
LS to LLO (Ascending)	1.9 km/s		
LLO to LEO	0.9 km/s	3.5 days	3.2 km/s

Figure 2-4: Trajectory data for the baseline Earth-Moon mission

2.2 Functional Requirements

Given the number of crew-days, one can estimate the required masses of food-stuffs, water, oxygen, etc. For example, as listed in [16]:

- food solids = $(0.62 \text{ kg/crew-day}) \times (3600 \text{ crew-day}) = 2,232 \text{ kg}$
- water = $(3.52 \text{ kg/crew-day (potable)} + 2.54 \text{ kg/crew-day (nonpotable)}) \times (3600 \text{ crew-day}) = 21,816 \text{ kg}$
- oxygen = $(0.84 \text{ kg/crew-day}) \times (3600 \text{ crew-day}) = 3024 \text{ kg}$

Similar tables exist for power requirements, etc.. Thus, the total landed mass can be calculated given these approximations. Knowing the landed mass and the required delta-V, given above, we may determine the total mass of the vehicles traveling to Mars or to the Moon.

In summary, the five vehicles and their associated masses are listed in Figure 2-5. The Lunar vehicle stacks are assembled in Low Earth Orbit, requiring four heavy lift launches and one crewed launch. The Mars vehicle stacks are also assembled in LEO, requiring nine heavy lift launches and one crewed launch.

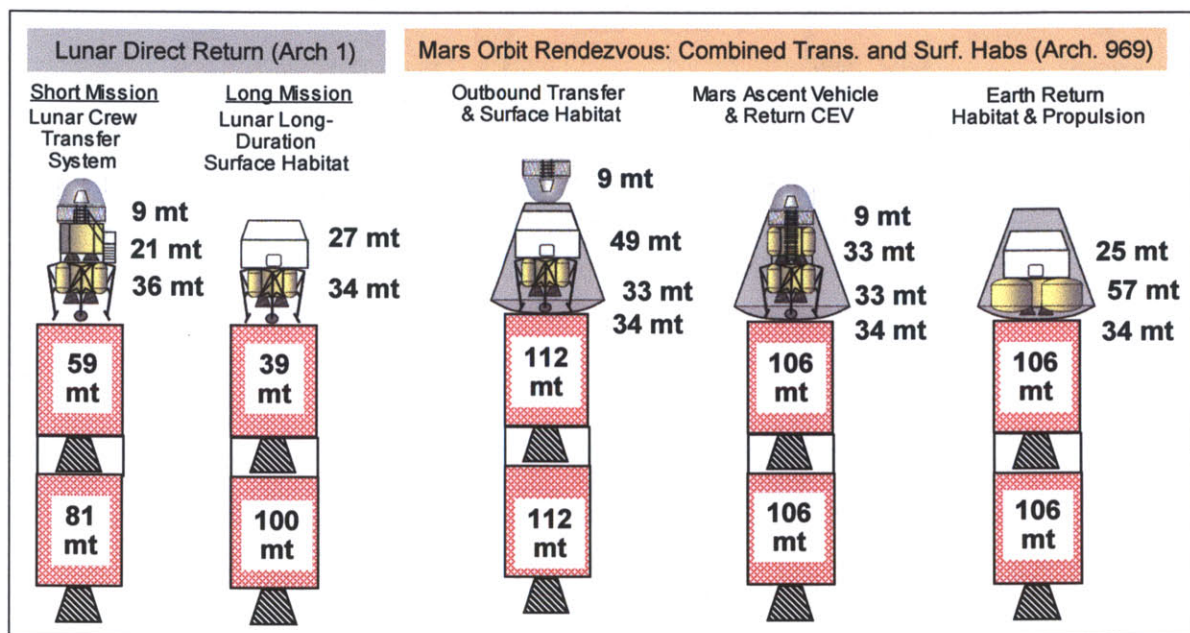


Figure 2-5: Lunar and Mars vehicle stacks. One metric ton equals one thousand kilograms.

Cargo

The cargo manifest for a Mars mission is shown in Figure 2-6. The habitable volume is listed in blue, propulsion in yellow, landing gear in purple, and cargo in green. This cargo must package within the prescribed vehicles, or else dedicated cargo flights must be made, at a high cost penalty.

Transfer and Surface Habitat	Mars Ascent Vehicle	Earth Return Vehicle
Habitat	CEV	Habitat
Descent stage	Descent stage Ascent stage	Trans-Earth Injection propulsion stage
Landing gear	Landing gear	
Cargo: Inflatable laboratory Science equipment Light duty rover (3x)	Cargo: Nuclear power plant Inflatable camper (2x) Heavy duty rover (2x)	Cargo: Trans-Earth Injection propellant

Figure 2-6: Cargo manifest for Mars vehicles.

These cargo elements require 10 - 100 m^3 of volume. Furthermore, the cargo must be packaged such that it can be deployed once the lander has reached the surface.

Nuclear Power

Nuclear power was selected as the surface power source, since dust storms may inhibit the use of solar panels on the surface of Mars. The radiator assembly is an inverted cone, with a height of 3.3 m , diameter of 4.8 m , and mass on the order of 6.5 mt [13]. A schematic of the nuclear reactor is shown in Figure 2-7.

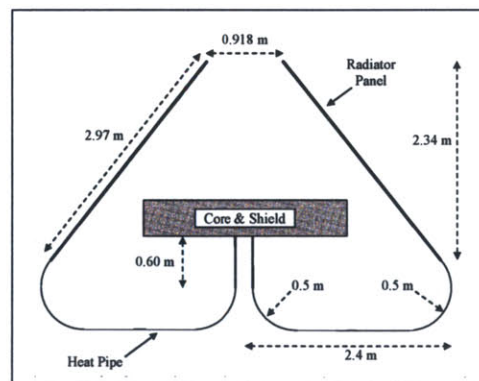


Figure 2-7: Dimensions of the surface nuclear reactor power plant [13].

Habitable Volume

Space systems that operate in micro-gravity generally concern themselves solely with habitable volume. In the case of a surface habitat which operates in both micro-gravity and partial gravity, the floor area and height are also major concerns [15]. The volume and floor area requirements are derived from NASA-STD-3000, based on the 95th percentile American male crewmember (who is approximately 1.93 *m* tall [19]). This person must perform activities such as command and control, science experiments, food preparation and eating, team meetings, exercise, and sleep. By assessing each of these activities for the amount of volume they require, a total pressurized volume of 285 *m*³ is determined for Mars missions. This includes laboratory space, cockpit, mess hall, crew quarters, etc. Although no target floor area requirement was set, an assumption was made that the habitat must be two stories tall in order to provide enough floor area.

2.2.1 Design Drivers

While the vehicle design must satisfy several requirements, four proved to drive the design significantly. They are Moon-Mars hardware commonality, Lunar launch vehicle architecture, Mars AEDL package and aerodynamic stability, and risk.

Moon-Mars Hardware Commonality

In order to create a sustainable exploration enterprise, NASA must strive to minimize hardware development costs. By applying the Mars-back design philosophy (explained in Section 2.3), the Draper-MIT team identified several common hardware elements between the Lunar and Mars transportation systems. While this commonality is essential for the economics of the enterprise, it does come at a cost to the vehicle design. For example, a propulsion stage optimized for Mars missions does not package within a side-mounted launch vehicle which may be used for Lunar missions.

Launch Vehicle Architecture

The ideal Mars exploration vehicle is short and squat; this has high passive-aerodynamic stability, has a low center of gravity for landing stability, and eases crew egress to the surface. The propulsion stage for this vehicle would have a diameter on the order of 10 *m*, too large to package on a side-mounted launch vehicle. If a side-mount, whose maximum fairing diameter would be 8 *m*, is desired for Lunar missions, then the propulsion stage must be tall and narrow, and this has negative performance implications for Mars missions, namely landing stability and aerodynamic stability.

Aerodynamic Stability and CG Location

The tall, narrow launch package of the side-mounted launch vehicle directly opposes the aerodynamic stability and landing stability enjoyed by short, wide vehicles. While landing stability may be mitigated via a large landing gear footprint, the center of gravity location requirement for aerodynamic stability is a design driver. Passive aerodynamic stability of a conic entry capsule requires x/D , the ratio of the distance from the nose to the center of gravity, x , to the heatshield diameter, D , to be less than 0.3 [3]. If $x/D < 0.3$, then the vehicle is passively stable, and mass savings may be realized in the Reaction Control System (RCS). If $x/D > 0.3$, then additional RCS propellant mass must be carried. Additionally, if the RCS system fails on a passively unstable vehicle, there is the risk that the vehicle will lose control.

Risk

Risk is not limited to active events such as aeroentry and landing. There also is operational risk in using restartable engines during long-duration missions. If the engines are damaged during touchdown or otherwise do not re-ignite, then the crew may perish. Here, aeroentry and landing risks are traded with operational risk of restartable engines.

2.3 Design Principles

In order to navigate the numerous physical, functional, and operational requirements driving the design of a complex engineering system, engineers use design principles to help steer their decisions. Four design principles guided the MIT-Draper team's efforts. They are [27]:

- Design for *sustainability*, which incorporates affordability
- A highly *modular* and *accretive* design, that allows for *extensibility* and *evolvability*
- A system that uses *Mars as a reference goal* to validate the Lunar exploration concept. (*Mars-back* design)
- A *holistic view* of the entire extended System of Systems (hardware, information, human, and organization)

2.3.1 Sustainability

The primary organizing principle of the MIT-Draper technical concept is the *sustainability* of the exploration effort. "Sustainability is about meeting today's goals in such a way as to ensure that we can meet tomorrow's goals" [6]. The four pillars of sustainability are: to communicate the value of exploration to the stakeholders, to yield a steady cadence of success in increasingly challenging missions, to understand, mitigate, and communicate the residual risks of exploration, and to design an affordable exploration system. There are several key points to affordability.

NASA must complete the design, production, and operation of several complex engineering systems within a prescribed yearly budget. In order to create an affordable enterprise, the architecture must allow for accretion of assets. Once the core system is designed, the accessories may be designed, and so on. The system must be extensible

to allow for the addition of these new elements with little re-design of the core system. To this effect, systems must be *modular*; they must be plug-and-play. Furthermore, the core system must be designed with Mars as a reference goal, such that hardware for the Mars missions may be added to the system seamlessly. The Mars-referenced design philosophy is called *Mars-back*.

2.3.2 Mars-Back

In order to create an affordable engineering system, engineers must make use of common hardware whenever possible. By designing hardware for the most strenuous use-case, one can reuse common hardware on all missions. In general, the most strenuous use-case is the extended Mars mission. Therefore, by designing with a *Mars-back* philosophy, engineers can create a highly modular, extensible system that may be used originally for human Lunar exploration and then for human Mars exploration.

2.4 Landing Gear System-Level Requirements

As examples of system-level requirements generation, the following two sections are presented. In this section, requirements for the landing gear system are developed from first principles, and in Section 2.4, airlock system requirements are developed from risk mitigation concerns.

The requirements of the landing gear are summarized in Figure 2-8. The Mars-back philosophy states that one should design for the worst-case scenario such that one common system may be used for both Lunar and Mars applications. In general, the Mars case is more strenuous; those functional requirements are highlighted peach. The functional requirements driven by the Lunar case are highlighted lavender. The less strenuous requirements, which are automatically fulfilled, are shaded gray.

LANDING GEAR HIGH-LEVEL FUNCTIONAL REQUIREMENTS	
1 Package within Lunar launch vehicle	Package within Mars entry aeroshell
2 Withstand vibratory loading during Earth launch	Withstand vibratory loading during TMI, Aerocapture, Mars descent, Aeroshell jettison Withstand vibratory loading during TLI, LOI, Lunar descent
3 Withstand aerothermal loading during Mars descent	
4 Deploy during Mars descent	Deploy during Lunar orbit
5 Withstand dust and debris impalement during Lunar landing	Withstand dust and debris impalement during Mars landing
6 Limit touchdown impact g-load	
7 Support touchdown impact g-load	
8 Attenuate kinetic energy at touchdown	
9 Prevent toppling	
10 Locate vehicle within specified ground clearance range	
11 Allow for ascent stage launch (level ascent stage)	
12 Monitor state of landing gear throughout mission	

Figure 2-8: High-level functional requirements of the landing gear.

The primary functions of the landing gear system are to safely and reliably absorb kinetic energy and to prevent toppling during touchdown. The landing gear must be robust to noise factors such as terrain, vehicle horizontal velocity, attitude deviation,

roll velocity, and in the Mars case, wind.

2.4.1 Suspension Design Process

The suspension design process is shown in Figure 2-9. First, the desired kinematic and dynamic responses of the suspension are prescribed in order to produce the desired vehicle dynamics. Locations of *hard points*, points where suspension members connect, are then determined. And finally, suspension members are designed.

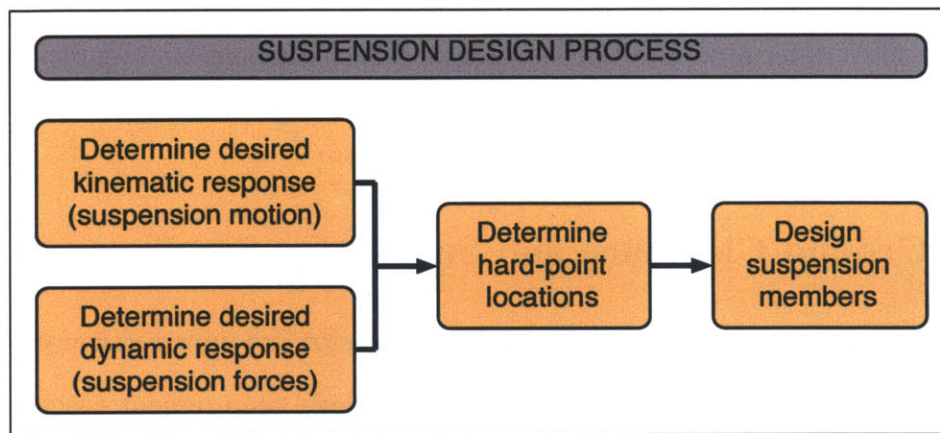


Figure 2-9: Suspension design process.

In the most simple case of the landing spacecraft, the kinematics are pure vertical motion and the dynamics are constant force. The vehicle lands with some initial ground clearance, compresses the suspension with constant force to attenuate the kinetic energy at touchdown, and comes to rest with some final ground clearance. Let us consider this case.

Next, the locations of the suspension hard-points are determined. A hard-point is an imaginary point where suspension forces act (i.e. where suspension-member axes intersect each-other, the suspended body, or the ground). The hard-points are numbered to facilitate discussion of their coordinates. In a simplified two-dimensional case, the suspension has three *external hard-points*: points (2) and (4) on the vehicle body and point (1) on the ground. These points are external, because these are the

locations where external forces act on the suspension. The locations of these points will be determined in the following two sections.

Once the locations of the external hard-points are known, suspension members may be designed. To facilitate this, one may define *internal hard-points* within the suspension. For example, the two-dimensional analogy of the Apollo cantilever system has two internal hard-points: point (3) where the lower control arm intersects the primary strut and point (5) where the upper truss supports the primary strut.

By defining the hard-points and kinematic and dynamic relationships between them, one may determine the forces acting on each suspension member and thus prescribe appropriately sized members.

2.4.2 Ground Clearance and Suspension Stroke

We have assumed that the kinematics of the suspension are pure vertical motion and the dynamics are constant force. The other vehicle-level requirement cascaded to the suspension system is that the final ground clearance after landing must be $c_f = 1.0m$.

The next step in the suspension design process is determining the location of the external hard-points. The simplified two-dimensional suspension has three external hard-points, points (2) and (4) on the vehicle body and point (1) on the ground. The heights of points (2) and (4) off the ground (z_2 and z_4) are determined to give the required initial ground clearance, allowing for *suspension stroke* during touchdown. See Figure 2-10.

The suspension must compress in order to attenuate the kinetic energy at touchdown; this compression is called the stroke. To determine the required suspension stroke, we consider the nominal vertical landing. We have assumed that the suspension provides a constant vertical force during compression. This could be achieved, as in the Apollo design, by using a perfectly-plastic shock-absorption material, such as a crushable honeycomb.

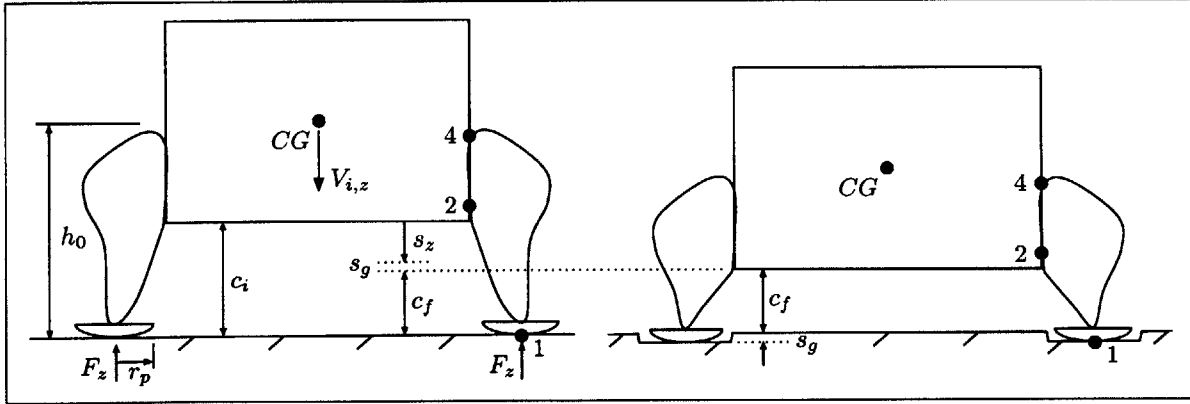


Figure 2-10: Sketch of the lander just prior to and long after touchdown.

If the craft is to decelerate at a constant rate of $a \left[\frac{m}{s^2} \right]$, then the work done on the lander is $W = mas_z$, where m is the landed *sprung mass* and s_z is the vertical suspension *stroke*. This work must attenuate the initial kinetic energy, $KE_i = \frac{1}{2}mV_{i,z}^2$, at touchdown. Solving for the stroke, we have

$$s_z = \frac{V_{i,z}^2}{2a} \quad (2.4.1)$$

Assuming the nominal mission sequence calls for hovering at a specified height, h_v , shutting off the engines, and falling to the surface, then the work done must attenuate the potential energy of the hover height

$$s_z = \frac{gh_v}{a} \quad (2.4.2)$$

where g is the acceleration due to gravity on the Moon (1.62 m/s^2) or on Mars (3.69 m/s^2).

Note that the stroke does not depend on the mass of the vehicle nor the number of legs. However, the ground reaction force acting on each leg does.

$$F_z = \frac{ma}{N} \quad (2.4.3)$$

Clearly, the suspension design is coupled to the impact load and to the touchdown velocity, which is coupled to the hover height, avionics performance, engine-out scenario propulsion-system performance, etc.

The suspension design is also coupled to the footpad size. The ground reaction pressure must be less than the soil bearing strength, or else the legs will pierce the soil like a knife stabbed into a loaf of bread. That is, $\sigma_b > F_z/A_p$, where A_p is the area of each footpad. Assuming the footpads are flat circular discs (they will really be convex) and solving for the radius of the footpad, we have

$$r_p = \sqrt{\frac{ma}{N\pi\sigma_b}} \quad (2.4.4)$$

Thus, these three parameters are coupled: hover height, h_v , touchdown g-load, a , and footpad radius, r_p . The choice of two determines the third. Intuitively, we foresee that we desire to minimize the stroke, since a larger stroke requires a higher initial ground clearance, which makes the craft more prone to toppling and, thus, requires a larger landing gear footprint, thereby increasing the mass of the system.

Finally, the initial ground clearance is

$$c_i = s_z + s_g + c_f \quad (2.4.5)$$

where s_g is the ground sinkage and c_f is the final ground clearance. Despite designing the footpads to float on the surface, let us allot $s_g = 0.1 \text{ m}$. (Recall that the vehicle requirement cascaded to the suspension system is $c_f = 1.0 \text{ m}$.)

A detailed depiction of this design process is best summarized in Figure 2-11. The gray parameters are assumed given, blue are chosen, orange are calculated, and yellow are influenced by the chosen design. In reality, the propulsion requirements may set the hover height (in order to prevent crater formation under the spacecraft). Alternatively, the initial ground clearance may be determined by landing stability

and package requirements, in which case the parameters will be calculated from right to left. In order to help navigate these decisions, this chart shows the relationships between each of the parameters in the system.

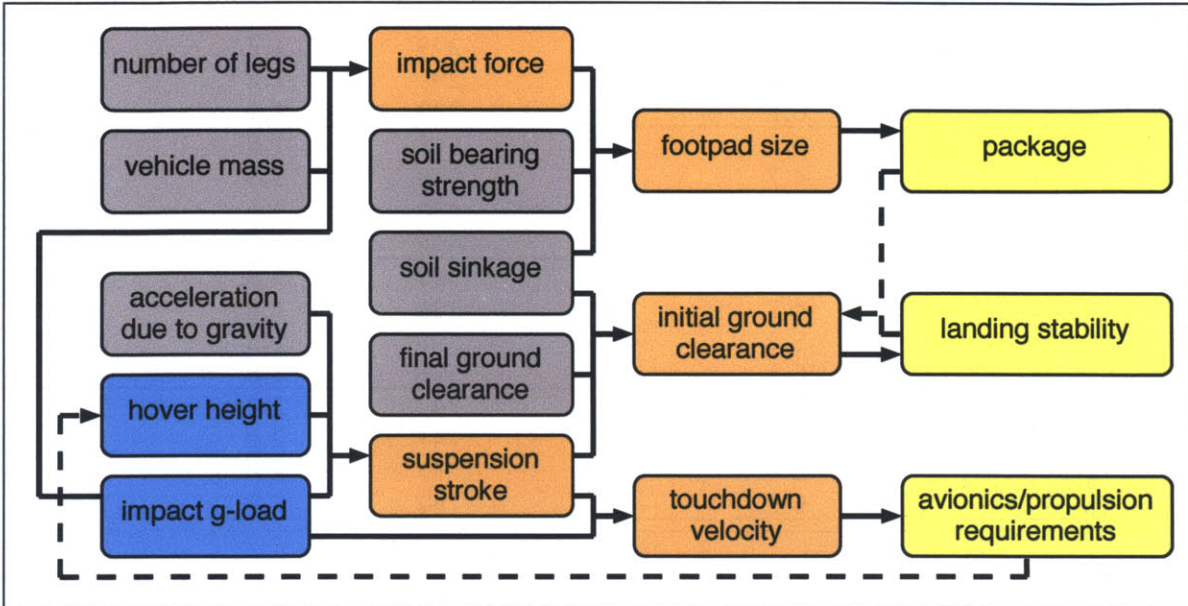


Figure 2-11: Design process for determining several suspension parameters. The gray parameters are assumed given, blue are chosen, orange are calculated, and yellow are performance metrics influenced by the chosen design.

Specifications: Architectures 1 and 969

Figures 2-12 and 2-13 show the calculated touchdown velocity, suspension stroke, impact force, footpad radius, and initial ground clearance, given selected touchdown impact g-loads and hover heights. In order to achieve a balance between small footpad for packaging and a small suspension stroke for landing stability, we choose the highlighted parameters for Mars, namely $a = 2g$ and $h_v = 2m$.

The Mars-back philosophy says that the Moon should be used to validate technology for Mars. It is anticipated that synthetic vision and radar sensors will be used during touchdown on Mars. These sensors must precisely determine the vehicle altitude, and the avionics must keep the vehicle at the prescribed hover height prior

a (g₀)	h_v (m)	V_{i,z} (m/s)	s_z (m)	F_z (kN)	r_p (m)	c_i (m)
-	-	(2.4.1)	(2.4.2)	(2.4.3)	(2.4.4)	(2.4.5)
1	2	3.8	0.8	149	0.9	1.9
1	3	4.7	1.1	149	0.9	2.2
1	4	5.4	1.5	149	0.9	2.6
1	5	6.1	1.9	149	0.9	3.0
2	2	3.8	0.4	299	1.2	1.5
2	3	4.7	0.6	299	1.2	1.7
2	4	5.4	0.8	299	1.2	1.9
2	5	6.1	0.9	299	1.2	2.0
3	2	3.8	0.3	448	1.5	1.4
3	3	4.7	0.4	448	1.5	1.5
3	4	5.4	0.5	448	1.5	1.6
3	5	6.1	0.6	448	1.5	1.7
4	2	3.8	0.2	598	1.8	1.3
4	3	4.7	0.3	598	1.8	1.4
4	4	5.4	0.4	598	1.8	1.5
4	5	6.1	0.5	598	1.8	1.6
5	2	3.8	0.2	747	2.0	1.3
5	3	4.7	0.2	747	2.0	1.3
5	4	5.4	0.3	747	2.0	1.4
5	5	6.1	0.4	747	2.0	1.5

Figure 2-12: Mars: suspension design parameters calculated, given touchdown deceleration and hover height. ($g_0 = 9.8 \text{ m/s}^2$) Assumptions: $N = 4$, $m = 61\text{mt}$ (Mars Ascent Vehicle), $\sigma_b = 61 \text{ MPa}$ (soil bearing strength for "drift material" on Mars [20]).

to engine shut-off. Since the hover height is critical to the operation of the avionics sensors, etc., it is anticipated that the hover height should remain the same for both Moon and Mars missions. Also, the initial ground clearance determines the center of gravity height during touchdown. Since the CG height is the most critical factor in determining landing stability and the landing gear footprint, it would be advantageous to hold the initial ground clearance constant as well. The highlighted row in Figure 2-13 shows the suspension design parameters which will yield the same hover height and initial ground clearance as the Mars case.

If the landing gear members are sized to withstand the load for the most massive of the vehicles, the Mars Ascent Vehicle, then one common suspension system may be used for every vehicle in the architecture. Of course, the energy absorption device

a (g₀)	h_v (m)	V_{i,z} (m/s)	s_z (m)	F_z (kN)	r_p (m)	c_i (m)
-	-	(2.4.1)	(2.4.2)	(2.4.3)	(2.4.4)	(2.4.5)
0.8	2	2.6	0.4	92	0.6	1.5
0.8	3	3.2	0.6	92	0.6	1.7
0.8	4	3.6	0.8	92	0.6	1.9
0.8	5	4.1	1.1	92	0.6	2.2
0.9	2	2.6	0.4	104	0.6	1.5
0.9	3	3.2	0.6	104	0.6	1.7
0.9	4	3.6	0.8	104	0.6	1.9
0.9	5	4.1	0.9	104	0.6	2.0
1	2	2.6	0.3	115	0.7	1.4
1	3	3.2	0.5	115	0.7	1.6
1	4	3.6	0.7	115	0.7	1.8
1	5	4.1	0.8	115	0.7	1.9
1.1	2	2.6	0.3	127	0.7	1.4
1.1	3	3.2	0.5	127	0.7	1.6
1.1	4	3.6	0.6	127	0.7	1.7
1.1	5	4.1	0.8	127	0.7	1.9
1.2	2	2.6	0.3	138	0.7	1.4
1.2	3	3.2	0.4	138	0.7	1.5
1.2	4	3.6	0.6	138	0.7	1.7
1.2	5	4.1	0.7	138	0.7	1.8

Figure 2-13: Moon: suspension design parameters calculated, given touchdown deceleration and hover height. ($g_0 = 9.8 m/s^2$) Assumptions: $N = 4$, $m = 47mt$ (Lunar Crew Transfer System), $\sigma_b = 82 MPa$ (soil bearing strength for the Moon [20]).

must be sized for the loads for each specific vehicle.

In summary, the radial locations of points (2) and (4), r_2 and r_4 , are determined by the vehicle width. The initial ground clearance, c_i , was determined in conjunction with the vertical suspension stroke, s_z , footpad size, r_p , vertical touchdown velocity, $V_{i,z}$, and impact g-load, a . Then, z_2 , z_4 , and the initial CG height, h_0 may be determined by the geometry of the spacecraft, as shown in Figure 2-10. Now we may determine the required radius of the landing gear footprint.

2.4.3 Landing Gear Footprint

The required radius of the landing gear footprint can be determined by a simplified landing stability analysis. The relevant dimensions of the spacecraft are the mass, m , height of the center of gravity, h_0 , radial distance from the CG to the footpad, r_0 , and the moment of inertia, I_{CG} , about an axis passing through the center of gravity and perpendicular to the page (see Figure 2-14). The remaining inputs to the stability analysis are the specifications for the horizontal and vertical touchdown velocities, $V_{i,x}$ and $V_{i,z}$, attitude deviation, ϕ_i (not shown), roll rate, ω_i , and maximum roll during touchdown, ϕ_f (not shown). Given these eight parameters, we seek to determine the radius of the landing gear footprint, r_0 .

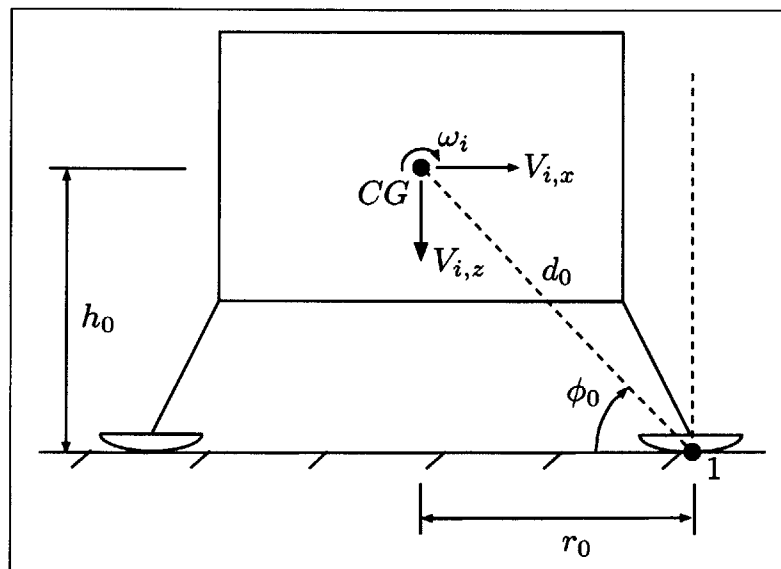


Figure 2-14: Relevant dimensions of the lander

For maximum stability, we seek to maximize the footprint of the landing legs. We trade landing stability with mass and package of the landing legs, as larger legs diminish both of these performance criteria.

Governing Equations

If the craft lands on level ground with the initial horizontal velocity $V_{i,x}$ and strikes a hard object, the craft may topple. This condition is exacerbated if the craft lands with an initial attitude deviation, ϕ_i , and angular velocity, ω_i , in the direction of the obstacle. We seek to determine the radius of the landing leg footprint, r_0 , such that the stability of the landing system is robust to this event. See Figure 4-5.

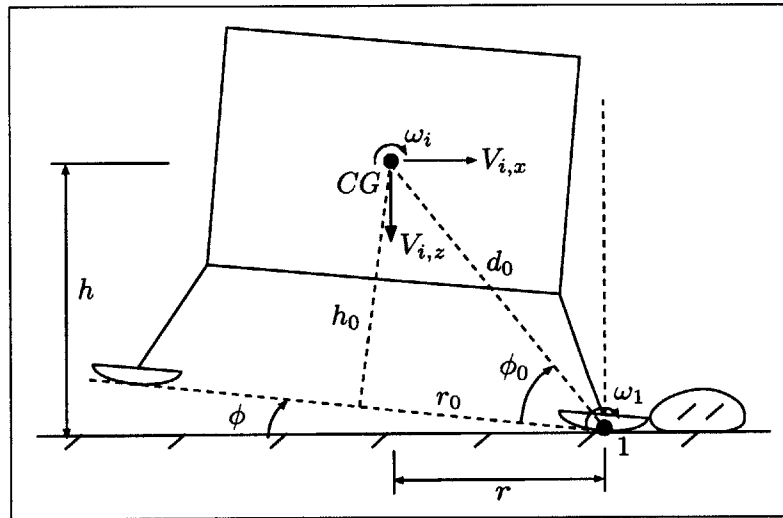


Figure 2-15: Sketch of lander during worst case scenario touchdown.

If the craft rotates about point (1) such that $\phi + \phi_0 > \frac{\pi}{2}$, then it will topple. The rotational kinetic energy at touchdown must be negated by the vehicle Reaction Control System (RCS) thrusters, or in the case of RCS failure, by the work done by gravity alone. Let us consider this case. We have

$$\int_{\phi_i}^{\frac{\pi}{2} - \phi_0} mgr d\phi \geq \frac{1}{2} I_1 \omega_1^2 \quad (2.4.6)$$

where $r = d_0 \cos(\phi + \phi_0)$ is given by the lander geometry.

Thus, we can evaluate the left hand side of (2.4.6)

$$\begin{aligned} \int_{\phi_i}^{\frac{\pi}{2}-\phi_0} mgd_0 \cos(\phi + \phi_0) d\phi &\geq \frac{1}{2} I_1 \omega_1^2 \\ mgd_0(1 - \sin(\phi_i + \phi_0)) &\geq \frac{1}{2} I_1 \omega_1^2 \end{aligned} \quad (2.4.7)$$

Let us assume that the initial attitude deviation, ϕ_i , is small, so

$$\sin(\phi_i + \phi_0) = \sin(\phi_i)\cos(\phi_0) + \cos(\phi_i)\sin(\phi_0) \approx \phi_i \frac{r_0}{d_0} + \frac{h_0}{d_0} \quad (2.4.8)$$

Evaluating terms in (2.4.7), I_1 is given by the Parallel Axis Theorem [2],

$$I_1 = I_{CG} + md_0^2 \quad (2.4.9)$$

and ω_1 is given by the total initial angular momentum about point (1):

$$I_1 \omega_1 = h_i m V_{i,x} - r_i m V_{i,z} + \omega_i I_{CG} \quad (2.4.10)$$

In the worst case for stability, the craft touches down with minimal vertical velocity ($V_{i,z} \approx 0$), and (2.4.10) becomes

$$I_1 \omega_1 \approx h_i m V_{i,x} + \omega_i I_{CG} \quad (2.4.11)$$

Substituting (2.4.8), (2.4.9), and (2.4.11) into (2.4.7) yields an implicit relationship for d_0 (and thus, r_0 , since $d_0 = \sqrt{r_0^2 + h_0^2}$).

$$mgd_0 \left(1 - \phi_i \frac{r_0}{d_0} - \frac{h_0}{d_0} \right) \geq \frac{(h_i m V_{i,x} + \omega_i I_{CG})^2}{2(I_{CG} + md_0^2)} \quad (2.4.12)$$

A factor of safety should be inserted in two places. First, we should restrict the lander to tip less than ϕ_f (as distinct from $\frac{\pi}{2}$), thus changing the 1 on the left hand

side of Equation (2.4.12) to $\sin(\phi_f)$. Second, we should multiply the initial rotational kinetic energy by a factor of safety, S_{KE} . Thus, (2.4.12) becomes

$$mgd_0 \left(\sin(\phi_f) - \phi_i \frac{r_0}{d_0} - \frac{h_0}{d_0} \right) \geq S_{KE} \frac{(h_i m V_{i,x} + \omega_i I_{CG})^2}{2(I_{CG} + m d_0^2)} \quad (2.4.13)$$

Note: True Radius of the Landing Leg Footprint

The radius, r_0 , used for the above landing stability analysis is *not* the true radius of the landing leg footprint. Rather, it is the distance from the center of gravity to the line of action of the ground reaction point, *or points*. In the worst case scenario landing, two legs impinge upon an obstacle simultaneously. See Figure 2-16. In order to design a four-leg system that is robust to this case, the landing leg footprint must be $\sqrt{2}$ times the radius determined above.

$$r_1 = \sqrt{2}r_0 \quad (2.4.14)$$

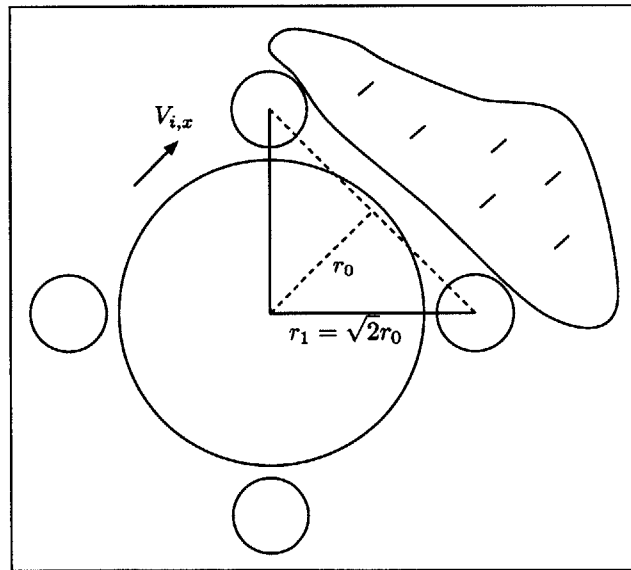


Figure 2-16: Plan view of the lander

Example: Apollo Lunar Module

In order to use Equations (2.4.13) and (2.4.14) to calculate r_1 for a particular spacecraft, one must know m , h_0 , and I_{CG} , specify the allowable $V_{i,x}$, ϕ_i , and ω_i , and choose ϕ_f and S_{KE} . The Apollo Lunar Module was designed for two landing cases. In case one: $V_{i,x} = 1.2 \text{ m/s}$, $\phi_i = 0 \text{ deg}$, and $\omega_i = 0 \text{ deg/s}$, and in case two: $V_{i,x} = 0 \text{ m/s}$, $\phi_i = 6 \text{ deg}$, and $\omega_i = 2 \text{ deg/s}$. The other parameters were:

$$\begin{aligned} m &= 6,600 && [kg] \\ h_0 &= 4, \text{ estimated} && [m] \\ I_{CG} &= 25,000, \text{ estimated} && [kg \cdot m^2] \end{aligned}$$

where I_{CG} and h_0 were estimated as follows. Model the Ascent Stage as a solid sphere; model the Descent Stage as a solid cylinder; and ignore the legs. See Figure 2-17 and note that some dimensions were estimated.

$$\begin{aligned} I_{CG} &= (I_{AS} + m_{AS}d_{AS}^2) + (I_{DS} + m_{DS}d_{DS}^2) \\ &= \frac{2}{5}m_{AS}r_{AS}^2 + m_{AS}d_{AS}^2 + \frac{1}{12}m_{DS}(3r_{DS}^2 + h_{DS}^2) + m_{DS}d_{DS}^2 \\ &= 22,800 \text{ kg} \cdot \text{m}^2 \end{aligned}$$

If one uses a hollow sphere, then one calculates $I_{CG} = 27,700 \text{ kg} \cdot \text{m}^2$. Thus, an approximate value of $I_{CG} = 25,000 \text{ kg} \cdot \text{m}^2$ is representative.

With the above values and factors of safety of $\phi_f = 60 \text{ deg}$ and $S_{KE} = 2$, Equation (2.4.14) prescribes $r_1 = 4.8 \text{ m}$ for case one and $r_1 = 4.2 \text{ m}$ for case two. The actual Apollo landing gear footprint had a radius of $r_1 = 4.45 \text{ m}$. Thus, the above model is consistent with the design of the Apollo system.

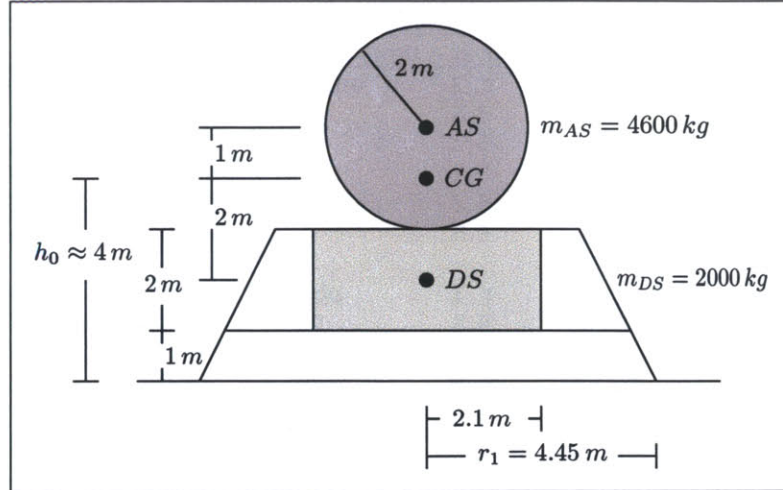


Figure 2-17: Sketch of the Apollo LM

Sensitivity Analysis of Landing Gear Footprint Radius Equation

The preceding landing stability analysis yielded the following equations which may be used to determine the necessary radius of the landing gear footprint

$$mgd_0 \left(\sin(\phi_f) - \phi_i \frac{r_0}{d_0} - \frac{h_0}{d_0} \right) \geq S_{KE} \frac{(h_i m V_{i,x} + \omega_i I_{CG})^2}{2(I_{CG} + m d_0^2)} \quad (2.4.13)$$

$$r_1 = \sqrt{2} r_0 \quad (2.4.14)$$

The radius is determined, given m , h_0 , and I_{CG} , by specifying the allowable $V_{i,x}$, ϕ_i , and ω_i , and by choosing ϕ_f and S_{KE} . Since the result depends on these eight parameters, it is useful to understand how the result is influenced by each. In Figure 2-18, the values for the landing gear footprint radius, r_1 , are given while varying one parameter at a time. The values for the Apollo baseline Case One and baseline Case Two are highlighted and in bold.

Similarly, in Figure 2-19, the values for the landing gear footprint radius, r_1 , are given while varying one parameter at a time. A first approximation for the values for the Architecture 969 Transfer and Surface Habitat baseline Case One and baseline Case Two are highlighted and in bold.

Sensitivity Analysis, Apollo Case One							
(varying one parameter at a time, baseline highlighted in bold)							
V ix	r 1	phi i	r 1	omega i	r 1	m	r 1
0	0	0	4.8	0	4.8	2600	4.6
0.6	3.7	3	5.2	1	4.8	4600	4.7
1.2	4.8	6	5.7	2	4.8	6600	4.8
1.8	6.0	9	6.2	3	4.9	8600	4.8
2.4	7.1	12	6.8	4	4.9	10600	4.8
h 0	r 1	I cg	r 1	phi f	r 1	S KE	r 1
0	3.8	15000	4.8	90	3.3	1	4.1
2	4.3	20000	4.8	80	3.5	1.5	4.5
4	4.8	25000	4.8	70	4.0	2	4.8
6	5.3	30000	4.8	60	4.8	2.5	5.1
8	5.7	35000	4.7	50	6.0	3	5.3

Sensitivity Analysis, Apollo Case Two							
(varying one parameter at a time, baseline highlighted in bold)							
V ix	r 1	phi i	r 1	omega i	r 1	m	r 1
0	4.2	0	3.3	0	0	2600	4.2
0.6	4.7	3	3.7	1	4.2	4600	4.2
1.2	5.7	6	4.2	2	4.2	6600	4.2
1.8	6.9	9	4.8	3	4.2	8600	4.2
2.4	8.1	12	5.4	4	4.2	10600	4.2
h 0	r 1	I cg	r 1	phi f	r 1	S KE	r 1
3	3.1	15000	4.2	90	1.2	1	4.2
3.5	3.7	20000	4.2	80	1.8	1.5	4.2
4	4.2	25000	4.2	70	2.9	2	4.2
4.5	4.7	30000	4.2	60	4.2	2.5	4.2
5	5.2	35000	4.2	50	5.9	3	4.2

Figure 2-18: Landing gear radius sensitivity to one-parameter variations.

This analysis reveals that the radius is very sensitive to $V_{i,x}$, ϕ_f , and S_{KE} , is moderately sensitive to h_0 and ϕ_i , and is less sensitive to m , I_{CG} , and ω_i . Also note that a very useful rule of thumb is that the suspension radius should be approximately equal to the center of gravity height.

2.4.4 Summary of Landing Gear Requirements

In summary, the suspension design process is shown in Figure ???. First, r_2 and r_4 are determined by the vehicle width. Then, the vertical suspension stroke, s_z , is determined in conjunction with the footpad size, r_p , vertical touchdown velocity, $V_{i,z}$,

Sensitivity Analysis, 969 TSH Case One							
(varying one parameter at a time, baseline highlighted in bold)							
<u>V_{ix}</u>	<u>r₁</u>	<u>phi_i</u>	<u>r₁</u>	<u>omega_i</u>	<u>r₁</u>	<u>m</u>	<u>r₁</u>
0	0	0	6.0	0	6.0	38500	5.9
0.6	5.4	3	6.7	1	6	48500	6.0
1.2	6.0	6	7.4	2	6.1	58500	6.0
1.8	6.8	9	8.3	3	6.1	68500	6.0
2.4	7.8	12	9.4	4	6.1	78500	6.0
<u>h₀</u>	<u>r₁</u>	<u>I_{cg}</u>	<u>r₁</u>	<u>phi_f</u>	<u>r₁</u>	<u>S_{KE}</u>	<u>r₁</u>
4.35	4.2	463000	6.0	90	2.8	1	5.6
5.35	5.1	513000	6.0	80	3.3	1.5	5.8
6.35	6.0	563000	6.0	70	4.4	2	6.0
7.35	6.9	613000	6.0	60	6.0	2.5	6.2
8.35	7.7	663000	6.0	50	8.2	3	6.4

Sensitivity Analysis, 969 TSH Case Two							
(varying one parameter at a time, baseline highlighted in bold)							
<u>V_{ix}</u>	<u>r₁</u>	<u>phi_i</u>	<u>r₁</u>	<u>omega_i</u>	<u>r₁</u>	<u>m</u>	<u>r₁</u>
0	6.6	0	5.2	0	0	38500	6.7
0.6	6.9	3	5.9	1	6.6	48500	6.7
1.2	7.5	6	6.6	2	6.6	58500	6.6
1.8	8.3	9	7.6	3	6.7	68500	6.6
2.4	9.2	12	8.6	4	6.7	78500	6.6
<u>h₀</u>	<u>r₁</u>	<u>I_{cg}</u>	<u>r₁</u>	<u>phi_f</u>	<u>r₁</u>	<u>S_{KE}</u>	<u>r₁</u>
4.35	4.6	463000	6.6	90	1.9	1	6.6
5.35	5.6	513000	6.6	80	2.9	1.5	6.6
6.35	6.6	563000	6.6	70	4.5	2	6.6
7.35	7.7	613000	6.7	60	6.6	2.5	6.7
8.35	8.7	663000	6.7	50	9.4	3	6.7

Figure 2-19: Landing gear radius sensitivity to one-parameter variations.

and impact g-load, a , according to Equations (2.4.1), (2.4.3), and (2.4.4). The ground clearance is determined according to Equation (2.4.5). Then, z_2 , z_4 , and the initial CG height, h_0 are determined by the geometry of the spacecraft.

The suspension radius, r_1 , is determined using Equations (2.4.13) and (2.4.14) given m , h_0 , and I_{CG} , by specifying the allowable $V_{i,x}$, ϕ_i , and ω_i , and by choosing $\phi_f = 60 \text{ deg}$ and $S_{KE} = 2$. The radius is chosen as the larger value determined using the two cases: $V_{i,x} = 1.2 \text{ m/s}$, $\phi_i = 0 \text{ deg}$, and $\omega_i = 0 \text{ deg/s}$ in case one, and $V_{i,x} = 0 \text{ m/s}$, $\phi_i = 6 \text{ deg}$, and $\omega_i = 2 \text{ deg/s}$ in case two.

2.5 Airlock System-Level Requirements

As a second example of system-level requirements generation, the following is presented. In this section, requirements for an airlock system are motivated primarily as a countermeasure to two significant mission risks: dust intrusion; and crew injury/illness. By employing a first-order analysis, we understand the feasibility of using an airlock, as well as the magnitude of the impact this has on the vehicle design as a whole.

During a short (4-6 day) Lunar mission, an airlock is not necessitated from mass concerns. In fact, it is more massive to carry an airlock than to exhaust all of the air out of the cabin prior to each EVA and repressurize upon return, as was done in the Apollo Lunar Module [18]. For this analysis, we make the following assumptions, in accordance with references [18],[25],[22], [24]:

- The minimum size airlock possible is a one-person cylinder of diameter, $d = 1.2m$, and length, $l = 2m$.
- The airlock may be constructed of an inflatable fabric of mass per unit surface area, $\rho_s = 5kg/m^2$.
- The airlock is pressurized with

$$\text{Oxygen: } R_g = 8.314 \frac{J}{mol \cdot K} / 0.016 \frac{kg}{mol} = 519.6 \frac{J}{kg \cdot K} \text{ at}$$

$$\text{Gauge pressure: } p_g = 33kPa \text{ and}$$

$$\text{Temperature: } T = 290K.$$

- The air leakage rate is less than $5 \times 10^{-3}kg/day$.
- The mass of each hatch is 20 kg. One hatch is an integrated part the vehicle and is not counted towards the airlock mass.

We find that the mass of the minimum possible sized airlock is approximately 60 kg by adding the mass of the walls, hatches, and air. The mass of the walls is:

$$m_{wall} = \rho_s * SA \quad (2.5.1)$$

Where SA is the surface area of the walls. For our cylinder, we have:

$$m_{wall} = \rho_s * \pi * d * l = 5kg/m^2 * \pi * 1.2m * 2m = 38kg.$$

By employing the Ideal Gas Law

$$pV = mR_gT \quad (2.5.2)$$

we may determine the mass of Oxygen required for the airlock:

$$m_{O_2} = \frac{pV}{R_gT} = \frac{33,000Pa * \frac{\pi * (1.2m)^2}{4} * 2m}{519.6 \frac{J}{kg \cdot K} * 290K} = 0.5kg$$

Assuming the vehicle life support system may be used to pressurize the airlock, then pump mass may be neglected, and the total mass of the airlock is, at minimum, $20kg + 38kg + 0.5kg \approx 60kg$.

If the lander does not have an airlock, the entire cabin must be evacuated into an air storage tank or simply depressurized by exhausting into space. Assuming here that:

- The Crew Exploration Vehicle habitable volume is $30m^3$.
- The mission duration is 6 days.
- There is 1 ExtraVehicular Activity (EVA) per day.

The mass lost by venting all of the air out of the vehicle prior to each EVA is:

$$m_{vent} = \frac{33,000 Pa * 30 \frac{m^3}{EVA} * 1 \frac{EVA}{day} * 6 day}{519.6 \frac{J}{kg \cdot K} * 290 K} = 39 kg$$

Thus, even without recycling air, the airlock is the more massive of the two options. So, if not for mass savings, then why carry an airlock?

The airlock serves as a countermeasure to two significant mission risks: Lunar dust intrusion and crew injury/illness. Lunar dust is a fine, yet highly abrasive powder. Apollo astronauts reported that Lunar dust contamination posed a significant issue with the proper functioning of EVA suits and surface assets and that every precaution should be taken to mitigate Lunar dust intrusion into the main habitat. An airlock or simply a separate pressurized volume from the main habitat may be used for EVA suit donning, thus keeping the cabin free from the bulk of the Lunar dust.

Problem	Time Period	Comments	Mitigation or Solution	End State
Dust	Constant	Solution must meet SMAC limits and hardware design specs.	Airlock	Majority of dust is controlled
			Separate volume (without airlock capabilities)	
			Dust removal method prior to ingress	
Crewmember illness or injury	Prior to donning suit	Needs a solution: too ill/injured to don suit, but not ill/injured enough to merit a return to Earth.	Airlock - crewmember remains inside crew cabin	Ill/injured crewmember refrains from EVA. No LOM.
			Internal pressurized volume houses affected crewmember	Mission continuance depends on status of ill/injured crewmember.
	During EVA	Crewmember needs to return to Lander and doff suit.	Cease all EVAs until illness/injury subsides	Mission continuance depends on status of ill/injured crewmember.
			Airlock - crewmember ingresses Lander	Other crewmembers' activities are unaffected. No LOM.
Suit Malfunction	Prior to initiation of Lunar Descent	Assume problem is too big to fix with available tools/parts.	Crewmember ingresses internal pressurized volume	All crewmembers return to Lander together. Mission continuance depends on status of affected crewmember.
			Operationally constrain EVA traverse distances and distances between EVA teams	All crew, except affected crewmember, performs EVA. No LOM.
			Airlock - crewmember remains inside crew cabin	Return to Earth
		Assume problem can be fixed with available tools/parts.	Affected crewmember uses Launch/Ascent suit	All crew performs EVA (affected crewmember joins when ready). No LOM.
			Mission is scrubbed	All EVA scrubbed until suit is fixed. No LOM.
			Airlock - crewmember remains inside crew cabin to fix suit	
Internal pressurized volume houses affected crewmember while fixing suit				
Scrub EVA until suit is fixed.				

Figure 2-20: Vehicle-level risks and countermeasures necessitating an airlock [25].

The second main advantage that the airlock provides is that not all crew members must don EVA suits when any wants to egress the vehicle. The level-zero functional requirement of an airlock is to allow for passage between a pressurized cabin and an unpressurized surroundings without changing cabin pressure. This allows crew to remain in the cabin in their coveralls while some members perform an EVA. This feature is especially needed when a crew member is too sick or injured to don an EVA suit, but not enough so to warrant a full mission abort. In terms of the hazard contingency analysis, the airlock allows the crew to continue the mission in an impaired state (e.g. without the ill/injured crew member). A summary of these two mission risks and countermeasures is listed in Figure 2-20.

We have now discussed the need for the airlock and two of its functional requirements. The remaining requirements and their associated design implications for the airlock are summarized in Figure 2-21. Identifying design implications helps bridge the gap between the requirements function-space and the concepts form-space.

Functional Requirement	Design Implication
Allow change in pressure without changing cabin pressure	Airlock
Mitigate dust intrusion	Don spacesuits outside spacecraft cabin Dust removal prior to ingress
Have a mass less than 150 kg for ascent	Lightweight airlock Jettison airlock before ascent Use a jetway (permanant surface-based airlock)
Provide ground-level egress (Required)	Pressurized volume extends to ground level, and airlock at ground level
Provide ground-level egress (Not Required)	Airlock at vehicle level, and exterior stairs or ramp
Cabin pressurized during ascent	Must have cabin hatch
Deploy tools, science equipment, etc., and return surface material samples	Desire large-volume airlock Desire no tight corners in gerbil tunnels

Figure 2-21: Airlock functional requirements and design implications.

[THIS PAGE INTENTIONALLY LEFT BLANK]

Chapter 3

Concepts

The landing vehicle is made up of four basic systems. They are the:

- Aeroshell (the heat shield and afterbody)
- Yellow Stage (the propulsion system)
- Habitat (which includes the cargo)
- Landing Gear (the suspension)

In this chapter, we explore and evaluate concepts for each of these systems, and we generate four whole-vehicle concepts for analysis in Chapter 4.

3.1 Design Space

In this section, the design space for the Mars aeroentry vehicle is explored, with attention to its relationship with the Earth launch vehicle. The dimensions given are based on the delta-V and mass assumptions consistent with the Draper-MIT NASA CE&R study. Unrealistic, or infeasible options are not listed. Due to physical packaging constraints, some of the architectural options are not available in combination with certain others.

3.1.1 Launch Vehicle Design Space

NASA Level 0 Requirements dictate that the crew shall be launched separately from cargo. Thus, the CEV will be launched on a single-stick launch vehicle, and the remaining design task concerns the Heavy Lift Launch Vehicle (HLLV) used to launch the other vehicles in the transportation architecture. The design space for the HLLV is shown in Figure 3-1. The drawings depict Shuttle-derived vehicles, but this is not integral to the architecture. The launch vehicle architecture is defined by the location of the payload, as this impacts the fairing diameter and thus, the payload package. Two orientations exist: in-line and side-mounted, and this gives rise to three realistic launch scenarios.

First, an in-line launch vehicle may be used for the Moon and extended for Mars. This requires moderate up-front monetary investment and development time and may require use of the Shuttle to complete construction of the International Space Station. However, this option is attractive because once the launch vehicle has been developed and flight tested for the Moon, few modifications must be made for Mars. This option affords the most flexibility in the package of the Mars aeroentry vehicle and affords the ability for the most possible hardware commonality.

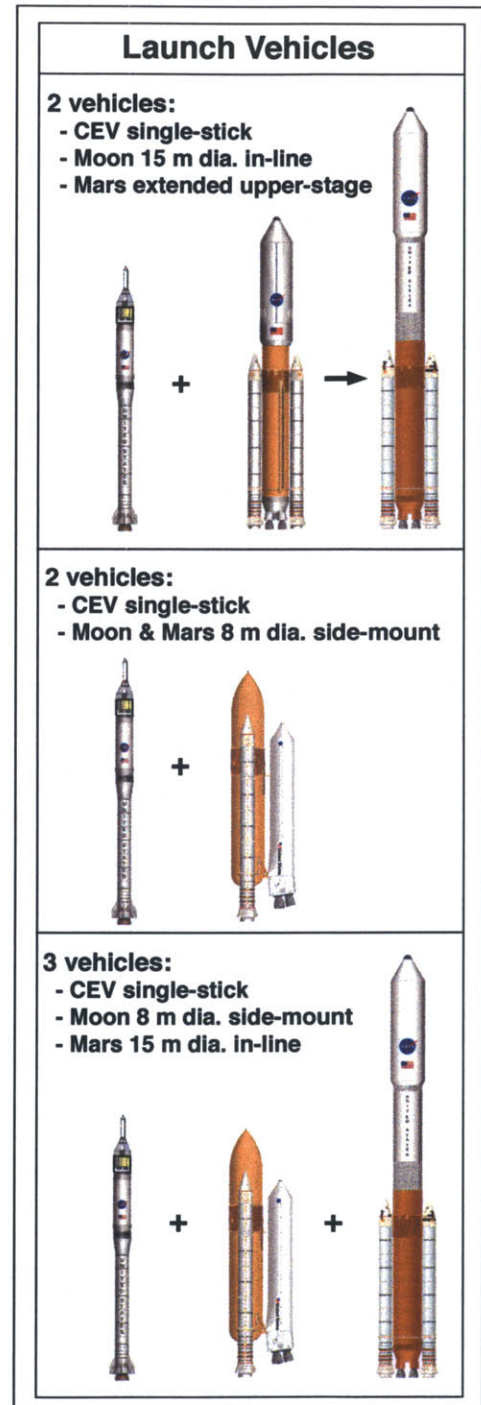


Figure 3-1: Launch vehicle design space.

Second, a side-mounted launch vehicle may be used for missions to both the Moon and Mars. This requires that the Mars aeroentry vehicle be an 8 m-diameter biconic shape, since it is not possible to package the entry vehicle within an 8 m-diameter conic aeroshell. Also, this option poses the operational risk of the foam striking the payload, as is the case with the current Shuttle launch system. Precautions will need to be made in order to ensure the safety of this system. However, this option does offer the least up-front and least downstream launch vehicle investment.

Third, a side-mounted launch vehicle may be used for ISS assembly and Lunar exploration, and then an in-line used for Mars. This option is attractive, because it requires little up-front development time and cost for the Lunar launch vehicle. However, the addition of the third launch vehicle development program may prove prohibitively costly, and there is increased risk in developing and operating two distinct HLLV systems.

3.1.2 Aeroshell Design Space

The design space for the aeroshell is shown in Figure 3-2. Four basic shapes exist. The Apollo and Soyuz entry vehicles are examples of the *conic* capsule design. The *heat shield and afterbody* (HSA) design is similar, except that the payload does not extend to the edge of the heat shield; there is no continuous aeroshell. The *biconic* design employs a conical section which tapers into a point via a sharper-angled conical section. This vehicle typically flies nose-first, as opposed to the conic and HSA, which fly blunt-end first. Finally, the Space Shuttle is an example of a *lifting body*; it is a streamlined vehicle with a high lift to drag ratio (L/D). This ratio, along with the ballistic coefficient ($C_b = m/C_dA$), determines the vehicle's crossrange, which is necessary for choosing landing locations after descent has begun. Let us reduce these options by two.

The Lifting Body architecture is attractive when a high lift to drag ratio is required. The MIT-Draper concept assumes that all vehicles will aerocapture into Mars orbit. The vehicle may then choose when and where to begin its descent. Consequently, extended crossrange maneuvers are not required, and the vehicle may have $0.1 < L/D < 0.3$. This can be achieved without the lifting body [3].

The Heat Shield & Afterbody is attractive when backshell heating is an issue. This geometry sacrifices package space to reduce heating; for a given heatshield diameter, the volume of usable space is less than that for a conic.

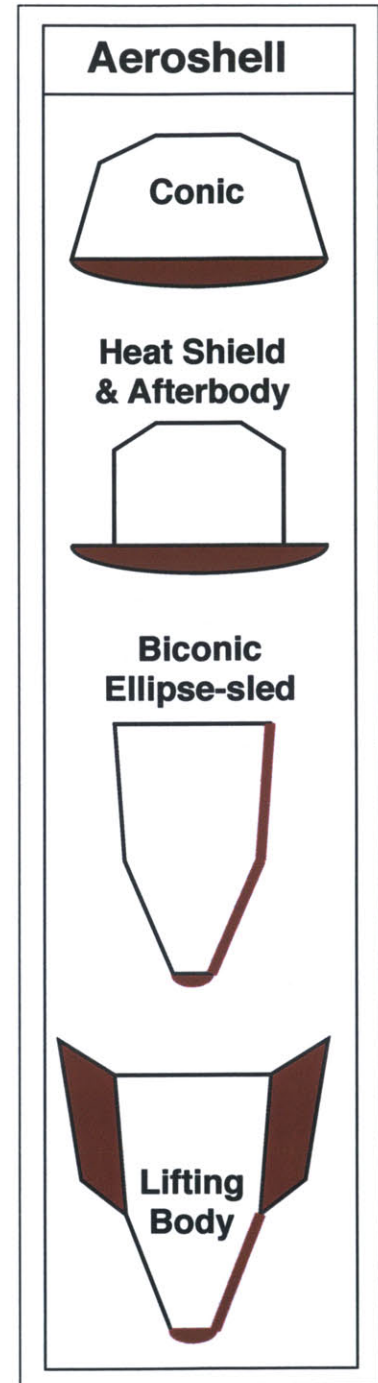


Figure 3-2: Aeroshell design space.

Preliminary analysis in Figure 3-3 shows that backshell heating is not significant in the operating region of the conic aeroshell. Therefore, the HSA may be eliminated.

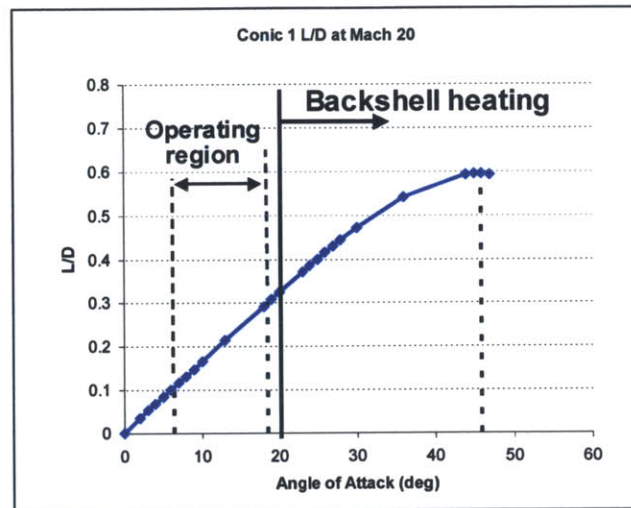


Figure 3-3: Backshell heating for the conic aeroshell, from [3].

The conic and biconic architectures are both feasible. However, the conic is the preferred shape for several reasons. For a given vehicle diameter and a given entry trajectory, the conic shape offers:

- Higher drag (less propellant required for propulsive descent)
- Lower heating rate (lower mass heatshield)
- Smaller TPS area (lower mass heatshield)
- Easier to package the center of gravity location
- Simpler heat-shield-ejection/engine-starting maneuver
- Flight heritage

Thus, the conic shape was chosen for the Draper-MIT baseline design. The baseline aeroshell is a 15-meter diameter capsule with a 70-degree sphere-cone forebody. This shape, similar to Viking and subsequent robotic landers, can fly at $L/D = 0.3$.

3.1.3 Yellow Stage and Habitat Design Space

The remaining vehicle elements are the descent/ascent propulsion stage (Yellow Stage), habitat, and cargo. Since the cargo package is coupled to its deployment, the means by which the cargo is deployed to the surface after landing must be accounted for up front in the design process. All of these elements must package within the aeroshell (and launch vehicle), and thus a holistic view of the design space must be taken. The design space for the aeroshell, Yellow Stage, habitat, cargo, and cargo deployment system is shown in Figure 3-4.




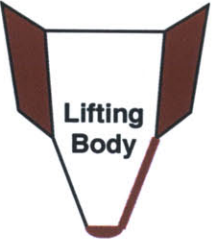
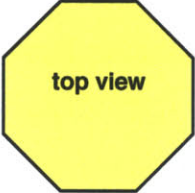
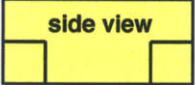


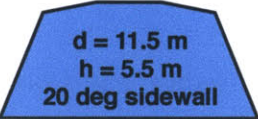
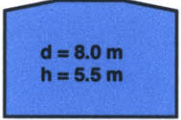




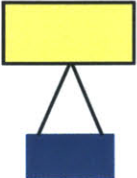
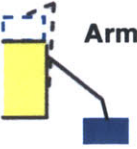

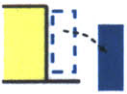
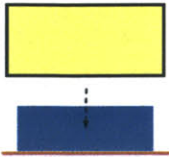
Aeroshell	Yellow Stage	Habitat	Cargo	Cargo Deploy
 <p>Conic</p> <p>Heat Shield & Afterbody</p>  <p>Biconic Ellipse-sled</p>  <p>Lifting Body</p> 	<p>1.5-stage octagonal prism</p>  <p>top view</p>  <p>side view</p> <p>d = 10 m h = 4.0 m</p> <p>2-stage square prism</p>  <p>top view</p>  <p>side view</p> <p>d = 7.5m h = 4.5m</p>	<p>Igloo</p>  <p>d = 11.5 m h = 5.5 m 20 deg sidewall</p> <p>Cylinder</p>  <p>d = 8.0 m h = 5.5 m</p> <p>Cylinder</p>  <p>d = 7.5 m h = 6.5 m</p>	<p>Top-mounted</p>  <p>Side-mounted</p>  <p>Underslung</p>  <p>Tethered</p> 	<p>Arm</p>  <p>Hinge</p>  <p>Manual (Apollo)</p>  <p>Release</p>  <p>(other)</p>

Figure 3-4: Aeroentry vehicle systems design space.

There are two architectures for the Yellow Stage. Namely, it may be a 1.5-stage core-ring design, with restartable descent/ascent engines and ascent propellant tanks mounted onto a core structure, and descent propellant tanks mounted in a surrounding ring. Alternatively, it may be a 2-stage design with separate engines and tanks for descent and ascent. Additionally, the Yellow Stage may be designed such that it does or does not package within the 8 *m*-diameter biconic aeroshell and side-mounted launch vehicle. Let us assume that it must be 7.5 *m* in diameter to package within the 8 *m* aeroshell. This yields a total of four Yellow Stage architectures. Note, only the two realistic options are shown in Figure 3-4. The 1.5-stage core-ring design is an octagonal prism inscribed within a 10 *m*-diameter circle with a height of 4 *m*. The 2-stage is a square prism inscribed within a 7.5 *m*-diameter circle, with each stage measuring 4.5 *m* high.

In order to minimize the structural mass of the habitat, a cylindrical pressure vessel is used. This should be vertically oriented in order to maximize its volume within the conic aeroshell and to maximize floor space of the habitat during surface operations. One notes that this cylindrical geometry does not use the volume between the vertical sidewall of the habitat and the tapered sidewall of the aeroshell. Alternatively, this volume (and associated floor area) may be recovered by use of an igloo-shaped habitat, at the expense of structural mass.

There are essentially four options for the cargo package: top-mounted, side-mounted, underslung, and tethered. Top- and side-mounted cargo may be used with the clustered engine package presupposed in the above Yellow Stage concepts. While underslung cargo may be more easily deployed, it requires outboard-mounted engines, which are deemed infeasible due to the increased risk of crashing in an engine-out scenario. The side-mounted cargo configuration was selected for detailed design. It offers the advantage of straightforward cargo deployment (via a hinge) while still allowing for clustered engines.

3.2 Landing Gear Concepts

The landing gear architecture does not drastically impact the packaging of the aeroentry vehicle. The salient feature is the size of the landing gear footprint, as a larger footprint requires longer legs and thus a more challenging package. The radius of the landing gear footprint is roughly equal to the height of the center of gravity at touchdown, as is shown in Figure 4-6.

There are, however, several landing gear architecture options. The Apollo Lunar Module employed a *cantilever* leg design. See Figure 3-5. The primary strut was supported by a lower control arm and an upper truss.

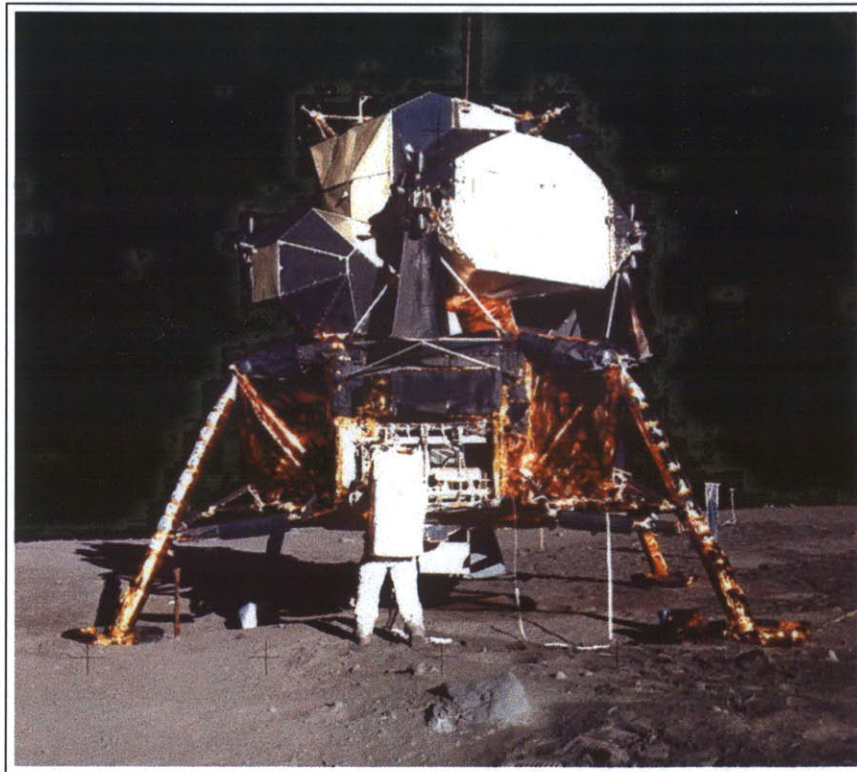


Figure 3-5: Apollo Lunar Module

The Surveyor spacecraft used a *radial* leg design. See Figure 3-6. The footpad was located by one upper member and two lower members which all attached to the pad itself.

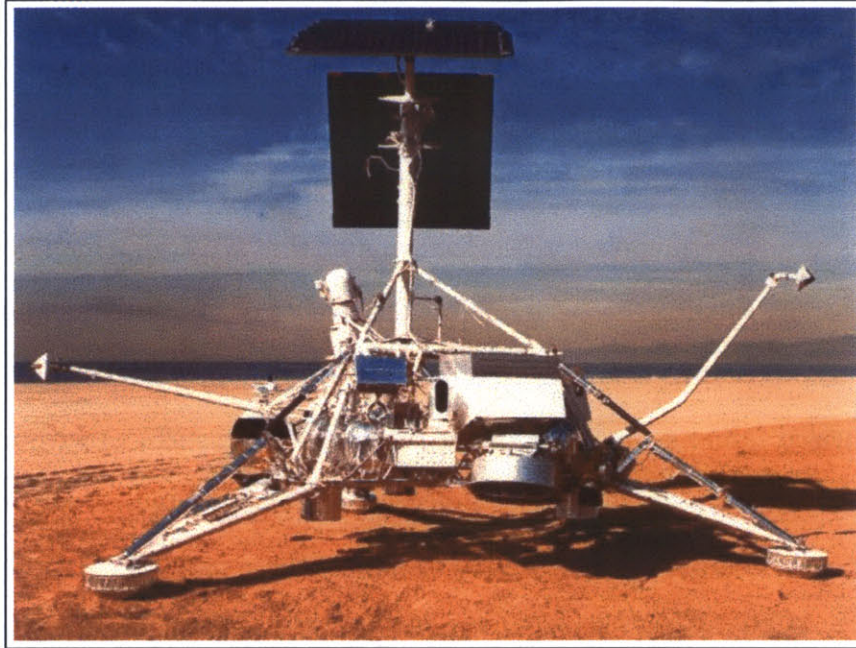


Figure 3-6: Surveyor on the beach in California

Other landing gear concepts include: articulating control arm (in the automotive industry, called the “short-and-long-arm” suspension), air bags, or a crushable underbody (with no legs). Each of these five concepts could be designed such that they are deployed during the mission or fixed from launch.

The deployable, cantilever design is the most feasible option. In Chapter 4, we will see that the legs must extend $O(7\text{ m})$ out from the center of and $O(1.5\text{ m})$ down from bottom of the landing vehicle. At this width and height, the fixed leg option is infeasible. Furthermore, airbags and a crushable underbody are infeasible. The radial suspension is attractive for small spacecraft and was used on Surveyor, Viking, Mars Polar Lander, LUNOX, etc.. However, the lower members violate the ground clearance requirement of 1 m as they extend out to the footpad itself.

In conclusion, the cantilever design is the most feasible option. While other options exist, the architecture of the landing gear itself is not critical to the overall vehicle design, so long as the gear packages within the aeroshell and provides adequate landing stability.

3.3 Airlock System Concepts

The airlock system is desired to mitigate two mission risks: dust intrusion into the habitat; and crew injury or illness requiring quarantine within the habitat. The airlock serves as an intermediate pressurized volume that EVA suits may be stored and donned in, thereby keeping the main habitat relatively free of Lunar (or Martian) dust. The airlock also serves as a means to allow passage from the pressurized habitat to the unpressurized Lunar surface (or lower pressure Martian surface) without changing the cabin pressure. These, and other system requirements and design implications were developed in Chapter 2. Concepts that satisfy these requirements are now listed in Figure 3-7. While many designers list only Functional Requirements and Design Parameters (i.e. Concepts), I prefer to include Design Implications to bridge the gap between the requirements function-space and the concepts form-space.

Functional Requirement	Design Implication	Concepts
Allow change in pressure without changing cabin pressure	Airlock	1-person gerbil tunnel 2-person room 4-person room
Mitigate dust intrusion	Don spacesuits outside spacecraft cabin	Large-volume airlock Pressurized volume between cabin and airlock
	Dust removal prior to ingress	Broom Dustbuster
Have a mass less than 150 kg for ascent	Lightweight airlock	Inflatable airlock
	Jettison airlock before ascent Use a jetway (permanant surface-based airlock)	Explosive bolts at vehicle Retractable docking port Predeployed airlock on a rover that docks with lander
Provide ground-level egress (Required)	Pressurized volume extends to ground level, and airlock at ground level	Inflatable tunnel Jetway
Provide ground-level egress (Not Required)	Airlock at vehicle level, and exterior stairs or ramp	Inflatable tunnel
Cabin pressurized during ascent	Must have cabin hatch	
Deploy tools, science equipment, etc., and return surface material samples	Desire large-volume airlock Desire no tight corners in gerbil tunnels	

Figure 3-7: Airlock functional requirements and concepts

The design parameters and concepts may be organized with aid of a so called *morphological matrix* [28]. In the leftmost column of the matrix, the design parameters are listed. Concepts for each parameter are listed across the row. System concepts are generated by choosing one concept from each row in the matrix.

Morphological Matrix			
Design Parameter	Concepts		
Airlock Location	Surface-level	Vehicle-level	
EVA Suit Donning Location	Intermediate pressurized volume	Airlock	
Airlock Capacity	1-Person	2-Person	4-Person
Deployment Time	Deployed during mission	Pre-deployed on vehicle	Pre-deployed on surface
Airlock Structural Material	Inflatable	Solid-walled	

Figure 3-8: Airlock Morphological Matrix

In order to use the morphological matrix to synthesize full system concepts, one must make ground rules and assumptions for combining the options. We make the following:

- Surface-level airlocks may not be pre-deployed on the vehicle.
- Vehicle-level airlocks may not be pre-deployed to the surface.
- Intermediate pressurized volumes may only be used with a surface-level airlocks.
- EVA suits may not be donned in a 1- or 2-person airlock.
- Airlocks that are deployed during the mission must be inflatable.
- Airlocks that are pre-deployed on the vehicle must be solid-walled.
- Airlocks that are pre-deployed on the surface must have an intermediate pressurized volume.

By combining design parameter options in accordance with the above rules, we arrive at six system concepts, as detailed in Figure 3-9.

Design Parameter	Airlock System Concept					
	1	2	3	4	5	6
Airlock Location	S	S	S	S	V	V
EVA Suit Donning Location	V	A	V	A	A	A
Airlock Capacity	2	4	2	4	4	4
Deployment Time	M	M	Pre-S	Pre-S	M	Pre-V
Airlock Structural Material	I	I	I	I	I	S

Figure 3-9: Airlock System Concepts

The ground rules and assumptions above merit several points of discussion. First, one notes that none of the system concepts utilize a 1-person airlock. Initially, the 1-person cylindrical airlock, similar in form to that used on the Voskhod 2 spacecraft, was considered. See Figure 3-10.

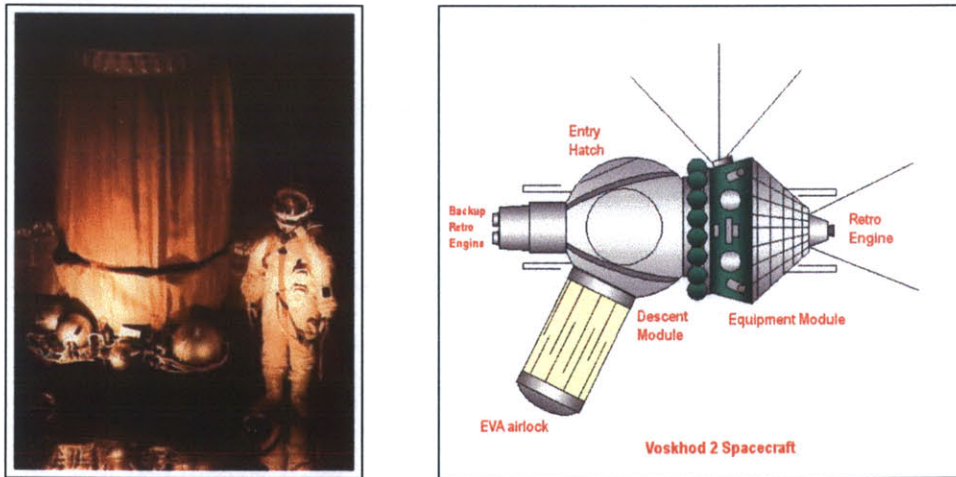


Figure 3-10: Voskhod 2 spacecraft, circa 1964.

The slender cylindrical shape employed for the Voskhod 2 affords a low volume to mass ratio; the maximum volume for a given mass is obtained with a spherical vessel.

Thus, a more squat cylinder, resembling a sphere, yields a higher volume/mass ratio. In fact, the 2-person airlock modeled here has a lower mass than the 1-person. See Figure 3-11 for the results and Section 4.3 for the analysis. In addition, the 2- and 4-person airlocks offer easier egress/ingress. Thus, the 2- and 4-person cylindrical airlocks are considered only.

Design Parameter	Airlock Capacity		
	1-Person	2-Person	4-Person
Shape	Cylinder	Cylinder	Cylinder
Diameter [m]	1.2	1.8	1.8
Length [m]	2.0	1.3	2.5
Crew Orientation	Lying	Seated	Seated
Volume [m³]	2.3	3.3	6.4
Surface Area [m ²]	7.5	7.3	14.1
Wall mass density [kg/m ²]	5.0	5.0	5.0
Pressure [kPa]	33.0	33.0	33.0
Gas Constant (O ₂) [J/kg*K]	519.6	519.6	519.6
Temperature [K]	290	290	290
Mass			
Walls [kg]	37.7	36.7	70.7
Gas [kg]	0.5	0.7	1.4
Hatch [kg]	20.0	20.0	20.0
Total Mass [kg]	58.2	57.5	92.0

Figure 3-11: First order airlock mass calculations

Second, it is conceivable that the two crew may don EVA suits inside a 2-person airlock. The functional requirement should read donning *and storage* of EVA suits. The functional requirement that the donning of the suits in the airlock satisfies is the mitigation of dust intrusion. Hence, it is assumed that the dust-laden suits will be stored in the same location they are donned in. It is also assumed that a 2-person airlock will not be large enough for two crew members to don suits while the other two suits are still in storage. Hence, the EVA suits may only be stored and donned in a 4-person airlock.

Finally, it is also conceivable that there may be an intermediate pressurized volume at vehicle level. However, this would add unnecessary complexity to the vehicle design. It is assumed that if the airlock is at vehicle level, it would be a single 4-person vessel.

3.4 Vehicle Architecture Concepts

The three launch scenarios may now be combined with aeroshell and Yellow Stage options to obtain four realistic vehicle architecture concepts. They are:

Option 1:

- HLLV: in-line, 15 *m*-diameter fairing, extended upper stage for Mars.
- Aeroshell: 15 *m*-diameter conic.
- Yellow Stage: 10 *m*-dia. octagonal prism, 1.5-stage with restartable engines.

Option 2:

- HLLV: in-line, 15 *m*-diameter fairing, extended upper stage for Mars.
- Aeroshell: 15 *m*-diameter conic.
- Yellow Stage: 7.5 *m*-diameter square prism, 2-stage.

Option 3:

- HLLV: side-mount, 8 *m*-diameter fairing for Moon and Mars.
- Aeroshell: 8 *m*-diameter biconic.
- Yellow Stage: 7.5 *m*-diameter square prism, 2-stage.

Option 4:

- HLLV: side-mount, 8 *m*-diameter fairing for Moon only.
- HLLV: in-line, 15 *m*-diameter fairing for Mars only.
- Aeroshell: 15 *m*-diameter conic.
- Yellow Stage: 7.5 *m*-diameter square prism, 2-stage.

In the following chapter, these four options are analyzed along selected performance criteria.

Chapter 4

Analysis

In the Chapter 3, four vehicle design concepts were generated that satisfy the functional requirements and system constraints. These concepts must now be analyzed along a set of performance criteria in order to determine the best option. Several performance metrics exist, and in this chapter, we analyze the architectural options along a finite set of criteria.

4.1 Selection Criteria

For a complex system such as a spacecraft, there are several performance criteria that could be evaluated. Here, we analyze nine criteria which may be grouped into three main categories: cost, risk and safety, and functional performance.

4.1.1 Cost

The design of a sustainable space exploration system must mind cost at all times. If the system architecture lends itself to becoming too costly, the entire program may grind to a halt. Launch vehicle costs are a prime focus, since this occupies a large percentage of the total exploration budget. The life-cycle cost of the launch

system may be broken down into three pieces: development cost, fixed recurring costs (overhead cost per year), and variable recurring costs (cost per flight). While the development cost is the largest portion (on the order of \$5 to \$8 billion), the fixed and variable costs may top \$500 million per year and \$1 billion per flight, respectively [27]. Clearly, the total cost of the transportation system is closely tied to the launch system cost.

But the cost of cargo flights is also a concern. A dedicated cargo flight will cost \$1 billion for the launch alone. If one designs a transportation system requiring dedicated cargo flights, they pay this penalty. Clearly, the need for dedicated cargo flights is a design selection criteria.

4.1.2 Risk and Safety

Risk is nominally defined by the severity and probability of an accident happening. An *accident* is an undesired or unplanned event that results in a specified level of loss. For example, a collision during docking results in mission abort. An accident may occur when the crew is exposed to a hazard. A *hazard* is a state (a set of conditions of the system) that may lead to an accident when combined with other conditions. For example, loss of attitude control is a hazard that may lead to the collision accident, provided that the loss of control occurred when the spacecraft were on intersecting trajectories. If a hazardous state is reached but does not result in an accident, this is called an *incident*. Each hazard may be characterized by its:

- Severity - the damage that would occur from a worst case scenario accident
- Likelihood - probability of hazard occurrence
- Danger - probability of hazard leading to an accident
- Latency - hazard exposure or duration

Risk is a function of the hazard severity, likelihood, danger, and latency. To reduce the risk posed by a hazard, several mitigation techniques may be done, namely:

- Eliminate - complete elimination of the hazard from the design (**likelihood** becomes zero)
- Prevent - reduction of the **likelihood** that the hazard will occur
- Control - reduction of the **danger** that the hazard results in an accident
- Reduce damage - reduction of the **severity** of the damage to the system if an accident does occur

Safety is defined as freedom from accidents, but can also be thought of as the freedom from hazards. This is distinct from reliability, which is the probability that a component will perform its intended function for a prescribed time under stipulated environmental conditions.

The best possible mitigation technique is to eliminate the hazard from the system completely. The hazard of foam falling off of the external fuel tank of the Shuttle launch system and striking the heat shield may be eliminated by selecting a top-mounted launch system.

In this chapter, *aeroentry stability* and *landing stability* are indicators of the likelihood that the vehicle will get into a hazardous state of unstable, uncontrolled motion. In Chapter 3, we selected Yellow Stage concepts with clustered engines, because that controls the danger that this unstable flight will lead to an accident.

But risk is not limited to mission events. *Operational risk* is the risk that system logistics may fail. For FedEx, inclement weather causes an operational risk that planes may be delayed and packages not delivered on time. Likewise, the same packages may be delayed if the pilot flying the plane has little experience with this particular plane. This reasoning may be extended to the introduction of any new system into

the exploration program. During the training period, there is increased risk of the system not operating properly. In this chapter, we use operational risk of the launch system as a proximate risk criteria.

4.1.3 Functional Performance

Finally, the functional performance of the architectures must be analyzed. Again, several performance criteria exist, and we evaluate only a small set here. The primary function of the astronauts while on the surface of Mars is to conduct science and exploration activities. The activity schedule will most likely call for on average one extravehicular activity (EVA) per day, so crew egress from the habitat will be a major concern. Also, the usable laboratory workspace, closely tied to the habitable volume and floor area, is a good measure of the astronauts' ability to perform scientific experiments. Here, the cargo package plays a major role as well. Larger-volume cargo bays may transport larger pieces of scientific or exploration equipment.

Section 4.2 presents the analysis along each of these criteria.

4.2 Comparison of Architectures

The following analysis presents the performance of the four vehicle architecture concepts over several criteria: launch vehicle implications, aeroentry stability, landing stability, crew egress, cargo package, and habitable volume.

4.2.1 Launch Vehicle Implications

Architecture Options 1 and 2 require the construction of an in-line Heavy Lift Launch Vehicle for missions to the Moon and Mars. This will likely be an Evolved Expendable Launch Vehicle-derived (EELV) system. Architecture Option 3 requires a side-mounted launch vehicle for missions to the Moon and Mars, most likely a Shuttle

Derived Vehicle (SDV). Architecture Option 4 requires a SDV for the Moon and an EELV-derived vehicle for Mars. The choice between these four options has implications on cost, timing, and risk.

The life-cycle cost of the launch system may be broken down into three pieces: development cost, fixed recurring costs (overhead cost per year), and variable recurring costs (cost per flight). See Figure 4-1.

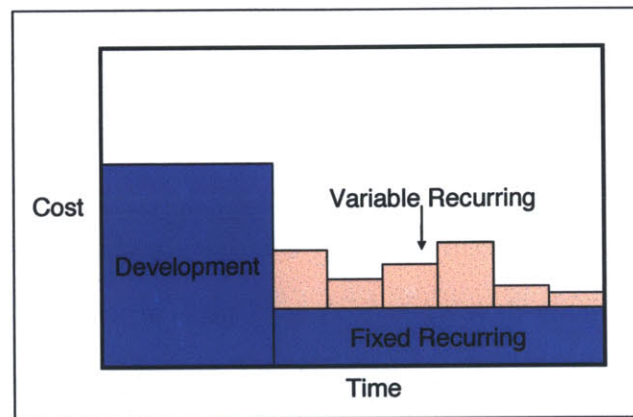


Figure 4-1: Elements of Launch Vehicle Life-Cycle Cost [27].

The total development cost for a Shuttle Derived Vehicle (SDV) is on the order of \$5.5 billion, fixed recurring cost on the order of \$900 million per year, and variable recurring costs on the order of \$1 billion per flight. The total development cost for an Evolved Expendable Launch Vehicle-derived system (EELV) is on the order of \$8.5 billion, fixed recurring cost on the order of \$400 million per year, and variable recurring costs on the order of \$450 million per flight [27]. Here, we see that while the initial investment for the EELV is on the order of \$3 billion more than the SDV, as demand for flights increases, the EELV quickly becomes the more economical option.

Architecture Options 1 and 2 use the EELV-derived system, which requires the \$8.5 billion up-front investment and may not be complete in time to assist in the construction of the International Space Station. To save cost and time in the near term, Option 3 is considered.

Architecture Option 3 requires the least launch vehicle investment. The current Shuttle design may be adapted with relatively little monetary and manpower investment. The additional benefit of the quickly-developed HLLV is that it may be used to ferry modules into Low Earth Orbit and assist in the completion of the International Space Station once the Shuttle is retired. However, precautions must be made to shield the payload from the external tank foam, as this will be a carry-over hazard from the current design. This option does require that the Mars aeroentry vehicles package within an 8 m fairing. Since it is not possible to package within an 8 m conic, a biconic must be used. If it is not possible to package within a biconic and a side-mounted lunar launch vehicle is still desired, then Option 4 must be selected.

Here, we see that Architecture Option 4 is clearly the worst option. The \$5.5 billion spent on the quickly-developed SDV for Lunar missions is a sunk cost. Before Mars exploration may begin, an additional \$8.5 billion must be invested to build the EELV-derived system. Thus, this option wastes money up front and puts a financial hurdle between the Moon and Mars. Additionally, the operational risk of this architecture is the highest, since two separate systems will be developed, tested, and used. The expertise gained using the side-mounted system will be lost when the in-line system is introduced.

4.2.2 Aeroentry Stability

The Mars vehicles must package within an aeroshell and heat shield to withstand the aerothermal heating during atmospheric descent to the Mars surface. The two reasonable architectures are the conic blunt body and the biconic bullet shape. Due to the large habitable volume and propellant volume required, the biconic shape must be elongated as a cylinder in order to package all of the elements. This may prove aerodynamically infeasible, and regardless, the thermal protection system will prove to be too massive, since its area will be much larger than the TPS area for the conic.

The parameter which indicates passive aerodynamic stability for a conic blunt body is x/D , the ratio of the distance from the nose of the vehicle to the center of gravity, x , to the maximum cross-sectional diameter, D . The x/D must be less than 0.3 for passive aerodynamic stability of a conic blunt body, and lower is better [3].

Figure 4-2 shows the x/D for the Earth Return Vehicle. The center of gravity location calculations are shown in Figure A-1.

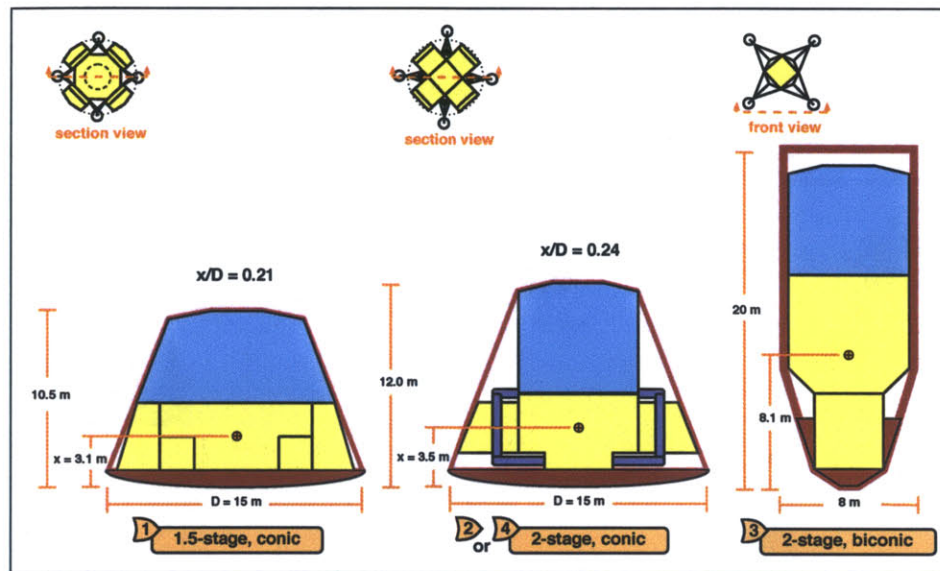


Figure 4-2: Earth Return Vehicle during aeroentry. Passive aerodynamic stability increases for lower x/D .

Due to the large propellant mass which may be located near the heat shield, the center of gravity for either conic design is within the acceptable limit, although architecture Option 1 offers a slight advantage. Since the biconic shape was extended as a cylinder, its passive aerodynamic stability is not directly quantifiable by the x/D ratio. The biconic is presented purely for illustration.

We see here that either the 2-stage or 1.5-stage designs are acceptable for the Earth Return Vehicle, yet the 1.5-stage architecture is preferable.

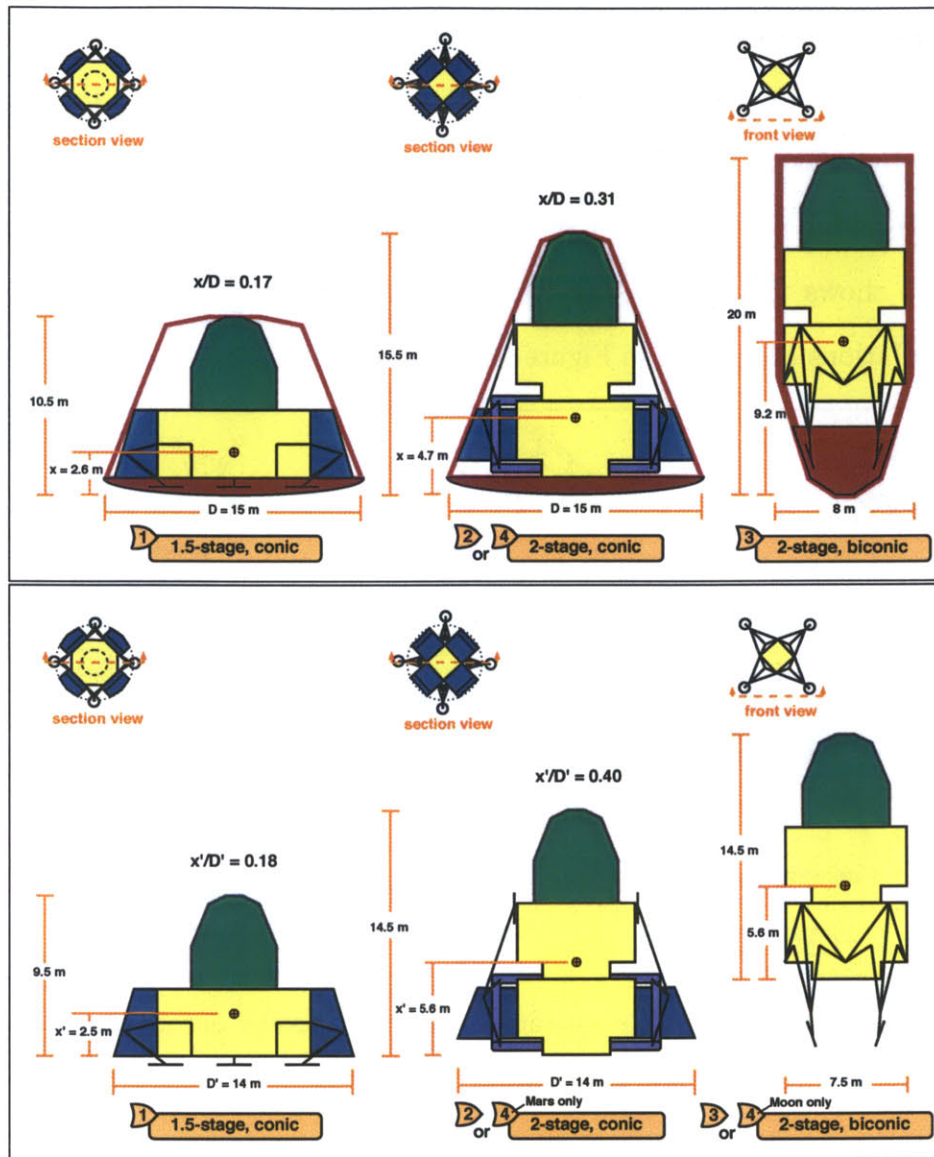


Figure 4-3: Mars Ascent Vehicle during aeroentry and immediately after heat shield jettison. Passive aerodynamic stability increases for lower x/D .

The x/D for the Mars Ascent Vehicle for Options 2 or 4 indicates the vehicle will not be passively stable during aeroentry. Between heat shield jettison and engine thrusting, the vehicle becomes unstable, as the center of gravity jumps 1.9 m rearward on the vehicle. The comparatively low CG in Option 1 makes the 1.5-stage Yellow Stage design preferable in this case.

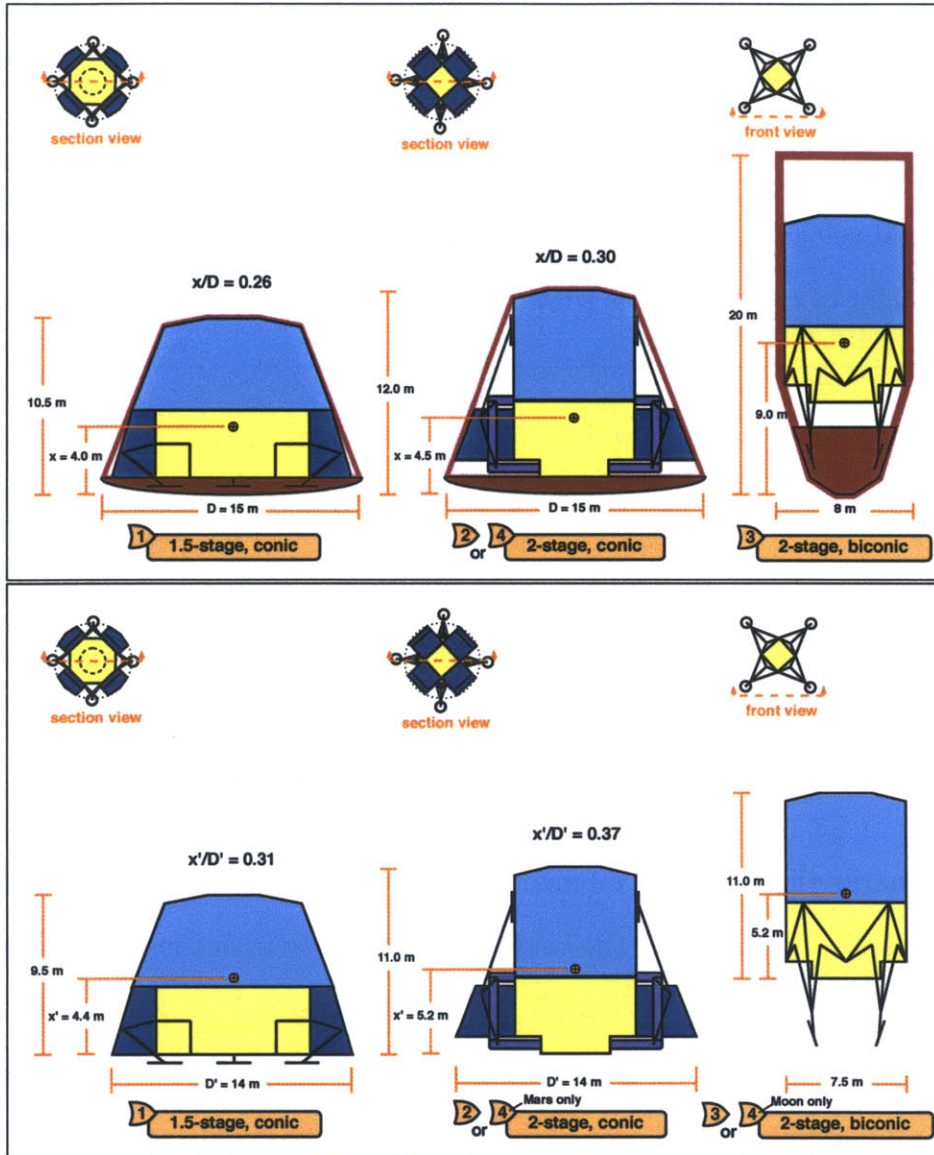


Figure 4-4: Mars Transfer and Surface Habitat during aeroentry and immediately after heat shield jettison. Passive aerodynamic stability increases for lower x/D .

For the Mars Transfer and Surface Habitat, we see the same results. The x/D of the Options 2 or 4 indicates instability, and the x/D of the Option 1 vehicle is favorable. We also note that for all conic vehicles, we see that storing massive elements in side-mounted cargo bays, close to the heat shield, will be required to increase aerodynamic stability.

4.2.3 Landing Stability

The radius of the landing gear footprint required to prevent toppling can be determined by a rigid-body landing stability analysis. The craft is assumed to land with some horizontal velocity, attitude deviation, and roll rate and to strike a hard object such as a boulder or crater wall, as shown in Figure 4-5.

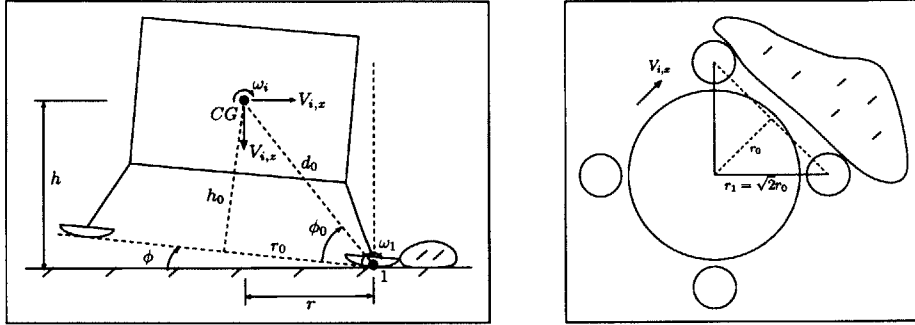


Figure 4-5: Sketch of lander during worst case scenario touchdown.

In this scenario, the rotational momentum about the incident footpad(s) will cause the craft to topple. By balancing the work done by gravity with the initial rotational kinetic energy, adding appropriate safety factors, and realizing that the radius, r_0 , is the distance from the center of gravity to the line of action of the ground reaction point(s), one determines the following equations for the required radius.

$$mgd_0 \left(\sin(\phi_f) - \phi_i \frac{r_0}{d_0} - \frac{h_0}{d_0} \right) \geq S_{KE} \frac{(h_i m V_{i,x} + \omega_i I_{CG})^2}{2(I_{CG} + m d_0^2)} \quad (2.4.13)$$

$$r_1 = \sqrt{2} r_0 \quad (2.4.14)$$

where m , h_0 , and I_{CG} are given by the spacecraft design; $V_{i,x}$, ϕ_i , and ω_i are design specifications; and $\phi_f = 60^\circ$ and $S_{KE} = 2$ are selected safety factors.

Using the above specifications, one finds that the radius is insensitive to the landed mass and the moment of inertia about the center of gravity and that the only vehicle parameter that influences the radius is the center of gravity height. Furthermore, the

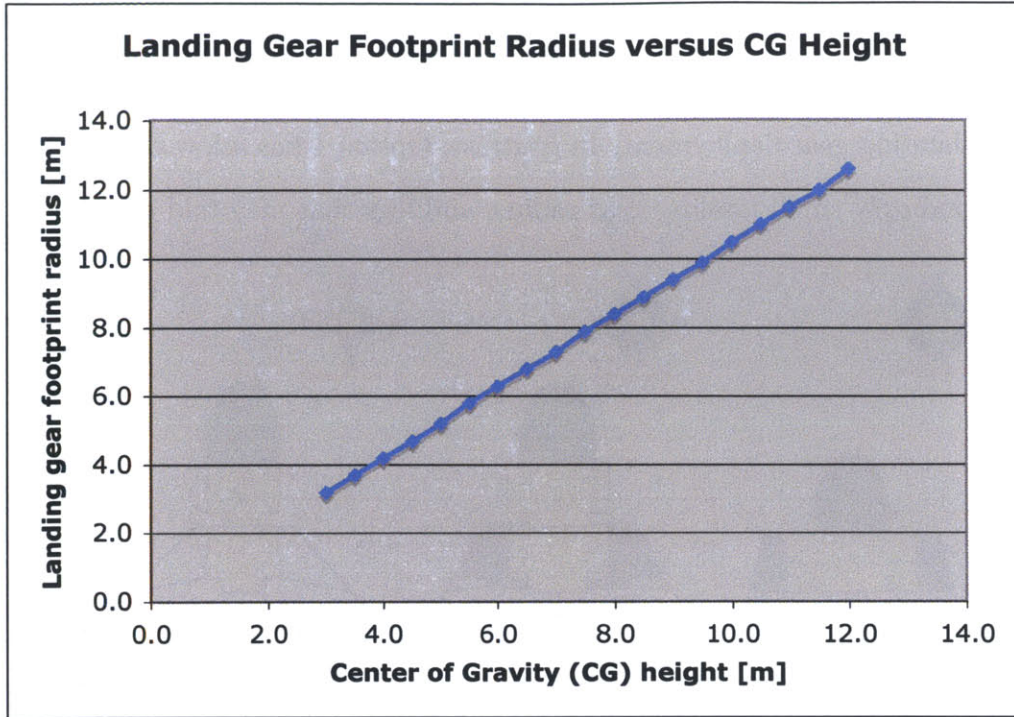


Figure 4-6: Required landing gear footprint radius versus center of gravity height. (Assuming $m = 51,000 \text{ kg}$ and $I_{CG} = 107,000 \text{ kg} \cdot \text{m}^2$, as is the case for the Mars Ascent Vehicle.)

required radius nearly equals the center of gravity height, as shown in Figure 4-6.

This result is consistent with the automotive industry *static stability factor*, which is the ratio of the distance from the vehicle centerline to the tire contact patch divided by the center of gravity height, which is usually between 1.1 (for SUV's) and 1.6 (for cars). The equivalent static stability factor prescribed by our analysis is 1.04.

The landing gear footprint radius was determined for each of the vehicles in the four architectural options using the above specifications. The results are shown in Figure 4-7. Because of the high center of gravity of the Mars Ascent Vehicle in Options 2, 3, and 4, the vehicles must have a wide footprint, requiring very long legs. This is not an issue for Option 3, since the legs may fold down and still package within the biconic aeroshell. For Options 2 and 4, we have seen that the aeroentry stability is perilous, at best. Folding these long legs down will require additional

separation between the Yellow Stage and heat shield, thus making the aeroentry vehicle less stable still. Therefore, the legs are shown stowed upwards. This leads to non-ideal landing gear deployment. In contrast, Option 1 has a low center of gravity, a correspondingly small landing gear radius, and legs that may fold down.

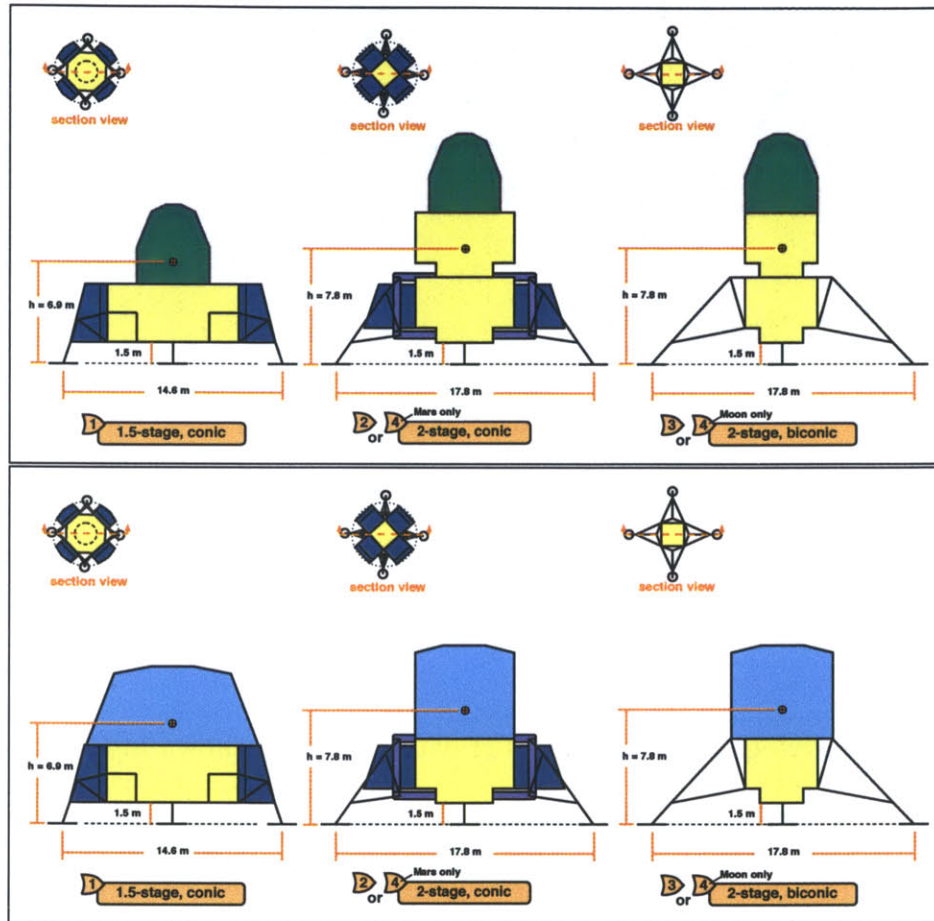


Figure 4-7: Mars Ascent Vehicle and Transfer and Surface Habitat during touchdown. Required landing gear radius shown.

The wide footprint in all four options prevents the use of airbags or a crushable underbody, as neither of these will have the required radius. One final note: the radius of the landing gear footprint for the Lunar vehicles is nearly identical to these for the Mars vehicles. Therefore, it is possible to design one carry-over system for both use cases. (Of course, the loading will be different for each vehicle, so a different energy absorption cartridge and different footpad size will be required for each vehicle.)

4.2.4 Crew Egress

In order to attenuate the kinetic energy at touchdown, the suspension compresses through a prescribed stroke. The requirements developed in Chapter 2 call for a 0.5 m stroke and final ground clearance of 1.0 m. The vehicles in their surface operating configurations, with respective crew egress heights, are shown in Figure 4-8.

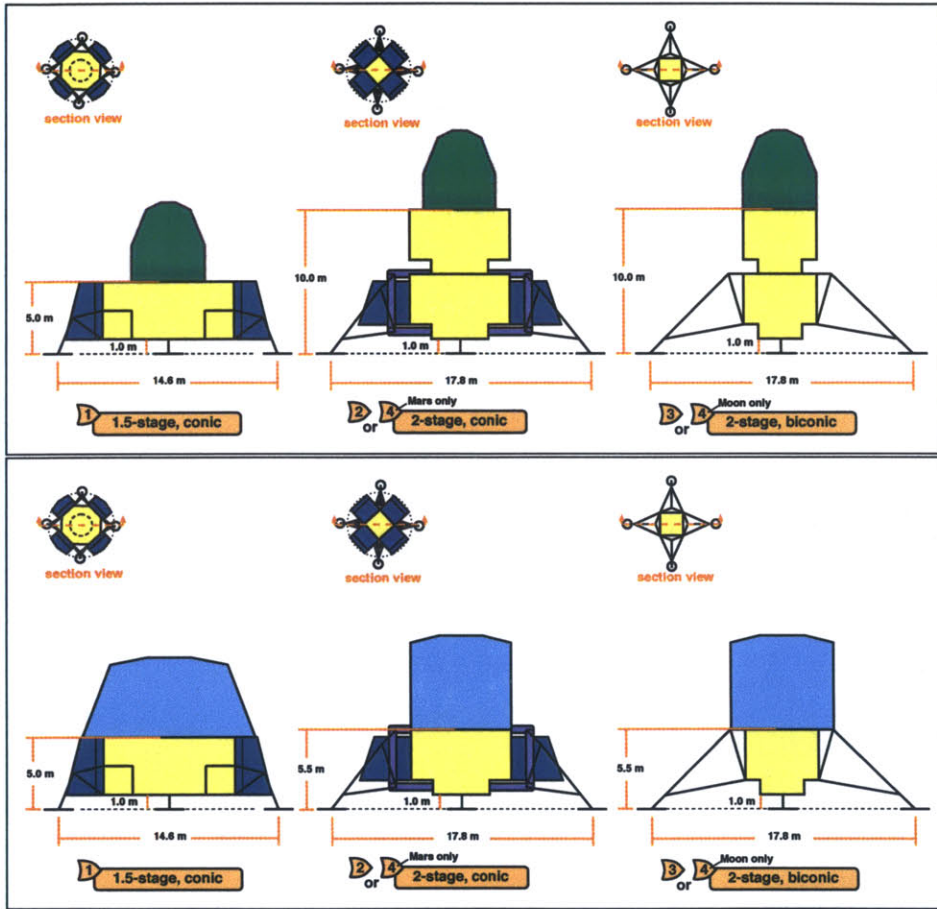


Figure 4-8: Crew egress heights for the Mars Ascent Vehicle and Transfer and Surface Habitat during surface operations.

The crew egress heights for the habitats are nearly equal for all vehicle configurations. However, for the Mars Ascent Vehicle, there is a 5 m height savings with the 1.5-stage Option 1. Note that for Options 1, 2, and 3, one common Moon and Mars suspension system may be developed, but for Option 4, both of the landing gear systems shown would have to be developed.

4.2.5 Habitable Volume and Floor Area

The required habitable volume for the Mars Transfer and Surface Habitat is 285 m³. The most structurally- and package-efficient shape for this pressure vessel, given the constraint to package within the aeroshell, is a vertically-oriented cylinder. Since this habitat will be used in the gravity environment of the Moon or Mars surface, the floor area is important in addition to the total volume, as the floor area determines the available workspace [15]. In vehicle architecture Option 1, an igloo-shaped habitat may be used, which yields nearly twice the floor area of the cylinder configurations. However, the igloo may not be used for Options 2 or 4, since the stowed landing gear interferes with the igloo package. It also may not be used in Option 3, since it does not package within the 8 m biconic aeroshell. The habitable volume and floor area of each of the habitats are listed in Figure 4-9.

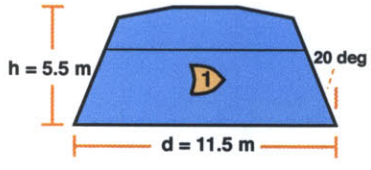
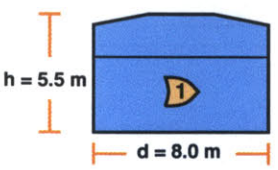
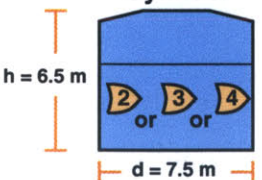
Configuration	Habitable Volume [m ³]	Floor Area [m ²] (1st floor + 2nd floor)
<p>Igloo</p> 	363	104 + 64
<p>Cylinder</p> 	276	50 + 50
<p>Cylinder</p> 	287	44 + 44

Figure 4-9: Habitable volume and floor area.

Inflatable Laboratory Module

Inflatable habitats are an attractive option for increasing the usable laboratory workspace on the surface of the Moon or Mars. An inflatable laboratory may offer over 250 m^3 of deployed volume, given less than 2 m^3 of cargo volume and less than 600 kg total mass.

An inflatable laboratory may be deployed from one of the cargo modules onto the surface of the Moon or Mars. This laboratory could be used as the primary location for 'indoor' scientific activity, thereby freeing the interior of the primary habitat for operations, etc. Another advantage of this separated lab/habitat configuration is to mitigate intrusion of foreign debris such as Lunar or Martian dust into the main habitat.

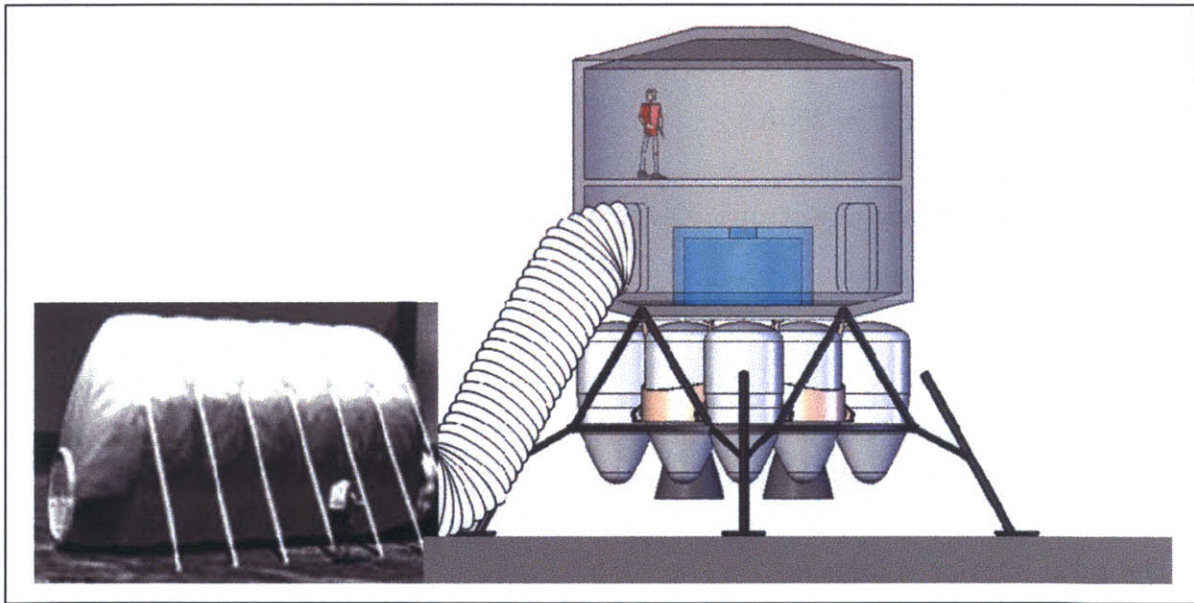


Figure 4-10: Moon or Mars habitat with surface inflatable tent deployed

The high-level parameters of the laboratory are the deployed volume (which is related to the available workspace), the stowed volume in the cargo module, and the total mass.

As an example, let us consider simple inflatable laboratory, consisting of a single cylindrical hallway of radius, r , and length, l , with spherical endcaps. Since the laboratory is a pressure vessel, the wall thickness may be sized using the familiar equation

$$\sigma = S_{pv} \frac{Pr}{t} \quad (4.2.1)$$

where σ is the tensile wall stress, P is the interior gauge pressure, r is the cylinder radius, t is the material thickness, and S_{pv} is a safety factor.

Let us assume $r_{lab} = 2.5 \text{ m}$, $l_{lab} = 10 \text{ m}$, $S_{pv} = 4$, and that the laboratory is filled with

- Oxygen: $R_g = 8.314 \frac{\text{J}}{\text{mol}\cdot\text{K}} / 0.016 \frac{\text{kg}}{\text{mol}} = 519.6 \frac{\text{J}}{\text{kg}\cdot\text{K}}$ at
- Absolute pressure: $P_{lab} = 33 \text{ kPa}$, and
- Temperature: $T = 290\text{K}$.

Let the walls be made of isotropic Kevlar 49 fabric, as suggested in [12]. The relevant material properties are:

- Tensile strength: $\sigma_K = 690 \text{ MPa}$ and
- Density: $\rho_K = 1442 \text{ kg/m}^3$.

The total interior volume is

$$V_{lab} = \pi r_{lab}^2 l_{lab} + 2 \cdot \frac{2}{3} \pi r_{lab}^3 = 262 \text{ m}^3 \quad (4.2.2)$$

Solving Equation (4.2.1) for t_{wall} , we have $t_{wall} = S_{pv} \frac{P_{lab} r_{lab}}{\sigma_K} = 1.5 \text{ mm}$. The mass of the fabric of the walls of the habitat is

$$m_{wall} = \rho_K A_s t_{wall} = 510 \text{ kg}$$

4.2.6 Cargo Package

The side-mounted cargo module configuration was selected for vehicle Architectures 1, 2, and 4 (Mars case only), because of the following features:

- Simple, straightforward cargo deployment
- Efficient usage of conic aeroshell volume
- Favorable center of gravity location within the conic aeroshell
- Modules accessible from surface, since bottom is $O(1\text{ m})$ from surface.
- Multiple uses for modules:

Cargo (science, surface transportation, power system, etc.)

Airlock

Inflatable Habitat

The side-mounted cargo configuration is shown in Figure 4-11.

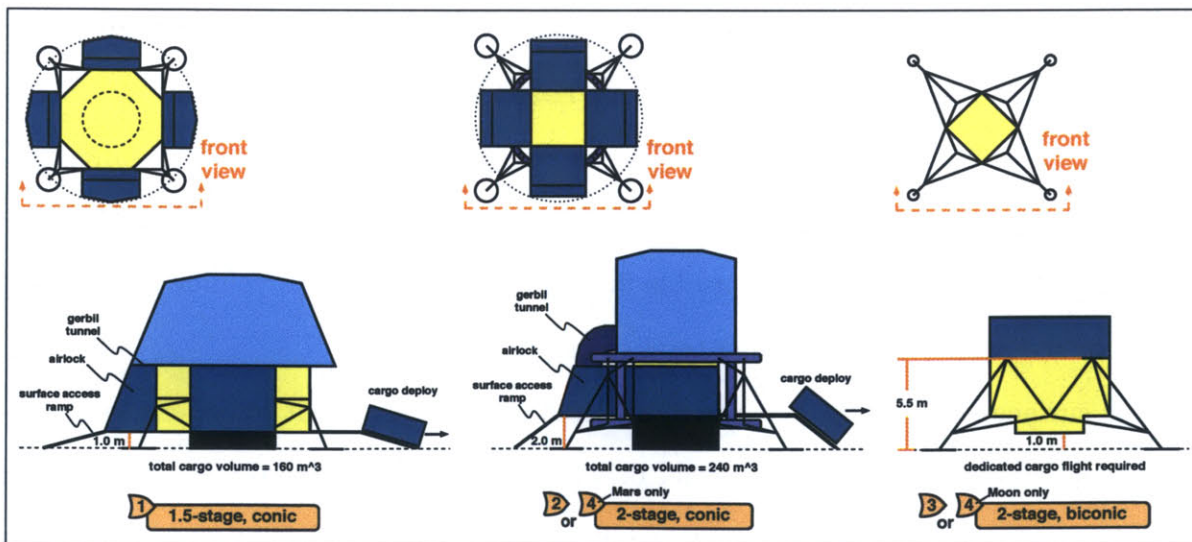


Figure 4-11: Cargo deployment for the Mars Transfer and Surface Habitat (or Lunar Long-Duration Habitat) for surface operations.

Where $A_s = 2\pi r_{lab} l_{lab} + 4\pi r_{lab}^2$ is the surface area. (Note that the mass per unit surface area of the wall is $1442\text{kg}/\text{m}^3 * 1.5\text{mm} = 2.1\text{kg}/\text{m}^2$.) The mass of the air required for inflation is given by the Ideal Gas relation

$$m_{air} = \frac{pV}{R_g T} = 57\text{kg}$$

Thus, the total mass of the laboratory walls and air is

$$m_{total} = m_{wall} + m_{air} = 567\text{ kg} \quad (4.2.3)$$

The total stowed volume of the habitat walls is obtained by multiplying the material volume,

$$V_{wall} = \frac{m_{wall}}{\rho_K} = 0.35\text{ m}^3$$

by a packing factor of 5 (per [24]), which accounts for any inefficiencies in packaging the cargo.

$$V_{stowed} \approx V_{wall} * 5 = 1.75\text{ m}^3 \quad (4.2.4)$$

The total mass of the inflatable laboratory is much less than that of a rigid pressure vessel, and the volumetric efficiency during Earth-Mars/Earth-Moon transport makes the inflatable lab an attractive option for increasing the scientific activity workspace.

Of course, a cylindrical laboratory is not the optimal shape. An elliptical cross-section would yield much more usable floor area, given the same volume and surface area of the walls (thus, the same total mass).

A surface-level laboratory also provides a significant benefit for operations. Astronauts returning from EVA's could bring samples directly into the lab, as opposed to carrying them up a 6 *m*-tall staircase into the main habitat. This system will ease sample return as well as mitigate dust intrusion into the main habitat.

For large cargo modules such as the power plant and rovers, Option 3 requires dedicated cargo flights, since these large cargo modules do not package within the biconic aeroshell. The 1.5-stage Yellow Stage employed in Option 1 supports cargo bays measuring 2.5 *m* deep at the bottom, 1 *m* deep at the top, 4 *m* high, and 5 *m* wide, yielding a total cargo volume of 140 *m*³ for the four bays. The 2-stage Yellow Stage used in Option 2 and Option 4 (for Mars missions only) houses cargo bays measuring 4.5 *m* deep at the bottom, 3.5 *m* deep at the top, 3 *m* high, and 5.3 *m* wide, yielding a total cargo volume of 254 *m*³ for the four bays. These large bays may directly deploy large items such as a nuclear reactor or pressurized rover. Those large items do package in the 1.5-stage Yellow Stage cargo bays, but may require assembly or inflation. Here, we see that Option 2 offers advantages in both gross cargo volume and large-item-deployment capabilities.

4.3 Airlock Analysis

We have shown that inflatable habitat structures are an effective means to increase habitable volume without suffering large mass penalties. Let us now consider the airlock system. The airlock system may contain up to four parts: a permanently pressurized access tunnel, permanently pressurized EVA suit donning room (called the *mud room*), the airlock itself, and in the case of a permanent surface airlock, a rover to transport it to the lander. System Concepts 1 through 6 and their parts manifest are listed in Figure 4-12.

A useful tool to assist the designer in organizing the design space, identifying critical design parameters for analysis, and identifying risks and countermeasures that may be built into the design, is a matrix such as the one shown in Figure 4-13. Recall that the first two functional requirements of the airlock system are countermeasures to the mission risks of crew injury or illness and dust intrusion into the habitat.

Design Parameter	Airlock Sytem Concept					
	1	2	3	4	5	6
Access Tunnel	Y	Y	Y	Y	N	N
Mud Room	Y	N	Y	N	N	N
Airlock Capacity	2	4	2	4	4	4
Rover	N	N	Y	Y	N	N
Airlock Structural Material	I	I	I	I	I	S

Figure 4-12: Airlock system concepts parts manifest

The system concepts are distinguished by their total mass, energy required for operation of the airlock, stowage volume, and risk. First, let us determine the total system mass. For this analysis, we make the following assumptions, in accordance with references [18],[25],[22], [24]:

- The minimum size airlock possible is a one-person cylinder of

diameter, $d = 1.2m$, and length, $l = 2m$.

- The airlock may be constructed of an inflatable fabric of mass per unit surface area, $\rho_s = 5kg/m^2$.

- The airlock is pressurized with

Oxygen: $R_g = 519.6 \frac{J}{kg \cdot K}$ at

Absolute pressure: $p_g = 33kPa$ and

Temperature: $T = 290K$.

- The air leakage rate is less than $5 \times 10^{-3}kg/day$.
- The mass of each hatch is 20 kg. One hatch is an integrated part the vehicle and is not counted towards the airlock mass.

Functional Requirement	Design Implication	Concepts	Analysis	Reference	Risk	Countermeasure
Allow change in pressure without changing cabin pressure	Airlock	1-person gerbil tunnel 2-person room 4-person room	Energy to recycle air Mass_airlock	Goodyear, Voskhod 2		
Mitigate dust intrusion	Don spacesuits outside spacecraft cabin	Large-volume airlock Pressurized volume between cabin and airlock	Volume required for donning?	Apollo LM		
	Dust removal prior to Ingress	Broom Dustbuster				
Have a mass less than 150 kg for ascent	Lightweight airlock	Inflatable airlock	Mass < 150 kg	Voskhod 2	Too massive	Conservative upfront design
	Jettison airlock before ascent	Explosive bolts at vehicle Retractable docking port		Voskhod 2	Bolts do not disengage	Bring wrench
	Use a jetway (permanant surface-based airlock)	Predeployed airlock on a rover that docks with lander	Mass_rover	Airport jetway Apollo rover	Land long	Use jettisonable airlock
Provide ground-level egress (Required)	Pressurized volume extends to ground level, and airlock at ground level	Inflatable tunnel Jetway	Mass_press.vol. Deployment?	Parachute packing	Does not deploy	Robust design and testing
Provide ground-level egress (Not Required)	Airlock at vehicle level, and exterior stairs or ramp	Inflatable tunnel		Apollo LM, Voskhod 2	Fall during ladder descent	Airlock at ground level
Cabin pressurized during ascent	Must have cabin hatch					
Deploy tools, equipment, etc., and return surface samples	Desire large-volume airlock Desire no tight corners in gerbil tunnels					

Figure 4-13: Airlock design matrix

Furthermore, let us assume that the 2-person airlock, 4-person airlock, access tunnel, and mud room are each cylinders, with dimensions given in Figure 4-14. These dimensions are representative of the required volume of an airlock, and the shape is selected to maximize useable interior volume while minimizing surface area.

Design Parameter	Airlock Capacity		Access Tunnel	Mud Room
	2-Person	4-Person		
Shape	Cylinder	Cylinder	Cylinder	Cylinder
Diamter [m]	1.8	1.8	0.8	1.8
Length [m]	1.3	2.5	8	3
Crew Orientation	Seated	Seated	Climbing	Seated
Volume [m ³]	3.3	6.4	4.0	7.6
Surface Area [m ²]	7.3	14.1	20.1	17.0

Figure 4-14: Airlock component dimensions.

4.3.1 Landed Mass

The landed mass encompasses the mass of the wall fabric, *air*, and hatch(es). (We use the term "air" to refer to the gas which is used to pressurize the airlock; in our case we use Oxygen instead of Earth air.) The mass of the walls is calculated as follows

$$(\text{mass of walls}) = (\text{mass of wall per unit surface area}) * (\text{surface area}) \quad (4.3.1)$$

The mass of the air required for inflation is given by the Ideal Gas relation

$$(\text{mass of air}) = \frac{pV}{R_g T} \quad (4.3.2)$$

Using equations 4.3.1 and 4.3.2, we may predict the mass of each of the components, as listed in Figure 4-15.

Design Parameter	Airlock Capacity		Access Tunnel	Mud Room
	2-Person	4-Person		
Shape	Cylinder	Cylinder	Cylinder	Cylinder
Diameter [m]	1.8	1.8	0.8	1.8
Length [m]	1.3	2.5	8	3
Crew Orientation	Seated	Seated	Climbing	Seated
Volume [m ³]	3.3	6.4	4.0	7.6
Surface Area [m ²]	7.3	14.1	20.1	17.0
Wall mass density [kg/m ²]	5.0	5.0	5.0	5.0
Pressure [kPa]	33.0	33.0	33.0	33.0
Gas Constant (O ₂) [J/kg*K]	519.6	519.6	519.6	519.6
Temperature [K]	290	290.00	290.00	290.00
Mass				
Walls [kg]	36.7	70.7	100.5	84.8
Gas [kg]	0.7	1.4	0.9	1.7
Hatch [kg]	20.0	20.0	20.0	0.0
Total Mass [kg]	57.5	92.0	121.4	86.5

Figure 4-15: Airlock component mass.

The sum total mass for each system concept is listed in Figure 4-16. Note that the mass of the rover is assumed to be 210 kg, which is the same as the mass of the Apollo Lunar Rover [1].

	Airlock Sytem Concept					
	1	2	3	4	5	6
Total system mass [kg]	265	213	475	423	92	440*

Figure 4-16: Total system mass. *The mass of Concept 6 is that of the Shuttle internal airlock [16], [11], which has similar dimensions.

We note that total system mass is highly dependent on the fabric mass per unit surface area, which has been estimated in previous studies to fall within a wide range, between $2kg/m^3$ [12] and $15kg/m^3$ [24]. Figure 4-18 shows the system sensitivity to fabric mass density.

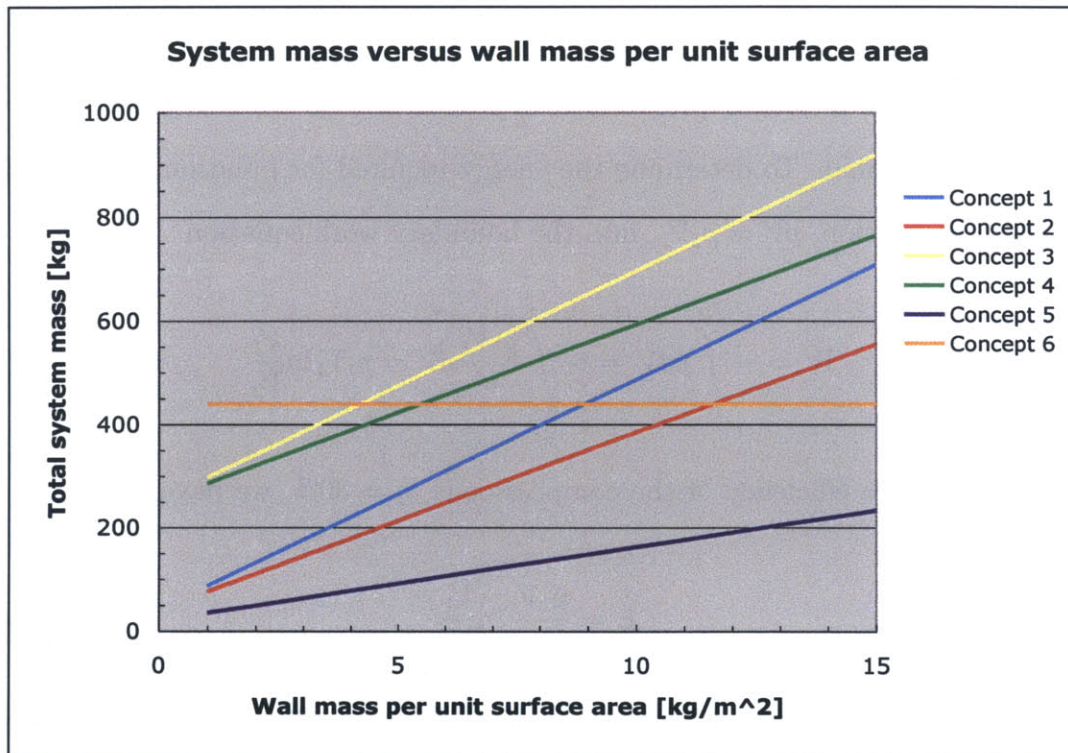


Figure 4-17: Total system mass versus airlock wall fabric mass per unit surface area. *The mass of Concept 6 is that of the Shuttle internal airlock [16], [11], which has similar dimensions.

Due to the large surface area of Concepts 1, 3, and 4, if these systems are to be used, engineering effort should be made to minimize fabric density.

4.3.2 Energy and Time for Decompression

In order to save mass on a long-duration mission, a compressor and storage tank could be used store most of the air prior to opening the exterior hatch. Such a system is used on the International Space Station in the Joint Airlock Module [17]. During an extended stay on Mars of 360 days, recycling the air could save as much as

$$\begin{aligned}(\text{mass}) &= (\text{mass of air in airlock}) * (\text{number of days}) * (\text{EVA's per day}) \\ &= 1.4kg * 360\text{days} * 2\text{EVA/day} = 1008kg\end{aligned}$$

Let us determine the energy required to compress the air into a $1m^3$ storage tank. This volume is arbitrary, and is chosen as unity as a first-order approximation. Assuming that the airlock is pressurized/depressurized slowly, this process may be considered isothermal. To determine the energy required for inflation, we substitute the Ideal Gas relation, $pV = p_1V_1$, into the boundary work equation

$$W = - \int_1^2 p dV = - \int_1^2 \frac{p_1 V_1}{V} dV = p_1 V_1 \ln \frac{V_1}{V_2}$$

Assuming that the efficiency of the compressor is, $\eta = 30\%$, we have that the total energy required is

$$E = \frac{p_1 V_1}{\eta} \ln \frac{V_1}{V_2} \quad (4.3.3)$$

Assuming that the compressor can draw $5kW$ of power [1], the time for decompression of the airlock is

$$T = \frac{E}{Pwr} \quad (4.3.4)$$

Equations 4.3.3 and 4.3.4 are plotted in Figure 4-18.

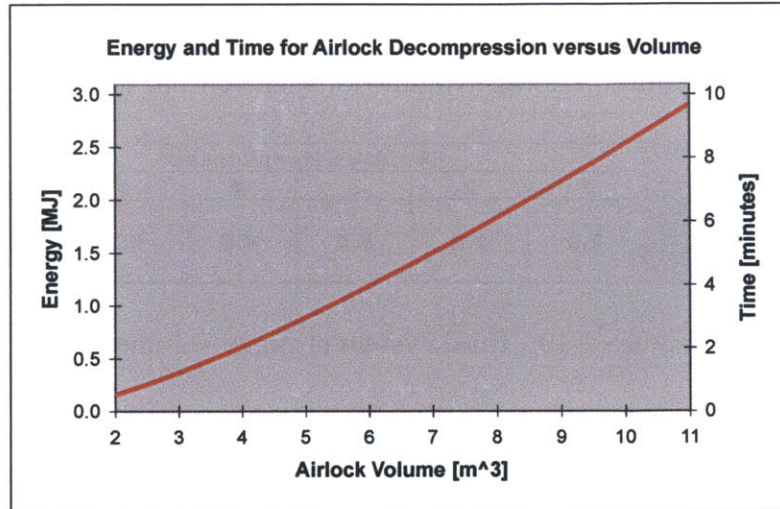


Figure 4-18: Energy and time for airlock decompression versus volume

Recall that the 2-person airlock had a volume of $3.3m^3$ and the 4-person airlock had a volume of $6.4m^3$. We see that while the 4-person airlock consumes about three times the energy as the 2-person, the required energy is still two orders of magnitude below the total energy stored in the Apollo Lunar Module batteries (180 MJ) [1]. Thus, it is feasible to recycle the air in the airlock system.

Finally, one notes that the compressor would be mass inefficient for use on short-duration missions. Therefore, it is desirable to either use a pump in the vehicle life support system or to design the system to be operable with or without the compressor, such that the compressor may not be carried during short-duration missions.

4.3.3 Stowage Volume

The thickness of the inflatable wall is assumed to be $8mm$, per [24]. We obtain the material volume by multiplying the surface area by the thickness, and we obtain the stowage volume by further multiplying by a packing factor of 5, per [24]. Thus, we have

$$(\text{stowage volume}) = (\text{surface area}) * (\text{thickness}) * (\text{packing factor}) \quad (4.3.5)$$

The stowage volume for the hatch is assumed to be $(\pi * (0.8m)^2/4) * 0.25m = 0.124m^3$. Thus, the required stowage volume for each concept is listed in Figure 4-19.

	Airlock Sytem Concept					
	1	2	3	4	5	6
Total system stowage volume [m³]	2.0	1.6	5.0	4.6	0.7	6.4

Figure 4-19: Total system stowage volume.

4.3.4 Risk

Concepts 1 and 2 dictate that the airlock and access tunnel will be deployed to the surface during the mission. Assuming that the airlock system will be deployed from the vehicle itself, at a height 6 to 8 meters above the surface, a deployment mechanism must be designed to lower the airlock on the ground. Furthermore, the airlock must be oriented and located on the ground in such a way as to allow passage through it and the tunnel. This deployment procedure poses a significant design challenge.

Concepts 3 and 4 depend on a permanent surface-based airlock, analogous to a jetway at an airport. The airlock, presumably on an unmanned rover, must locate the spacecraft after landing, traverse to it, and dock with the craft. This rover must be pre-deployed and assembled before sending humans to the surface. Since this system requires pre-deployment and assembly of the rover, these concepts may not be used for the initial "sortie" missions. In addition, this system carries the risk that if the spacecraft "lands long" (i.e. out of the range of the rover airlock), then the crew may not use the airlock during their mission.

Concepts 5 and 6 are the most simple, employing a vehicle-level airlock for suit donning and EVA activities. Concept 5 offers the lowest mass, and Concept 6 does not require deployment. However, these two concepts require the crew to descend to the surface on an external ladder while wearing EVA suits. This carries the risk of

crew falling during descent/ascent of the ladder.

All six systems pose some level of risk. However, the risk for Concepts 1 and 2 is technical and may be retired via robust design and testing of the deployment system. The risks for Concepts 3, 4, 5, and 6 are operational and will persist for every mission.

4.3.5 Airlock System Concept Selection

Concepts 2 and 5 most effectively meet the functional requirements. Selecting between these two airlock systems depends on two main factors: the mass per unit surface area of the fabric walls, which dictates total system mass; and whether a deployment mechanism may be engineered to deploy a surface-level airlock. If lightweight materials and a robust deployment mechanism can be realized, then Concept 2 should be selected. If not, Concept 5 offers the lowest system mass and stowage volume of any concept, and it affords a relatively simple deployment operation.

4.4 Vehicle Architecture Concept Selection

In this chapter, the four realistic architectural options were evaluated on several performance criteria. Option 1 was the best in nearly every criteria. Option 2 offers a better cargo package, but this comes at the expense of increased risk during aeroentry and landing and Lunar mission crew egress. Options 3 and 4 offer near-term savings in launch vehicle investment but have significant performance disadvantages. This analysis is summarized in Figure 5-1.

The Draper-MIT baseline design in the CE&R Base Period was architecture Option 1. During the Option Period, the baseline was changed to Option 2 in an effort to decouple the Mars aeroentry architecture from the launch architecture. However, decoupling the descent/ascent propulsion stage from the launch vehicle comes at a cost. By selecting Option 2, one gains three things: lower operational risk, due to not

depending on restartable engines, a slightly better cargo package, and the ability to exercise Option 4. These come at the expense of the performance difference between Option 1 and Option 2. While the lower risk and better cargo package are desirable, Option 4 is not.

Using the side-mounted lunar launch vehicle in Option 4 is attractive in the near-term, but the architecture performs the worst in the long-term. A side-mounted launch vehicle should only be used for Lunar exploration if it can also be used for Mars exploration, as in Option 3. This requires a biconic entry vehicle, which, as shown in Section 4.2.2, packages perilously at best. If the biconic aeroshell does not package, then NASA should invest money up front to develop the in-line heavy lifter. In that case, if restartable engines are deemed acceptable from a risk perspective, then Option 1 is clearly the best. If not, then Option 2 should be selected.

Chapter 5

Conclusion

In summary, there exist four realistic package scenarios, which may be selected from by answering these three questions:

- Is a side-mounted or in-line launch vehicle preferred for Lunar missions?
- Are restartable descent/ascent engines acceptable (from a risk perspective)?
- Is it possible to package the Mars vehicle stacks in an 8m-diameter biconic aeroshell?

Figure 5-1 shows this decision tree, the four architectural options, and the functional performance of each. The Draper-MIT baseline design is Option 2, with an in-line HLLV, 2-stage Yellow Stage, and a conic aeroshell. (The Draper-MIT baseline in the CE&R Base Period was Option 1.)

In Chapter 4, the four architectural options were evaluated on several performance criteria. Option 1 was the best in nearly every criteria. Option 2 offers a better cargo package, but this comes at the expense of increased risk during aeroentry and landing and Lunar mission crew egress. Options 3 and 4 offer near-term savings in launch vehicle investment but have significant performance disadvantages.

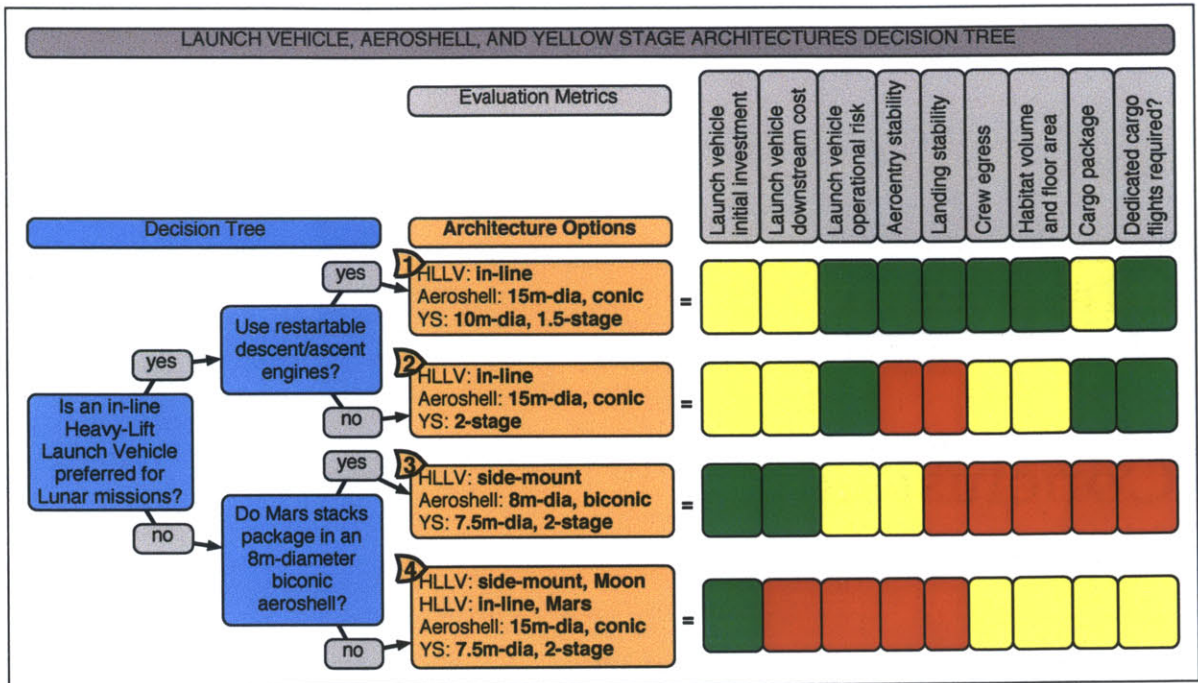


Figure 5-1: Architecture options and functional performance.

Using the side-mounted lunar launch vehicle in Option 4 is attractive in the near-term, but the architecture performs the worst in the long-term. A side-mounted launch vehicle should only be used for lunar exploration if it can also be used for Mars exploration, as in Option 3. If the biconic aeroshell does not package, then NASA should invest money up front to develop the in-line heavy lifter. Then, if restartable engines are deemed acceptable from a risk perspective, then Option 1 is clearly the best. If not, then Option 2 should be selected.

5.1 Vehicle Design Concept

Architecture Option 2 was selected for detailed design. The following images were created by Mitchell Hansberry, and much gratitude is owed to him for his excellent work.

The Moon storyboard is as follows. The Lunar Crew Transportation System (LCTS) (pictured left) consists of the Crew Exploration Vehicle (CEV), two-stage Yellow Stage (YS), and two interplanetary propulsion stages (dubbed Red Stages), one for Trans-Moon Injection (TMI) and one for Trans-Earth Injection (TEI). The

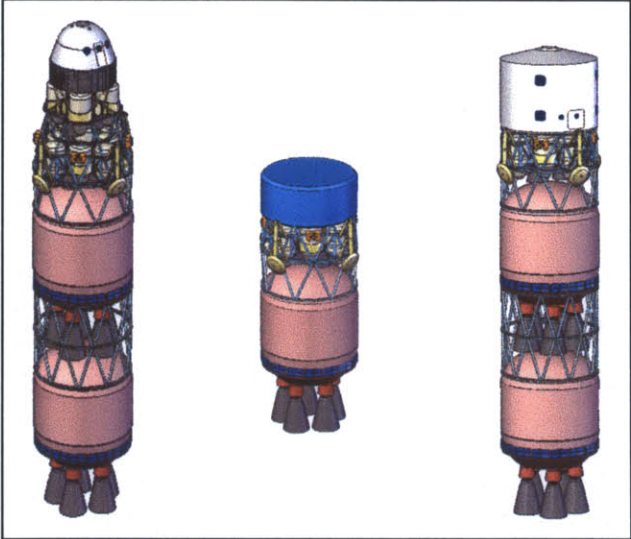


Figure 5-2: Lunar mission Earth-departure configurations

LCTS is assembled in LEO after three launches consisting of: one red stage, one red stage and the yellow stage, and the CEV and crew. The LCTS expends one red stage for the TMI engine burn.

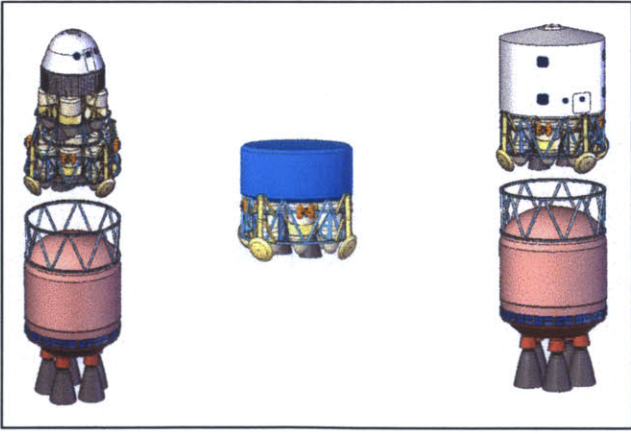


Figure 5-3: Lunar mission transit configurations

The YS and CEV then undock from the remaining red stage and descend to the surface, consuming the propellant in the descent stage of the YS. On a short Lunar mission, the crew only uses the LCTS. However, for an extended 60-day mission, the Lunar Long-Duration Surface Habitat (LLDSH) (pictured right) would be prepositioned for use by the crew on the surface.



Figure 5-4: Lunar mission descent configurations

This vehicle architecture does not require the 15m diameter launch vehicle fairing for Lunar missions. However, if the launch vehicle fairing is not large enough to house cargo side-mounted on the descent stage of the LCTS or LLDSH YS, dedicated cargo flights must be made using the Cargo Vehicle (pictured center). The cargo (blue) would be deployed to the surface via a mechanical arm.

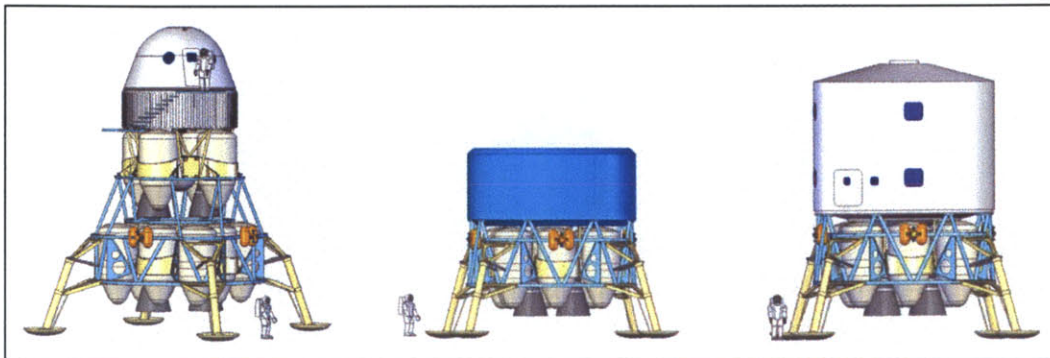


Figure 5-5: Lunar mission surface configurations

At the conclusion of surface operations, the ascent stage of the YS propels the CEV into LMO and performs the TEI burn, and the crew returns to Earth.

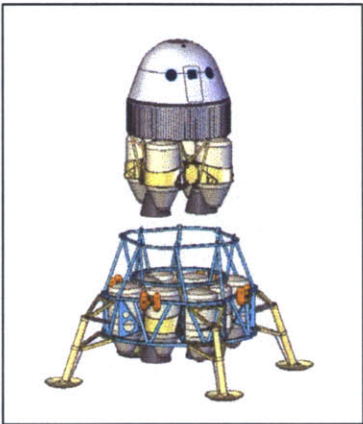


Figure 5-6: Lunar mission ascent configuration

The CEV retains the YS ascent stage to perform mid-course correction burns, if necessary.

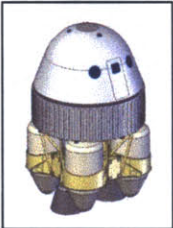


Figure 5-7: Lunar mission Earth-transit configuration

Finally, the CEV undocks from the YS and performs Earth entry, descent, and landing (EDL).



Figure 5-8: Lunar mission Earth-entry configuration

The Mars storyboard is similar. However, since the Mars vehicles must perform aerocapture and AEDL, those configurations are also included. The Earth Return Vehicle (ERV) (pictured left) consists of two RS and inside the aeroshell (AS), a single-stage YS with large external strap-on propellant tanks and a habitat (HAB). The ERV is assembled in LEO after three launches. Similarly, the Mars Ascent Vehicle (MAV) is assembled in LEO after three launches. The MAV consists of two

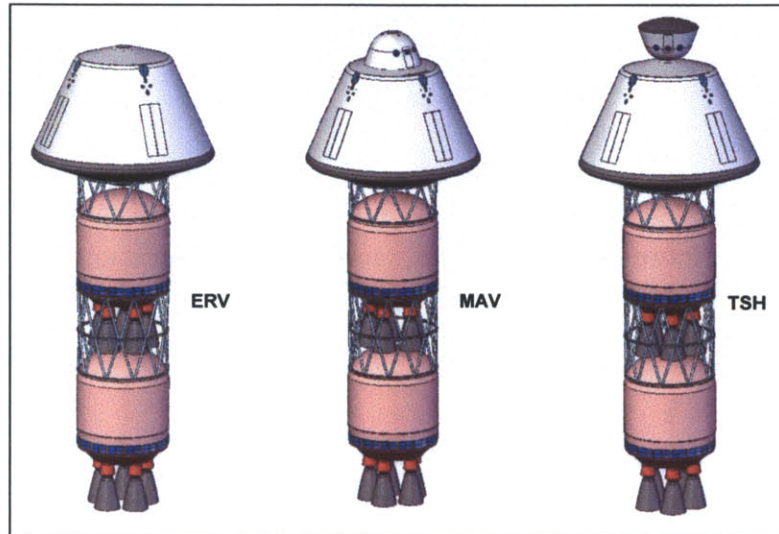


Figure 5-9: Mars mission Earth-departure configurations

RS, an AS with a two-stage YS (one for descent and one for ascent), four cargo pods (CP), and a CEV. The ERV and MAV are propositioned in Mars orbit and on Mars surface, respectively. Finally, the Transfer and Surface Habitat (TSH) consists of two RS, one AS with a one-stage YS, four CP, and one HAB. The crew is launched in another CEV, which docks with the assembled TSH and travels to LMO.

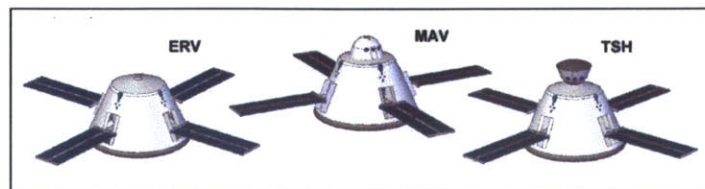


Figure 5-10: Mars mission transit configurations

The crew travels to Mars in the TSH, with the CEV remaining attached. The CEV may be used as an alternate habitable volume and cockpit in the case of mission abort (e.g. the Apollo 13 scenario). If the mission proceeds nominally, the CEV is jettisoned prior to aerocapture. The AS is equipped with retracting solar panels which provide power during the six-month travel time to Mars. During aerocapture, the panels retract.

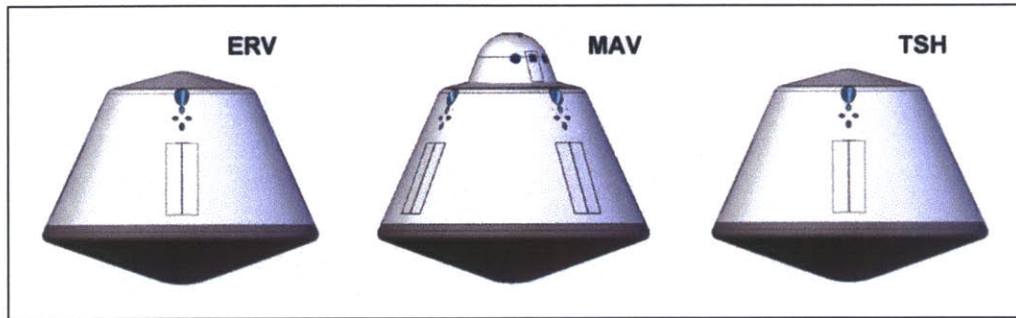


Figure 5-11: Mars mission aerocapture configurations

Once captured into orbit, the MAV and TSH may descend to the surface at any time, weather permitting. If they must remain in orbit for more than three days, the solar panels are deployed once again to sustain power. While the MAV and TSH retain their aeroshells for AEDL, the ERV jettisons its. The ERV remains in orbit until the crew has completed surface operations. Further analysis is required to determine if the MAV and TSH must carry two separate heat shields, or if one, reusable heat shield is sufficient. This design employs one reusable heat shield.

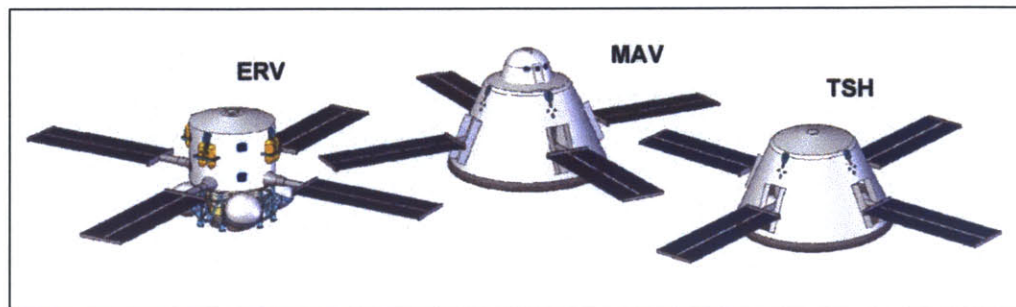


Figure 5-12: Mars mission Low Mars Orbit configurations

Mars AEDL is a two phase event. Following a de-orbit burn, the TSH (or MAV) follows an elliptical transfer orbit for approximately fifty minutes to reach the far side of the planet. The final nine to twelve minutes of this coast phase are spent decelerating ballistically through the Martian atmosphere from Mach 14 to Mach 4 (Note: the speed of sound on Mars is approximately 240 m/s).

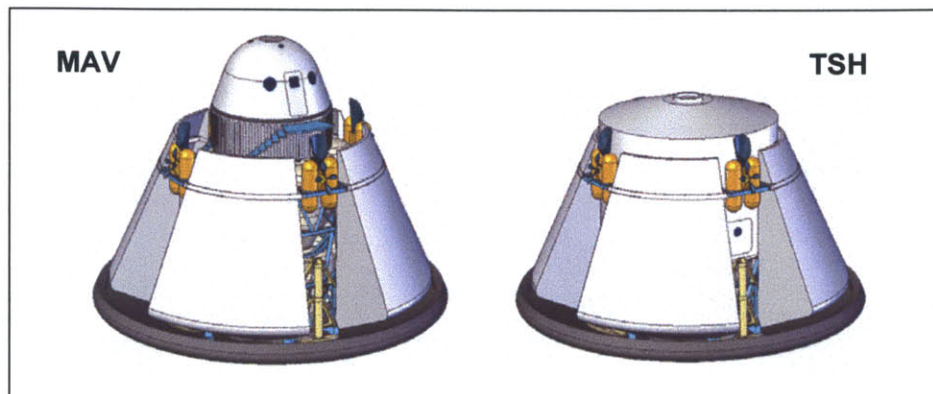


Figure 5-13: Mars mission ballistic descent configurations

At this point, the vehicle altitude is approximately 12 km . The vehicle ejects its heat shield, ignites its engines, and begins powered descent. It is in this dynamic maneuver that aerodynamic stability is most important. The powered descent phase lasts two minutes. During Lunar missions, the thrust vector is aligned to oppose the velocity vector (called a gravity turn), as this is the most efficient configuration for

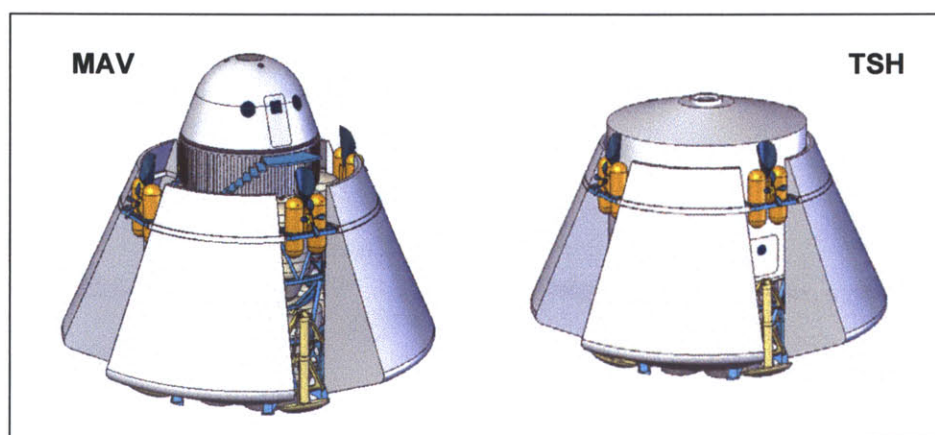


Figure 5-14: Mars mission propulsive descent configurations

deceleration in the absence of drag. However, for Mars missions, the vehicle may make use of aerodynamic forces. The vehicle may orient itself such that its thrust vector acts above its drag vector (as shown in Figure 5-15) in order to loft the vehicle. This, in fact, requires less propellant, since drag acts in tandem with thrust to reduce the speed of the craft [27].

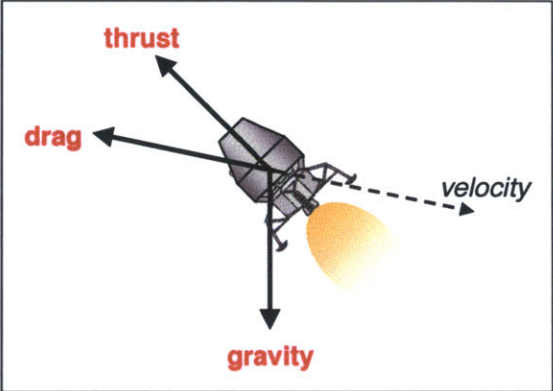


Figure 5-15: Mars mission propulsive descent configuration

During terminal descent, the landing gear deploys, and the vehicle rights itself. The remaining fuel may be used for hovering while the pilot selects a touchdown location. These vehicles require synthetic vision systems, as the astronauts will not have a direct view of the ground.

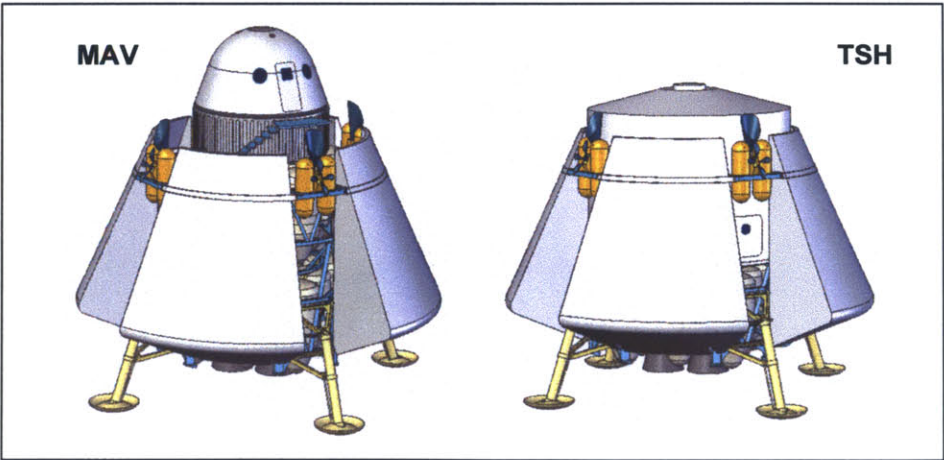


Figure 5-16: Mars mission terminal propulsive descent configurations

Cargo is stored in modular pods hinged to the sides of the descent stage. After touchdown, the cargo is readily deployed to the surface. The 7.5 m diameter YS affords ample room in the cargo pots to transport large items such as a fully-assembled nuclear reactor or pressurized rover.

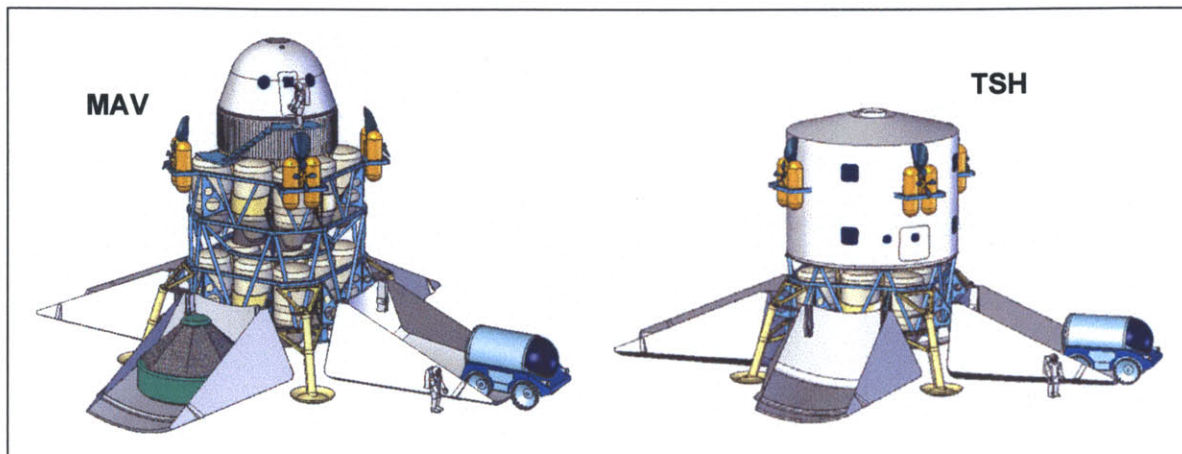


Figure 5-17: Mars mission surface configurations

At the conclusion of surface operations, the astronauts travel to the MAV. The ascent stage of the SAM propels the CEV into LMO. The CEV docks with the ERV in LMO, performs the TEI burn, and returns to Earth. The ERV retains the YS to

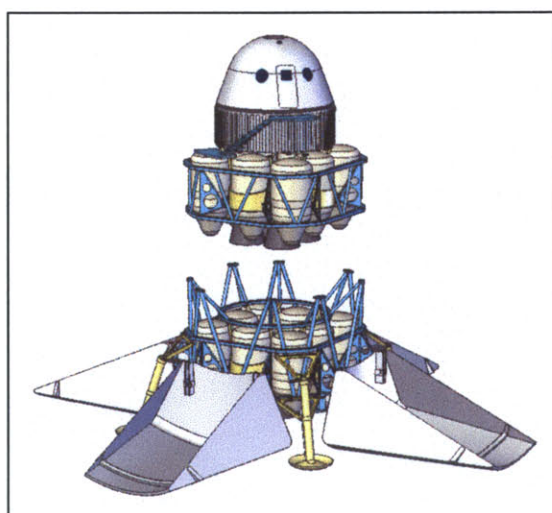


Figure 5-18: Mars mission ascent configurations

perform mid-course correction burns, if necessary. Here we see the utility of the conic aeroshell. The oversized strap-on fuel tanks for the ERV easily package within the conic shape. Packaging the fuel near the heatshield serves a dual purpose; the fuel mass increases aerodynamic stability during aerocapture, and the heat shield shades the fuel from solar radiation, thereby mitigating cryogenic fuel boil-off.



Figure 5-19: Mars mission Earth-transit configurations

Finally upon Earth arrival, the CEV undocks from the ERV and performs Earth EDL and recovery.

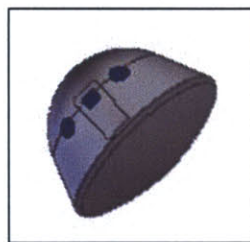


Figure 5-20: Mars mission Earth-entry configurations

One notes that the landing gear shown in these images is not representative of the landing gear required for this design. A realistic set of landing gear would have a span over twice as wide as what is shown in Figures 5-2 through 5-18. This gear would be stowed upwards, or in a folded configuration.

5.2 Vehicle-level Design Recommendations

The design concept presented in Section 5.1 is the result of many trades and analyses. The key takeaways from these analyses are as follows. Mars AEDL should be achieved using a blunt-body (conic entry capsule), since an L/D of only 0.3 is sufficient for Mars aerocapture and entry from orbit, and since the blunt-body maximizes drag and minimizes the ballistic coefficient. This recommendation assumes that precision guidance and navigation systems for Mars AEDL alleviate the need for extensive cross-range maneuvers, thus not requiring an L/D greater than 0.3. The required heat shield diameter for this conic entry capsule is 15 m , in order to accommodate the large habitable volume.

Precipitating this diameter through the transportation system, we see that a 15 m -diameter fairing, in-line heavy lift launch vehicle is then required for Mars exploration. This, of course, assumes that the heat shield may not be assembled in LEO. Although this same vehicle may also be used for Lunar missions, the core system does package within a 7.5 m fairing. Thus, a 15 m -diameter or a 7.5 m -diameter HLLV may be used for the Moon. However, if the 7.5 m diameter fairing is used, then dedicated cargo flights are necessitated, at a one billion dollar per flight price-tag. We also note that while this 7.5 m diameter launch vehicle may either be an in-line or a side-mount, development of a 15 m -diameter in-line HLLV for Mars is more straightforward, and operational risk is minimized if the Lunar mission HLLV is also an in-line.

The center of gravity of the vehicles should be as close to the heat shield as possible for passive aero-entry stability. Thus, cargo should be mounted on the sides of the descent stage to increase aero-entry and landing stability. This also solves the problem of how to deploy cargo to the surface after touchdown.

Both the 1.5-stage and 2-stage Yellow Stage designs are feasible for Mars exploration vehicles. However, both have disadvantages. Crew egress heights will be in excess of 10 m for the two-stage YS design. The 1.5-stage design affords a 5 m crew

egress height. The 1.5 stage Yellow Stage design requires reuse of engines which may be damaged by projectile debris during hovering and touchdown.

We have seen that the design of the Lunar launch vehicle is closely tied to the design of the Mars lander. We have also seen that the size of the habitat is a major design driver, as this dilates the aeroshell diameter, and thus, launch vehicle diameter. Finally, we have discovered that aerodynamic stability is a major design driver in the package of the vehicles that land on Mars, as this both restricts aeroshell height and dilates aeroshell diameter.

5.3 Airlock System Design Recommendations

The recommended airlock system is Concept 2: a surface-level, 4-person airlock that is deployed from the lander to the surface during the mission. This affords the second lowest system mass (193kg) and stowage volume (1.6m³) of any of the six concepts, the most versatility with crew number during egress, and few operational risks. A summary of the system concepts and performance metrics is presented in Figure 5-21.

Design Parameter	Airlock System Concept					
	1	2	3	4	5	6
Access Tunnel	Y	Y	Y	Y	N	N
Mud Room	Y	N	Y	N	N	N
Airlock Capacity	2	4	2	4	4	4
Rover	N	N	Y	Y	N	N
Airlock Structural Material	I	I	I	I	I	S
Total system mass [kg]	265	193	475	403	92	440*
Total system stowage volume [m³]	2.0	1.6	5.0	4.6	0.7	6.4
Major Risk	Deployment	Deployment	Land long	Land long	Ladder descent	Ladder descent

Figure 5-21: Performance metrics for the six airlock system concepts. *This is the mass of the solid-walled internal airlock on the Shuttle [16], [11].

Concepts 2 and 5 are highlighted, because these two designs most effectively meet the functional requirements. Concept 2 has been selected, with the recommendations that:

- Engineering resources should be allocated towards developing lightweight structural fabric materials, since the wall mass per unit area is the largest mass driver of the total system.
- Robust design and testing must be done to validate the deployment system for the surface-level airlock in order to retire the technical risk of the airlock not deploying properly during the mission.

Several additional design recommendations can be made, based on the analysis in Section 4.3. Specifically, they are

- A 2-person airlock is mass inefficient. The mass penalty for using a 2-person airlock is the mass of the mud room, assumed to be the same size as the 4-person airlock itself. The mass penalty for using the 4-person airlock is less in either case:

The excess mass of air exhausted from the airlock during a short-duration mission, or

The excess mass of batteries required to store the energy required for airlock decompression

- A compressor/storage tank should be protected for in the design, but not required for operation of the airlock. It is mass efficient to recycle air during long-duration missions but inefficient during short-duration missions. Therefore, the compressor should be made modular such that it may or may not be flown with each vehicle, depending on the mission duration.

- The energy required to recycle the air is two orders of magnitude below the reasonably expected amount of energy stored in the spacecraft batteries. This energy may be replenished by the vehicle power generation system.
- The amount of power required to recycle the air is within the expected power capabilities of the vehicle.
- Packaging of the stowed airlock system requires $1 - 2m^3$ cargo volume.
- Permanent surface airlock systems (i.e. jetway) do not support sortie missions and, thus, should not be used.

In conclusion, an inflatable airlock is an attractive alternative to the conventional solid-walled design. An inflatable airlock may be deployed once on the Lunar/Martian surface and jettisoned prior to ascent. This portable system is a minimum-ascent-mass solution to the problem of providing mitigation for the mission risks of dust intrusion and crew injury or illness.

5.4 Summary

In this thesis, we have examined the conceptual design of a the landing spacecraft for Moon and Mars exploration, and we have examined the design of the spacecraft airlock system. We followed the mechanical engineering design process: define the product, determine requirements, generate concepts, evaluate concepts on selected performance criteria, and select the most desirable concept. We then developed a conceptual design that satisfies all of the imposed design requirements, noting the design drivers. Design recommendations have been made; a report has been submitted to NASA; and the project has concluded.

[THIS PAGE INTENTIONALLY LEFT BLANK]

Bibliography

- [1] Astronautix. <http://www.astronautix.com/craft/apollo1m.htm>.
- [2] H. Baruh. *Analytical Dynamics*. McGraw-Hill, 1999.
- [3] Robert D. Braun. TPS Report. Technical report, Georgia Institute of Technology, 2005.
- [4] George W. Bush. The Vision for Space Exploration, 2004.
- [5] Edward Crawley. Lecture notes - MIT course ESD.34 System Architecture. Fall 2005.
- [6] Edward Crawley. NASA Concept Exploration & Refinement BAA 04-01. Technical report, Massachusetts Institute of Technology, 2005.
- [7] Robert W. Fox and Alan T. McDonald. *Introduction to Fluid Mechanics*. John Wiley & Sons, Inc., fifth edition, 1998.
- [8] GlobalSecurity.org. <http://www.globalsecurity.org/space/systems/als.htm>.
- [9] Yousef Haik. *Engineering Design Principles*. Thomson, Brooks/Cole, 2003.
- [10] Barry Hyman. *Fundamentals of Engineering Design*. Prentice Hall, 2003.
- [11] Artemis Society International. <http://www.asi.org/adb/06/07/04/10/airlock-pictures.html>

- [12] Ted A. Bateman Jenine E. Abarbanel. A Framing System for a Lunar/Martian Inflatable Structure. Technical report, Colorado State University, 1998.
- [13] S.C. Kane and T.S. Ellis. The Martian Surface Reactor: An Advanced Nuclear Power Station for Manned Extraterrestrial Exploration. Technical report, Massachusetts Institute of Technology, 2004.
- [14] John F. Kennedy. "Man on the Moon". Special Message to the Congress on Urgent National Needs, 1961.
- [15] Howard Kleinwaks. A Mars-back Approach to Lunar Surface Operations. Master's thesis, Massachusetts Institute of Technology, 2005.
- [16] Wiley J. Larson and Linda K. Pranke, editors. *Human Spaceflight: Mission Analysis and Design*. McGraw-Hill, 1999.
- [17] NASA. http://science.nasa.gov/headlines/y2001/ast06jul_1.htm
- [18] NASA. Nasa Apollo 11 press kit. Technical report, NASA, 1969.
- [19] NASA. Man-systems Integration Standards (nasa-std-3000). Technical report, NASA, 1995.
- [20] International Academy of Astronautics. http://www.iaonet.org/p_papers/chap61.html.
- [21] Gerhard Phal and Wolfgang Beitz. *Engineering Design*. London: Design Council, 1988.
- [22] M. Roberts. Inflatable Habitation for the Lunar Base. In *The Second Conference on Lunar Bases and Space Activities of the 21st Century*, volume 1, 1992.
- [23] Willard Simmons, Benjamine Koo, and Edward Crawley. Architecture generation for moon-mars exploration using an executable meta-language. Technical report, Massachusetts Institute of Technology, 2005.

- [24] Frederick J. Stimler. System definition study of deployable, non-metallic space structures. Technical report, Goodyear Aerospace Corporation, 1984.
- [25] NASA ESAS team. Exploration Systems Architecture study final report. Technical report, NASA, 2006.
- [26] Karl Ulrich and Stephen Eppinger. *Product Design and Development*. McGraw-Hill, 2000.
- [27] John West. Concept Exploration & Refinement study, final report. Technical report, The Charles Stark Draper Laboratory, Inc., 2005.
- [28] Fritz Zwicky. *The Morphological Method of Analysis and Construction*. New York Wiley-Interscience, 1948.

[THIS PAGE INTENTIONALLY LEFT BLANK]

Appendix A

Center of Gravity Calculations

The center of gravity was calculated for each vehicle using the mass specifications consistent with the Draper-MIT CE&R study. The cargo bays were assumed empty, and the mass of the corset and landing gear was accounted for in the descent stage. The center of gravity location and mass of the biconic heat shield was assumed the same as the conic heat shields, although in reality, the mass will be greater for the biconic. The following Figures A-1 through A-3 detail the center of gravity calculations:

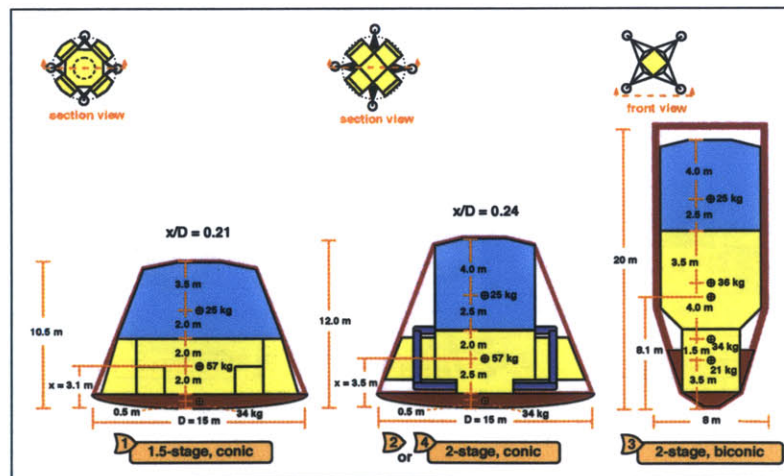


Figure A-1: Center of gravity location for the Earth Return Vehicle during aéroentry.

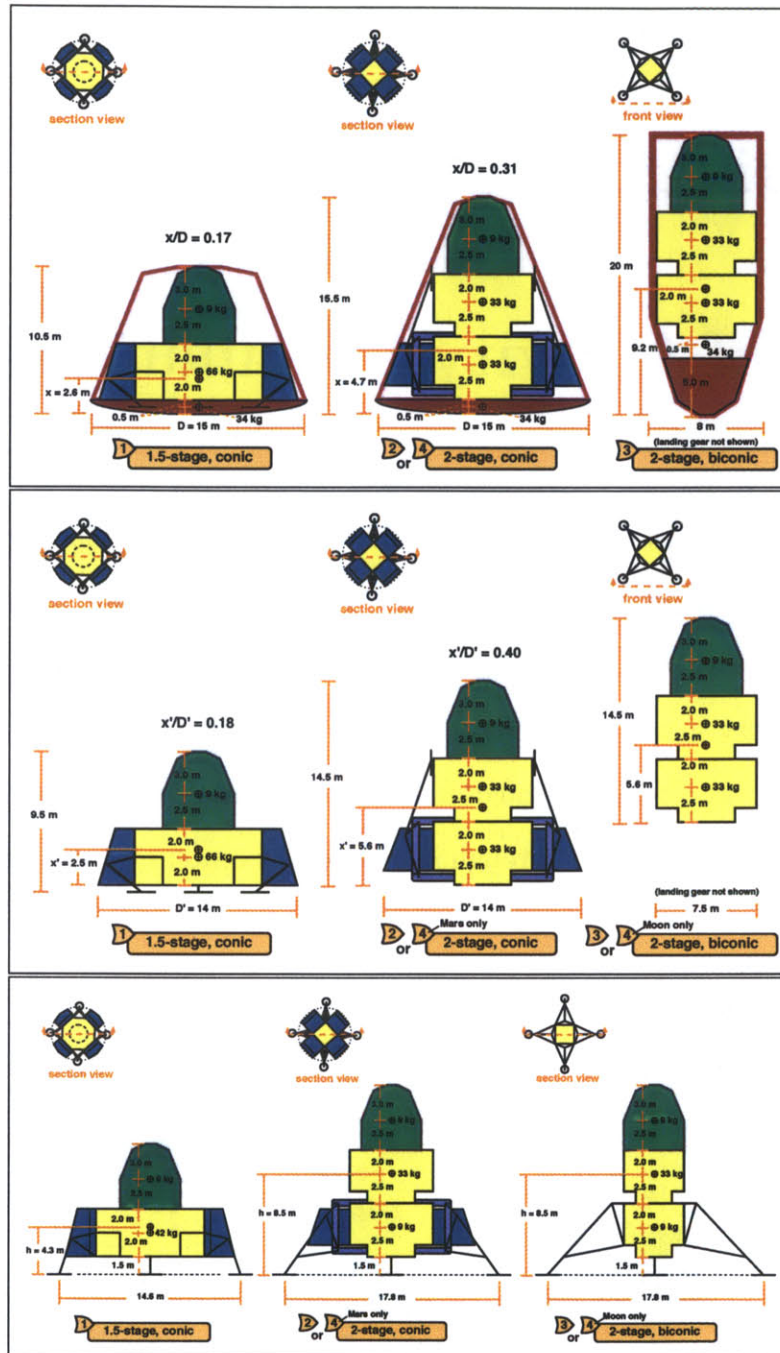


Figure A-2: Center of gravity locations for the Mars Ascent Vehicle during aeroentry, heat shield jettison, and touchdown, respectively.

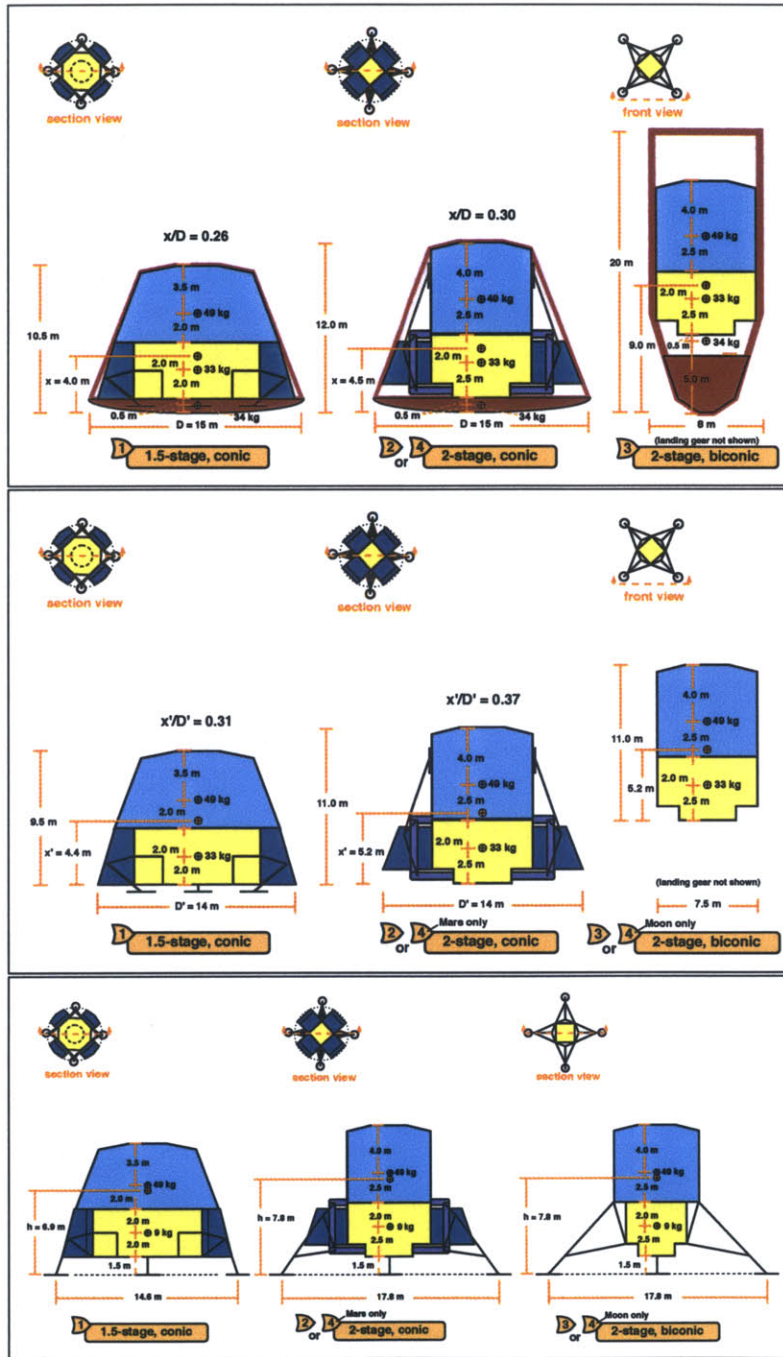


Figure A-3: Center of gravity locations for the Mars Transfer and Surface Habitat during aeroentry, heat shield jettison, and touchdown, respectively.

[THIS PAGE INTENTIONALLY LEFT BLANK]

Appendix B

Matlab Code

B.1 Landing Gear Footprint Radius Program

```
%%%%%%%%%%%% Landing Gear Footprint Radius Program %%%%%%%%%%%%%%
%
% Uses the bisection method for finding roots of functions. %
% Requires y = fun(x) to be defined. For example, if %
% y = x^2 - 11, you need a script titled fun.m that has the %
% following text: %
%
% function [y] = fun(x) %
% y = x^2 - 11; %
%
% The Bisection Method: %
% Step 1: Plot function and determine two initial guesses %
% for the root %
% Step 2: Check that the guesses bound the root %
% Step 3: Iterate until convergence %
```

```

%           Let the center x be the average of the left   %
%           and right x's.                               %
%           Determine fun(x_l), fun(x_c), and fun(x_r)   %
%           If fun(x_c) has same sign as fun(x_l), then  %
%           let x_l = x_c.                               %
%           Else, let x_r = x_c.                         %
%                                                       %
% By Brenden Epps, June 10, 2005                        %
%%%%%%%%%%%%%%%%%%%%%%%%%%%%%%%%%%%%%%%%%%%%%%%%%%%%%%%%%%%%%%%%%%%%%%%%%%

clear
close all

%%%%%%%%%%%%%%%%%%%%%%%%%%%%%%%%%%%%%%%%%%%%%%%%%%%%%%%%%%%%%%%%%%%%%%%%%% Step 0: Specify Input Parameters %%%%%%%%%%%
%                                                       %
V_ix   = [1.2, 0];           % m/s, 0 (case 1), 1.2 (case 2) %
phi_i   = [0, 6*pi/180];     % rad, 6 (case 1), 0 (case 2)   %
omega_i = [0, 2*pi/180];    % rad, 2 (case 1), 0 (case 2)   %
phi_f   = 60*pi/180;        % rad, 60                       %
S_KE    = 2;                % [ ], 2                       %
%                                                       %
h_0     = 8.5;              % m,                  %
I_cg    = 1073000;          % kg*m^2              %
m       = 51000;            % kg                  %
g       = 3.69;             % m/s^2, 1.622 (moon), 3.69 (mars)%
%                                                       %
R = zeros(1,2);           %

```

```

%
%%%%%%%%%%%%%%%%%%%%%%%%%%%%%%%%%%%%%%%%%%%%%%%%%%%%%%%%%%%%%%%%%%%%%%%%

%%%%%%%%%%%%%%%%%%%%%%%%%%%%%%%%%%%%%%%%%%%%%%%%%%%%%%%%%%%%%%%%%%%%%%%% Main Program %%%%%%%%%

%
% Case 1 and Case 2
for i_case = 1:2,

%%%%%%%%%%%%%%%%%%%%%%%%%%%%%%%%%%%%%%%%%%%%%%%%%%%%%%%%%%%%%%%%%%%%%%%% Step 1: Determine Initial Guesses %%%%%%%%%
%
% In general, one plots the function and picks off the graph
% two points that bound the root. For this problem, we know
% that the radius of the landing leg footprint must be between
% zero and twenty meters.
x_l = 0;
x_r = 20;

%%%%%%%%%%%%%%%%%%%%%%%%%%%%%%%%%%%%%%%%%%%%%%%%%%%%%%%%%%%%%%%%%%%%%%%%

%%%%%%%%%%%%%%%%%%%%%%%%%%%%%%%%%%%%%%%%%%%%%%%%%%%%%%%%%%%%%%%%%%%%%%%% Step 2: Check that the Guesses Bound the Root %%%%%%%%%
%
f_l = fun(x_l, V_ix(i_case), phi_i(i_case), omega_i(i_case), ...
          phi_f, S_KE, h_0, I_cg, m, g);
f_r = fun(x_r, V_ix(i_case), phi_i(i_case), omega_i(i_case), ...
          phi_f, S_KE, h_0, I_cg, m, g);

if x_l == x_r
    STOP = 'Error: Initial guesses must be different.'

```

```

        continue %
end %
%
if f_l == 0 %
    STOP = 'CAUTION: Initial guess is a root.' %
    ROOT = x_l %
    continue %
elseif f_r == 0 %
    STOP = 'CAUTION: Initial guess is a root.' %
    ROOT = x_r %
    continue %
end %
%
if f_l > 0 %
    if f_r > 0 %
        STOP = 'ERROR: Initial guesses do not bracket root.' %
        continue %
    end %
elseif f_r < 0 %
    STOP = 'ERROR: Initial guesses do not bracket root.' %
    continue %
end %
%
%%%%%%%%%%%%%%%%%%%%%%%%%%%%%%%%%%%%%%%%%%%%%%%%%%%%%%%%%%%%%%%%%%%%%%%%%%
%%%%%%%%%%%%%%%%%%%%%%%%%%%%%%%%%%%%%%%%%%%%%%%%%%%%%%%%%%%%%%%%%%%%%%%%%% Step 3: Iterate %%%%%%%%%%%%%%%%%%%%%%%%%%%%%%%%%%%%%%%%%%%%%%%%%%%%%%%%%%%%%%%%%%%%%%%%%%%
%
```

%% Step 4: Report Results %%

%%%

```

%
%
end
%
delta = x_r - x_l;
%
%
end
%
x_l = x_c;
%
else
%
x_r = x_c;
%
elseif f_l*f_c < 0
%
break
%
XROOT = x_c
%
if f_c == 0
%
%
omega_i(i-case), phi_f, S_KE, h_0, I_cg, m, g); %
f_r = fun(x_r, V_ix(i-case), phi_i(i-case), ...
%
omega_i(i-case), phi_f, S_KE, h_0, I_cg, m, g); %
f_c = fun(x_c, V_ix(i-case), phi_i(i-case), ...
%
omega_i(i-case), phi_f, S_KE, h_0, I_cg, m, g); %
f_l = fun(x_l, V_ix(i-case), phi_i(i-case), ...
%
%
x_c = (x_l+x_r)/2;
%
while delta > 0.00001
%
%
delta = x_r - x_l;

```

```

%                                                                    %
    XROOT = (x_l+x_r)/2;                                           %
    R(i_case) = sqrt(2)*XROOT;                                     %
end                                                                    %
                                                                    %
R                                                                    %
%                                                                    %
%%%%%%%%%%%%%%%%%%%%%%%%%%%%%%%%%%%%%%%%%%%%%%%%%%%%%%%%%%%%%%%%%%%%%%%% End Program %%%%%%%%%%
%%%%%%%%%%%%%%%%%%%%%%%%%%%%%%%%%%%%%%%%%%%%%%%%%%%%%%%%%%%%%%%%%%%%%%%% Notes %%%%%%%%%%
% To use this program, edit the fun.m file to input the          %
% correct function. The accuracy of the result depends on        %
% the argument in the 'while' loop. For a more accurate         %
% result, change it to 'delta > 0.000000001' or so...          %
%%%%%%%%%%%%%%%%%%%%%%%%%%%%%%%%%%%%%%%%%%%%%%%%%%%%%%%%%%%%%%%%%%%%%%%%
%%%%%%%%%%%%%%%%%%%%%%%%%%%%%%%%%%%%%%%%%%%%%%%%%%%%%%%%%%%%%%%%%%%%%%%% Function Definition Script %%%%%%%%%%
%                                                                    %
% This script is used in conjunction with the program:           %
% 'Landing Gear Footprint Radius Program'                         %
%                                                                    %
% Here we define the function to be evaluated. For example,     %
% if the function we are evaluating is  $y = x^2 - 11$ , then the %
% text in this script would read:                                 %
%                                                                    %
% function [y] = fun(x)                                           %
% y = x.*x - 11;                                                  %
%                                                                    %

```



```

% By Brenden Epps, June 10, 2005 %
%%%%%%%%%%%%%%%%%%%%%%%%%%%%%%%%%%%%%%%%%%%%%%%%%%%%%%%%%%%%%%%%%%%%%%%%

%%%%%%%%%%%%%%%%%%%%%%%%%%%%%%%%%%%%%%%%%%%%%%%%%%%%%%%%%%%%%%%%%%%%%%%%
% %
function [y] = fun(r_0, V_ix, phi_i, omega_i, phi_f, S_KE,... %
                h_0, I_cg, m, g) %
%
d = sqrt(r_0^2 + h_0^2); %
h_i = 0.1*r_0 + h_0; %
%
y = m*g*(sin(phi_f)*d - phi_i*r_0 - h_0) -... %
    S_KE*(h_i*m*V_ix + ... %
    omega_i*I_cg)^2/(2*(I_cg + m*d^2)); %
% %
%%%%%%%%%%%%%%%%%%%%%%%%%%%%%%%%%%%%%%%%%%%%%%%%%%%%%%%%%%%%%%%%%%%%%%%%

```

B.2 Landing Gear Sizing Program

```
%%%%%%%%%% Cantilever Landing Gear Design Program %%%%%%%%%%%
%
% This script determines the optimal positions of points 3 and%
% 5 for the cantilever leg design. Inputs to the script are %
% the positions of points 1, 2, and 4, and the desired F_y %
% and F_x touchdown forces. %
%
% The program computes the best package for the landing gear. %
%
% By Brenden Epps, July 16, 2005 %
%%%%%%%%%%

clear

close all

%%%%%%%%%% Step 0: Specify Input Parameters %%%%%%%%%%%
%
m      = 62000;      % kg, touchdown mass %
g      = 9.8;       % m/s^2, acceleration due to gravity %
N      = 4;        % [], number of legs %
F_Y    = m*2*g/N;   % N, vertical impact force %
F_X    = m*g;      % N, horizontal impact force %
r1     = 9.4       % m, z location of point 1 %
z1     = 0.0;     % m, r location of point 1 %
r2     = 3.5;     %
z2     = 2.5;     %
```

```

r4      = 3.5;                                     %
z4      = 6.0;                                     %
rT      = 5.6;                                     %
zT      = 5.5;                                     %
r_6     = rT;                                     %
z_6     = zT;                                     %
r2s     = r2+0.1;                                  %
z2s     = z2;                                     %
alpha   = 20*pi/180;                               %
t       = 0.5;      % heat shield thickness        %
                                                %
pt3_1   = 0.40;      % percent of the way up the leg %
r5      = 6.0;                                     %
z5      = 4.0;                                     %
%                                               %
%%%%%%%%%%%%%%%%%%%%%%%%%%%%%%%%%%%%%%%%%%%%%%%%%%%%%%%%%%%%%%%%%%%%%%%%%%

%%%%%%%%%%%%%%%%%%%%%%%%%%%%%%%%%%%%%%%%%%%%%%%%%%%%%%%%%%%%%%%%%%%%%%%%%% Main Program %%%%%%%%%%%%%%%%%%%%%%%%%%%%%%%%%%%%%%%%%%%%%%%%%%%%%%%%%%%%%%%%%%%%%%%%%%%
%                                               %
l_ps    = sqrt((r1-r5)^2+(z5)^2);                 %
theta   = atan(z5/(r1-r5));                       %
phi_B   = atan((z5-z2)/(r5-r2));                 %
phi_C   = atan((z4-z5)/(r5-r4));                 %
                                                %
% Determine stowed position %                   %
phi_S   = atan((z5-z2s)/(r5-r2s));               %
r1s     = r5 - l_ps*cos(phi_S);                  %

```

```

z1s    = z5 - l_ps*sin(phi_S);                                %

%%%%%%%%%%%%%%%%%%%%%%%%%%%%%%%%%%%%%%%%%%%%%%%%%%%%%%%%%%%%%%%%%%%%%%%% Determine Aeroshell Size %%%%%%%%%%
r_1s    = r1s;                                                %
z_1s    = z1s;                                                %

%%%%%%%%%%%%%%%%%%%%%%%%%%%%%%%%%%%%%%%%%%%%%%%%%%%%%%%%%%%%%%%%%%%%%%%% Step 1: Determine initial guesses %%%%%%%%%%
%
% For this problem, we know that the radius of the aeroshell %
% must be larger than the width of the yellow stage and      %
% probably less than 10 m.                                    %
%
x_l = 5;                                                        %
x_r = 10;                                                       %
%
%%%%%%%%%%%%%%%%%%%%%%%%%%%%%%%%%%%%%%%%%%%%%%%%%%%%%%%%%%%%%%%%%%%%%%%%%

%%%%%%%%%%%%%%%%%%%%%%%%%%%%%%%%%%%%%%%%%%%%%%%%%%%%%%%%%%%%%%%%%%%%%%%% Step 2: Check that the guesses bound the root %%%%%%%%%%
%
f_l = aeroshell_fun(x_l, r_1s, z_1s, r_6, z_6, alpha);      %
f_r = aeroshell_fun(x_r, r_1s, z_1s, r_6, z_6, alpha);      %
%
if x_l == x_r                                                  %
    STOP = 'Error: Initial guesses must be different.'        %
    continue                                                  %
end                                                            %
%
```

```

if f_l == 0 %
    STOP = 'CAUTION: Initial guess is a root.' %
    ROOT = x_l %
    continue %
elseif f_r == 0 %
    STOP = 'CAUTION: Initial guess is a root.' %
    ROOT = x_r %
    continue %
end %
%
if f_l > 0 %
    if f_r > 0 %
        STOP = 'ERROR: Initial guesses do not bracket root.' %
        continue %
    end %
elseif f_r < 0 %
    STOP = 'ERROR: Initial guesses do not bracket root.' %
    continue %
end %
%
%%%%%%%%%%%%%%%%%%%%%%%%%%%%%%%%%%%%%%%%%%%%%%%%%%%%%%%%%%%%%%%%%%%%%%%%%%
%%%%%%%%%%%%%%%%%%%%%%%%%%%%%%%%%%%%%%%%%%%%%%%%%%%%%%%%%%%%%%%%%%%%%%%%%% Step 3: Iterate %%%%%%%%%%%%%%%%%%%%%%%%%%%%%%%%%%%%%%%%%%%%%%%%%%%%%%%%%%%%%%%%%%%%%%%%%%%
%
delta = x_r - x_l; %
%
while delta > 0.00001 %

```

```

x_c = (x_l+x_r)/2; %
%
f_l = aeroshell_fun(x_l, r_1s, z_1s, r_6, z_6, alpha); %
f_c = aeroshell_fun(x_c, r_1s, z_1s, r_6, z_6, alpha); %
f_r = aeroshell_fun(x_r, r_1s, z_1s, r_6, z_6, alpha); %
%
if f_c == 0 %
    XROOT = x_c %
    break %
elseif f_l*f_c < 0 %
    x_r = x_c; %
else %
    x_l = x_c; %
end %
%
delta = x_r - x_l; %
end %
%
%%%%%%%%%%%%%%%%%%%%%%%%%%%%%%%%%%%%%%%%%%%%%%%%%%%%%%%%%%%%%%%%%%%%%%%%
%%%%%%%%%%%%%%%%%%%%%%%%%%%%%%%%%%%%%%%%%%%%%%%%%%%%%%%%%%%%%%%%%%%%%%%% Step 4: Report Results %%%%%%%%%%%%%%%%%%%%%%%%%%%%%%%%%%%%%%%%%%%%%%%%%%%%%%%%%%%%%%%%%%%%%%%%%
% %
XROOT = (x_l+x_r)/2; %
% %
r_c0 = XROOT; %
z_c0 = z_6 - (r_c0-r_6)/tan(alpha); %
z_n0 = z_c0 - 0.261*r_c0; %

```

```

                                                                                                                                 %
r_c  = r_c0 + t*sin(alpha);                                                                                                                                 %
z_c  = z_c0 - t*cos(alpha);                                                                                                                                 %
z_n  = z_c - 0.261*r_c;                                                                                                                                 %
                                                                                                                                 %
%%%%%%%%%%%%%%%%%%%%%%%%%%%%%%%%%%%%%%%%%%%%%%%%%%%%%%%%%%%%%%%%%%%%%%%% End Aeroshell Routine                                                                                                                                 %
                                                                                                                                 %

%%%%%%%%%%%%%%%%%%%%%%%%%%%%%%%%%%%%%%%%%%%%%%%%%%%%%%%%%%%%%%%%%%%%%%%% Determine Leg Forces                                                                                                                                 %
                                                                                                                                 %
l_2  = l_ps*(1-pt3_l);                                                                                                                                 %
                                                                                                                                 %

r3    = r1 - pt3_l*l_ps*cos(theta);                                                                                                                                 %
z3    = z1 + pt3_l*l_ps*sin(theta);                                                                                                                                 %
phi_A = atan((z2-z3)/(r3-r2));                                                                                                                                 %
                                                                                                                                 %

% Solve matrix equation A*X=B for the forces %                                                                                                                                 %
forcesA = [-cos(phi_A) -cos(phi_B) -cos(phi_C);...                                                                                                                                 %
           sin(phi_A) -sin(phi_B)  sin(phi_C);...                                                                                                                                 %
           -l_2*sin(theta-phi_A) 0 0];                                                                                                                                 %
                                                                                                                                 %

% Case 1: F_Y = m*5*g/N, F_X=0 %                                                                                                                                 %
% forcesB=[F_X;-F_Y;F_X*l_ps*sin(theta)-F_Y*l_ps*cos(theta)]; %                                                                                                                                 %
forcesB = [0; -F_Y; -F_Y*l_ps*cos(theta)];                                                                                                                                 %
forcesX = linsolve(forcesA,forcesB);                                                                                                                                 %
F_Ay    = forcesX(1); % N, force in member A (+ for tension) %                                                                                                                                 %
F_By    = forcesX(2); % N, force in member B (+ for tension) %                                                                                                                                 %
F_Cy    = forcesX(3); % N, force in member C (+ for tension) %

```

```

% Case 2: F_Y = 0, F_X=m*3*g %
% forcesB=[F_X;-F_Y;F_X*l_ps*sin(theta)-F_Y*l_ps*cos(theta)]; %
forcesB = [F_X; 0; F_X*l_ps*sin(theta)]; %
forcesX = linsolve(forcesA,forcesB); %
F_Ax = forcesX(1); % N, force in member A (+ for tension) %
F_Bx = forcesX(2); % N, force in member B (+ for tension) %
F_Cx = forcesX(3); % N, force in member C (+ for tension) %
%
%%%%%%%%%%%%%%%%%%%%%%%%%%%%%%%%%%%%%%%%%%%%%%%%%%%%%%%%%%%%%%%%%%%%%%%% End Main Program %%%%%%%%%%

```

```

%%%%%%%%%%%%%%%%%%%%%%%%%%%%%%%%%%%%%%%%%%%%%%%%%%%%%%%%%%%%%%%%%%%%%%%% Function Definition Script %%%%%%%%%%

```

```

%
% This script is to be used in conjunction with the program: %
% 'Aeroshell Sizing' %
%
% Here we define the function to be evaluated. For example, %
% if the function we are evaluating is  $y = x^2 - 11$ , then the %
% text in this script would read: %
% function [y] = fun(x) %
% y = x.*x - 11; %
%
% By Brenden Epps, June 10, 2005 %

```

```

%%%%%%%%%%%%%%%%%%%%%%%%%%%%%%%%%%%%%%%%%%%%%%%%%%%%%%%%%%%%%%%%%%%%%%%%

```

```

%%%%%%%%%%%%%%%%%%%%%%%%%%%%%%%%%%%%%%%%%%%%%%%%%%%%%%%%%%%%%%%%%%%%%%%%

```

```

%
function [y] = aeroshell_fun(r_c, r_1s, z_1s, r_6, z_6, alpha)%

```